STRUCTURE-PROPERTY RELATIONSHIPS IN BIMODAL AND TRIMODAL END-LINKED POLYDIMETHYLSILOXANE ELASTOMERS

A Dissertation

Presented to the Faculty of the Graduate School

of Cornell University

In Partial Fulfillment of the Requirements for the Degree of

Doctor of Philosophy

by

Geoffrey David Genesky

August 2009

STRUCTURE-PROPERTY RELATIONSHIPS IN BIMODAL AND TRIMODAL END-LINKED POLYDIMETHYLSILOXANE ELASTOMERS

Geoffrey David Genesky, Ph.D.

Cornell University 2009

This thesis investigates the structure and properties of end-linked polydimethylsiloxane (PDMS) elastomers prepared with multiple, discrete molar mass distributions. Even in unimodal networks, which contain elastic chains of a single molar mass distribution, the length of the precursors used to synthesize an end-linked polymer network will have a great influence on the network's mechanical properties. When the average molar masses of the short and long chain components in bimodal networks are widely separated, improved mechanical properties can result. For instance, these elastomers can be stretched to high elongation ratios and display an upturn in stress before fracture. Therefore, the best bimodal networks can absorb more energy before failure than unimodal networks with similar low strain properties. Experimental determination of mechanical properties for a wide variety of bimodal networks systematically identifies which compositions demonstrate optimal performance. These results are combined with theoretical calculations and comparisons to models of rubber elasticity to provide evidence of the microstructure connected with mechanical reinforcement. The methods are then extended to a series of PDMS elastomers with three precursor molar mass distributions. Some of these trimodal networks have mechanical properties which surpass even the bimodal networks.

The relationship between the structure of these end-linked networks and their mechanical properties under applied stress are examined at the molecular scale using ^{2}H-NMR spectroscopy. Unimodal networks show decreasing spectral wings with

increasing precursor molar mass, indicating that the longer chains are less perturbed from their initial states when changing from the melt state to the elastic state. These general lineshapes persist for the selectively labeled short and long chains in bimodal networks, and the short chain networks with the best mechanical properties show the most prominent spectral wings. ^{2}H-NMR experiments on stretched samples reveal that the short chains sustain more of the applied load than the long chains in optimal networks. Longer chains in unimodal or bimodal samples can display inner and outer doublets at high strain that are related to the excluded volume interactions between segments and the effect of the chemical cross-links, respectively.

BIOGRAPHICAL SKETCH

Geoffrey Genesky was born in Batavia, NY on March 26, 1981. After graduating from Batavia High School in 1999, he attended the University at Buffalo and received a B.S. in Chemical Engineering in 2003. Upon completion of the requirements for a Ph.D. in Chemical Engineering at Cornell University, Geoffrey will join the Research and Development department at L'Oréal USA in Clark, NJ.

To my family and friends

ACKNOWLEDGEMENTS

Thank you to Prof. Claude Cohen for being such a patient and helpful advisor.

Thank you to Prof. Mike Duncan and Prof. Herbert Hui for serving on my thesis committee and helping me at various points along the way.

Thank you to Prof. Fernando Escobedo and Bernardo Aguilera-Mercado for being such integral parts of our collaborative work.

Thank you to Dr. Ashish Batra for training me during my early years at Cornell.

Thank you to all of the undergraduate and graduate students who have worked in the Cohen Lab during my graduate school career.

Thank you to the National Science Foundation Polymers Program for support of this research under grants DMR-0349952 and DMR-0705565.

Thank you to my parents and my sister for bringing me up right.

Thank you to my grandparents for being good role models and good people.

Thank you to my friends for helping to make life fun.

TABLE OF CONTENTS

LIST OF FIGURES

LIST OF TABLES

CHAPTER 1

INTRODUCTION*

1.1 Bimodal Network Précis and Material of Choice

Bimodal polymer networks consist of two sets of telechelic polymer chains of different molar mass that are chemically identical and end-linked together from the melt state. It has been reported that when such networks are prepared from short and long chains whose molar mass differ by a factor greater than 10, enhanced mechanical properties can result.[1] For example, these bimodal networks can withstand higher loads than long chain unimodal networks without the usual decrease in extensibility found in networks prepared with shorter chains. Therefore, bimodal networks can have both a large ultimate stress and a large ultimate strain. The mechanical enhancement is aided by a characteristic upturn in stress at high strain values. This leads to an improvement in toughness – the energy per unit volume required to rupture the material, which is found by integrating under the stress-elongation ratio curve.

Polydimethylsiloxane (PDMS) is an important component of many silicone elastomers. Its unique properties, such as low glass transition temperature (-127^{o}C) and high chain flexibility, make it a rather ideal elastomer to study. The properties of PDMS chains with unimodal chain length distribution end-linked with tetrafunctional cross-linkers have been well characterized.[2-7] For these reasons, and the fact that unimodal PDMS elastomers have been successfully modeled by Monte Carlo simulations,[8-11] PDMS has been employed in the present study of bimodal elastomers.

1.2 Reported Hypotheses for Reinforcement in Bimodal Networks

A number of experimental studies of bimodal networks have been previously reported. However, the reasons for the upturn in stress and enhancement in mechanical properties have been debated and are not clear. The two main hypotheses for the improvement in properties are finite extensibility of the short chains, as originally proposed by J.E. Mark[1,12,13], and the clustering of the short chains into heterogeneous structures.[14-18] Mark's experiments used hydroxyl terminated PDMS chains cross-linked with tetraethyl orthosilicate to create networks with tetrafunctional cross-linking. The short chains always had number average molar mass (M_n) less than 1100 g/mol, while the long chains were typically about 20,000 g/mol. Mark attributed the increased toughness of bimodal networks to good extensibility due to reapportionment of strain to the long chains during the early stages of deformation, followed by an increase in stress at high elongations due to the limited extensibility of the short chains. However, some researchers have credited the improved properties to heterogeneous domains of short chains in the bimodal networks. Stein et al.[14] used small-angle neutron scattering (SANS) to observe an increase in the scattered intensity I(q) upon curing of bimodal networks with deuterium-labeled short chains. This observation, along with additional SANS experiments on bimodal networks that showed two characteristic length scales,[15] indicates segregation between the short and long chains. Additional evidence from stress-optical,[16] dynamic light scattering,[17] and nuclear magnetic resonance[18] studies shows that the short chains can segregate into clusters. Proponents of the clustering hypothesis for toughness enhancement envision the smaller chain heterogeneities acting as large multifunctional cross-links similar to the filler particles that are often added to elastomers. Some have theorized that these short chain clusters cause increased toughness through dissipation of elastic energy as the network is deformed.[19]

A number of theoretical studies have also been performed to describe the properties of bimodal networks. Several studies have used free energy minimization techniques to generate stress-strain properties. Rotational isomeric state (RIS) or Fixman-Alben distributions were used to describe the end-to-end distances of the chains.[20-24] While these studies are able to describe the short, non-Gaussian chains as they reach their extended state, the network connectivity and resulting interactions between chains are ignored. On the other hand, von Lockette et al.[25] developed a micromechanics-based eight-chain model to take into account network connectivity based on a proposed microcomposite arrangement. Each of the eight chains in the model is a "bimodal" chain consisting of a long chain and short chain connected in series with two pairs of cross-links. The model is successful in describing stress-stretch experimental results of Mark's bimodal networks with high concentration of short chains, but it fails to describe others at lower short chain concentrations. The authors speculate that this may be due to the fact that their proposed microcomposite arrangement does not describe all experimental systems. Their model does not incorporate the role of the faster curing kinetics of the much smaller and more mobile short chains.

1.3 Methodology and Thesis Outline

The overall goal of this research is to determine the effect of both the number of discrete precursor molar masses and their respective average chain lengths on the mechanical properties of polymer networks. These properties are measured using macroscopic testing methods which include stress-elongation in uniaxial extension, fracture energy via pure shear cut growth, and swelling in toluene. Connections between these properties and the network structure are probed at the microscopic length scale using ^{2}H-NMR spectroscopy.

The mechanical and swelling properties of bimodal networks are studied in a systematic fashion in Chapter 2. Bimodal network properties are examined in experimental studies of polydimethylsiloxane elastomers and compared with Monte Carlo simulations mimicking such flexible chains.[11] Since the experiments and simulations show good qualitative agreement, evidence from each is combined to evaluate the hypotheses for mechanical reinforcement in bimodal networks.

Chapter 3 treats networks with three molar mass distributions. Mechanical properties of these trimodal networks are compared to unimodal and bimodal networks with similar low strain properties. Bimodal networks with very widely separated precursor molar masses are also investigated. Microstructures necessary for enhanced mechanical properties in these special systems are proposed based on theoretical calculations and comparison to the model of ideal rubber elasticity.

In Chapter 4, elastomers with a long pre-cut are tested to determine their threshold fracture energies. Unimodal network results are compared to the classical Lake-Thomas theory[26] and to previous measurements of fracture energy for randomly cross-linked PDMS networks.[27] The theory is used to investigate the respective contributions from chemical cross-links and chain entanglements to fracture energy. Bimodal and trimodal fracture energies are compared to the unimodal network results.

^{2}H-NMR is used to monitor segmental orientation in unimodal PDMS networks in Chapter 5. Lineshapes in the rest state vary with precursor molar mass, revealing the shorter chains to be more perturbed from their initial melt states upon cross-linking. Stretched long chain networks display two distinct doublets that are associated with segment alignment due to the constraints of the cross-links and

interactions between neighboring chains.

Chapter 6 extends the ^{2}H-NMR studies to bimodal networks. Short or long chains are selectively labeled to monitor chain segment behavior in each. Lineshapes of unstretched networks provide clues into the microstructure of bimodal networks. Stretched networks are then examined to compare segment orientations of each chain component and connect these microscopic measurements with mechanical performance.

REFERENCES

1. Andrady, A. L.; Llorente, M. A.; Mark, J. E. *J. Chem. Phys.* **1980**, *72*, 2282-2290.

2. Patel, S. K.; Malone, S.; Cohen, C.; Gillmor, J.; Colby, R. *Macromolecules* **1992**, *25*, 5241-5251.

3. Valles, E. M.; Macosko, C. W. *Macromolecules* **1979**, *12*, 673-679.

4. Meyers, K. O.; Bye, M. L.; Merrill, E. W. *Macromolecules* **1980**, *13*, 1045-1053.

5. Sivasailam, K.; Cohen, C. *J. Rheology* **2000**, *44*, 897-915.

6. Urayama, K.; Kohjiya, S. *Polymer* **1997**, *38*, 955-962.

7. Kawamura, T.; Urayama, K.; Kohjiya, S. *J. Polym. Sci. Pol. Phys.* **2002**, *40*, 2780-2790.

8. Chen, Z.; Cohen, C.; Escobedo, F. A. *Macromolecules* **2002**, *35*, 3296-3305.

9. Stepto, R .F. T; Taylor, D. J. R. *J. Chem. Soc. Faraday Trans.* **1995**, *91*, 2639-2647.

10. Stepto, R. F. T; Cail, J. I.; Taylor, D. J. R. *Mat. Res. Innovat.* **2003**, *7*, 4-9.

11. Genesky, G. D.; Aguilera-Mercado, B. M.; Bhawe, D. M.; Escobedo, F. A.; Cohen, C. *Macromolecules* **2008**, *41*, 8231-8241.

12. Llorente, M. A.; Andrady, A. L.; Mark, J. E. *J. Polym. Sci. Pol. Phys.* **1981**, *19*, 621-630.

13. Mark, J. E.; Tang, M. -Y. *J. Polym. Sci. Pol. Phys.* **1984**, *22*, 1849-1855.

14. Wu, W. L.; Jong, L.; Hanyu, A.; Coyne, L .D.; Stein, R. S. *Macromolecules* **1990**, *23*, 351-353.

15. Hecht, A. -M.; Horkay, F.; Geissler, E. *J. Phys. Chem. B* **2001**, *105*, 5637-5642.

16. Subramanian, P. R.; Galiatsatos, V. *Makromol. Chem. - M. Symp.* **1993**, *76*, 233-240.

17. Oikawa, H. *Polymer* **1992**, *33*, 1116-1119.

18. Saalwachter, K.; Ziegler, P.; Spyckerelle, O.; Haidar, B.; Vidal, A.; Sommer, J. -U. *J. Chem. Phys.* **2003**, *119*, 3468-3482.

19. Smith, T. L.; Haidar, B.; Hedrick, J. L. *Rubber. Chem. Technol.* **1990**, *63*, 256-264.

20. Mark, J. E.; Curro, J. G. *J. Chem. Phys.* **1983**, *79*, 5705-5709.

21. Curro, J. G.; Mark, J. E. *J. Chem. Phys.* **1984**, *80*, 4521-4525.

22. Llorente, M. A.; Rubio, A. M.; Freire, J. J. *Macromolecules* **1984**, *17*, 2307-2315.

23. Erman, B.; Mark, J. E. *J. Chem. Phys.* **1988**, *89*, 3314-3316.

24. Zhang, L. -X.; Jiang, Z. -T.; Zhao, D. -L. *J. Polym. Sci. Pol. Phys.* **2002**, *40*, 105-114.

25. von Lockette, P. R.; Arruda, E. M.; Wang, Y. *Macromolecules* **2002**, *35*, 7100-7109.

26. Lake, G. J.; Thomas, A. G. *P. R. Soc. Lond. A. Mat.* **1967**, *300*, 108-119.

27. Gent, A. N.; Tobias, R. H. *J. Polym. Sci. Pol. Phys.* **1982,** *20*, 2051-2058.

CHAPTER 2

MECHANICAL PROPERTIES OF BIMODAL NETWORKS IN UNIAXIAL EXTENSION*

2.1 Introduction

Mechanical and swelling properties of a series of PDMS bimodal networks are determined experimentally in this chapter and compared with Monte Carlo simulations mimicking such flexible chains.[1] Several different combinations of short and long chains are employed, including short chains that are long enough to assume a Gaussian distribution of end-to-end vectors when in the unperturbed state. Carefully controlled chemistry allows for the creation of networks with a very low soluble fraction, and these specimens have fewer defects than those employed in many previous experiments. Experimental stress-strain and swelling measurements are compared to Monte Carlo simulation predictions with good qualitative agreement. Therefore, results from both experiments and simulations are used to test the two hypotheses of finite extensibility and non-homogeneous distribution of short chains that have been used to explain the mechanical improvement seen in bimodal networks.

2.2 Experimental Procedures

2.2.1 Synthesis of precursor chains

Except for the 800 g/mol chains, which were purchased from Gelest, Inc., PDMS precursor chains were synthesized via an anionic ring-opening polymerization from hexamethylcyclotrisiloxane monomer[2,3] (Gelest, Inc.). The monomer was dissolved in 50 wt% toluene and an empirically determined amount of HPLC water

* Reproduced in part with permission from *Macromolecules* **2008**, *41*, 8231-8241. Copyright 2008 American Chemical Society.

was added to control the molecular weight of the resulting polymer. After heating the solution to 60°C, the reaction began with the addition of benzyltrimethylammoniumbis(o-phenylenedioxy)-phenylsiliconate catalyst and dimethylsulfoxide promoter. After 2 hours the reaction was complete and the mixture of toluene and PDMS chains was allowed to cool to room temperature. Addition of an excess of pyridine (an acid scavenger) and vinyldimethylchlorosilane converted the PDMS chain ends to vinyl groups. The polymer chains were then washed with water and precipitated in a mixture of toluene and methanol. Any remaining solvent was removed by drying in an oven for 3 days.

The molar mass distributions were characterized by gel permeation chromatography (GPC). The columns were calibrated using polystyrene standards with narrow polydispersity, and equivalent PDMS molar masses were obtained using a well-established conversion.[4] For the 800, 4500, 10000, 21000, 29000, and 91000 number-average molar mass chains used in this study, the corresponding polydispersity indexes were 1.43, 1.18, 1.33, 1.25, 1.27, and 1.38.

2.2.2 Synthesis of bimodal networks

For the bimodal networks studied here, the mole percentage of short chains was varied from 60 to 98%. The total mass of short chains required was calculated using:

$$g_{short} = g_{total} \times \left[\frac{x_{short} \times M_{n,short}}{x_{short} \times M_{n,short} + x_{long} \times M_{n,long}} \right] \quad (1)$$

Here, g is the mass in grams, M_n is the number averaged molar mass in g/mol, and x is the mole fraction. The short chain and long chains masses were measured and combined. Next, the necessary volume of tetrakis(dimethylsiloxy)silane cross-linker

($\mu l_{cross\text{-}linker}$) (Gelest, Inc.) was calculated using:

$$\mu l_{cross-linker} = 1.86 \times 10^5 \times r \times \left[\frac{g_{short}}{M_{n,short}} + \frac{g_{long}}{M_{n,long}} \right] \quad (2)$$

In this equation, the prefactor 1.86 x 10^5 (in μl per mole) is calculated from the density and molar mass of the cross-linker to balance the number of reactive ends of the tetrafunctional cross-linker with chain ends of the difunctional PDMS. The parameter *r* is defined to represent the ratio of cross-linker arms to polymer chain ends such that *r* = 1 represents a stoichiometric balance between the two. Past work has shown that *r* = 1.7 yields the highest quality unimodal networks[5] when the precursor chains have molar masses greater than 10,000. Therefore, *r* = 1.7 was used to produce optimal (low soluble fractions) long chain unimodal networks. Other researchers have demonstrated that the highest quality short chain unimodal networks are formed at lower *r* ratios.[6] Thus, bimodal networks with 800 g/mol short chains required less cross-linker to produce optimal networks, so *r* was reduced to 1.1 as the mol% of short chains increased. For the 4500-91,000 M_n bimodal network series, *r* = 1.7 was used for all bimodal networks.

After the short chain, long chain, and cross-linker were added, they were well-mixed with a spatula and placed on a rotator overnight to ensure homogeneity. The catalyst for the network formation, cis-dichlorobis(diethylsulfide)platinum(II), was dissolved in a minimal amount of toluene and then mixed into the PDMS and cross-linker. After transfer to Teflon molds, the networks were cured at 35°C for 3 days.

2.2.3 Mechanical testing to fracture in uniaxial extension

After the networks were cured, they were removed from the molds and a sample puncher was employed to produce test pieces of uniform width and thickness. Typical samples were 0.5-1 mm thick and 4.3 mm wide. The distance between the two

clamps was 40-45 mm. Engineering stress (force/initial cross-sectional area) versus extension ratio (length/initial length) data were measured with an Instron uniaxial extension setup. The samples were clamped in their undeformed state at room temperature and extended at 20 mm/min until fracture. This strain rate was selected after verifying that the stress-strain data were independent of strain rate at this slow extension speed. Young's modulus (E) was determined by calculating the slope of the best fit line through the first 5% of the stress-strain curve, where the trend is linear.

2.3 Results and Discussion

2.3.1 Stress-elongation

Experimental stress-extension ratio curves up to network rupture for three series of bimodal networks are presented in Figure 2.1. The area under each curve is the energy needed to break the network. This energy is sometimes referred to as the fracture energy, and will depend on the size of the sample and the sizes of the flaws that cause the sample to fail. Throughout this thesis, this energy (as measured by uniaxial extension testing) is referred to as the toughness. Toughness values, other mechanical and swelling properties, and the swelling ratio Q are listed in Table 2.1.

Each sample produced 4 to 6 test pieces. While the stress-strain curve was reproducible from sample to sample, inherent flaws in the test pieces varied the breaking point. Therefore, the average and standard deviation are presented for the modulus, toughness, and ultimate stress data. A few samples broke prematurely near one of their edges due to the clamping force and were not included in this statistical analysis. Since presenting all measured data in Figures 2.1-2.5 would be too cluttered, only the data of the test pieces that reached the highest elongation ratios is shown in these plots.

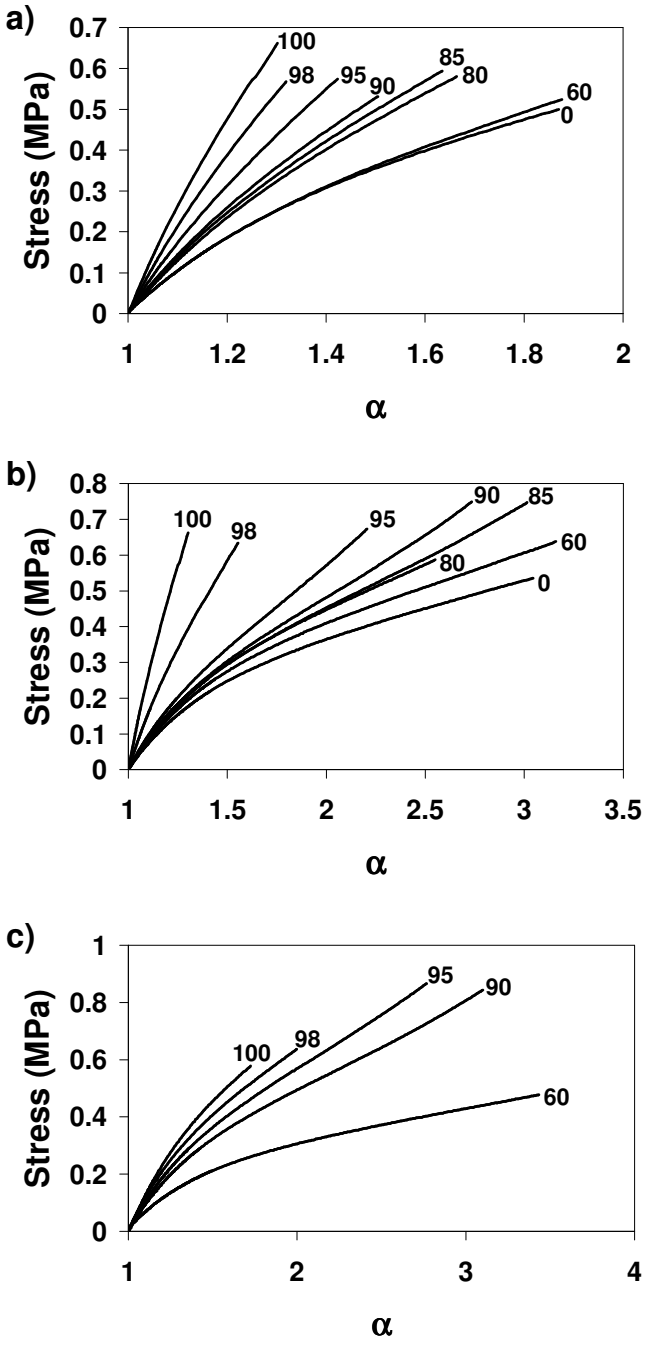

Figure 2.1. Engineering stress f/A* (force divided by initial cross-sectional area) vs. extension ratio α for bimodal networks (a) 800-10,000 g/mol networks; (b) 800-29,000 g/mol networks; (c) 4500-91,000 g/mol networks. Curves are labeled with mol% short chains.

Table 2.1. Bimodal network compositions and properties. Modulus, Toughness, and Ultimate Stress values reported are the average and standard deviation of 4 to 6 test pieces.

M_n of short chains	M_n of long chains	mol%, mass% of short chains	E (MPa)	Q	w_{sol} (mass%)	Toughness (MPa)	Ultimate Stress (MPa)
800	10,000	0	1.04 ± 0.03	3.16	0.34	0.20 ± 0.06	0.44 ± 0.06
		60, 11	1.06 ± 0.02	3.16	0.49	0.17 ± 0.08	0.43 ± 0.08
		80, 24	1.33 ± 0.02	2.74	0.76	0.16 ± 0.05	0.50 ± 0.07
		85, 31	1.38 ± 0.03	2.73	0.73	0.15 ± 0.06	0.49 ± 0.09
		90, 42	1.46 ± 0.03	2.67	1.02	0.10 ± 0.04	0.44 ± 0.07
		95, 60	1.74 ± 0.03	2.44	0.70	0.08 ± 0.04	0.45 ± 0.09
		98, 80	2.14 ± 0.11	2.30	1.07	0.07 ± 0.02	0.47 ± 0.07
		100	2.72 ± 0.11	2.06	0.90	0.09 ± 0.02	0.59 ± 0.10
800	29,000	0	0.74 ± 0.04	3.75	0.78	0.53 ± 0.12	0.48 ± 0.04
		60, 4	0.82 ± 0.04	3.57	0.71	0.51 ± 0.24	0.51 ± 0.09
		80, 10	0.89 ± 0.02	3.53	0.36	0.44 ± 0.12	0.53 ± 0.05
		85, 14	0.88 ± 0.02	3.54	0.38	0.85 ± 0.03	0.74 ± 0.01
		90, 20	0.88 ± 0.03	3.47	0.90	0.63 ± 0.14	0.68 ± 0.09
		95, 34	0.95 ± 0.04	3.10	0.49	0.37 ± 0.08	0.60 ± 0.06
		98, 57	1.43 ± 0.03	2.66	0.88	0.15 ± 0.03	0.57 ± 0.10
		100	2.72 ± 0.11	2.06	0.90	0.09 ± 0.02	0.59 ± 0.10
4500	91,000	60, 7	0.64 ± 0.03	5.17	3.74	0.64 ± 0.10	0.45 ± 0.02
		90, 31	0.94 ± 0.01	3.62	0.26	0.90 ± 0.09	0.79 ± 0.04
		95, 48	1.09 ± 0.03	3.40	0.22	0.79 ± 0.09	0.82 ± 0.04
		98, 71	1.24 ± 0.04	3.15	1.00	0.28 ± 0.09	0.57 ± 0.07
		100	1.34 ± 0.06	3.06	0.93	0.24 ± 0.01	0.57 ± 0.02

2.3.2 Toughness

For the 800-10,000 g/mol series a), no toughness enhancement was seen. The 60 mol% short chain network performs similarly to the unimodal 10,000 g/mol samples. At higher concentration of short chains, the networks do not exhibit an upturn in stress at high elongations and do not show improved toughness. The only effect of bimodality here seems to be to alter the elastic modulus E. It is important to note that in this system, the ratio of molar masses in this bimodal system has only a moderate value of 12.5.

With a short chain of 800 g/mol and a long chain of 29,000 g/mol (Figure 2.1b), however, some of the bimodal networks have better toughness than their unimodal counterparts. When the short chain concentration is 85-95 mol%, the stress turns upward before rupture. The 85 mol% short chain network gives the best combination of elongation, ultimate stress, and toughness. Comparison to the performance of 800-10,000 g/mol networks suggests that greater enhancements in mechanical properties are seen when the molar masses of the precursor chains are quite widely separated.

While the improvement in toughness can clearly be seen in 800-29,000 M_n networks, it is only of the order of 25-50%. This enhancement is less than previously reported.[7-9] This can be attributed to the fact that this study uses an "optimal" 29,000 g/mol network that leads to a very low soluble fraction (w_{sol}) and few inelastic chains. Previous researchers used a stoichiometric amount of cross-linker corresponding to r = 1.0 for both bimodal and unimodal networks.[7-9] Since the optimal r for these bimodal samples at 85-95 mol% is about 1.1 due to the large amount of short chain ends, earlier studies had fortuitously employed bimodal networks of higher quality than the unimodal networks they were being compared to. Here, all networks were prepared as

defect-free as possible, as evidenced by soluble fraction values of 1.07% or less for samples in the 800-10,000 and 800-29,000 M_n series.

2.3.3 Stress upturn

The stress-strain performance of bimodal networks with short chains of molar mass 4500 g/mol also reveals stress upturns at high strains. Therefore, enhanced mechanical properties in bimodal networks cannot be solely attributed to the presence of very short chains that are non-Gaussian in the undeformed state. Because the long chain component (91,000 g/mol) contains so few chain ends, it is difficult to completely end-link a pure long chain melt or mixtures with low % short chains in a reasonable cure time. As shown in Table 2.1, the 60 mol% short chain network in this series had a soluble fraction of 3.74%.

It is instructive to normalize the stress σ by the initial elastic modulus E, as plotted in Figure 2.2 for the 800-29,000 and 4500-91,000 M_n bimodal systems. This allows for comparison to the model of ideal rubber elasticity:

$$\frac{\sigma}{E} = \frac{\alpha - \alpha^{-2}}{3} \tag{3}$$

For both systems, all curves initially follow the ideal model (the dashed curve), but deviate downward as α increases. This downward deviation for elastomers is usually attributed to the presence of entanglements (often associated with the C_2 term in the Mooney-Rivlin representation).

However, due to non-Gaussian behavior and limited extensibility at large values of α, some of the experimental curves upturn at higher concentrations of short chains. These curves again approach the ideal rubber elasticity values of σ/E once they are stretched far enough. In fact, the data of the 95 mol% 800 – 5 mol% 29,000 network slightly overtake the ideal curve. Thus, the presence of the short chains

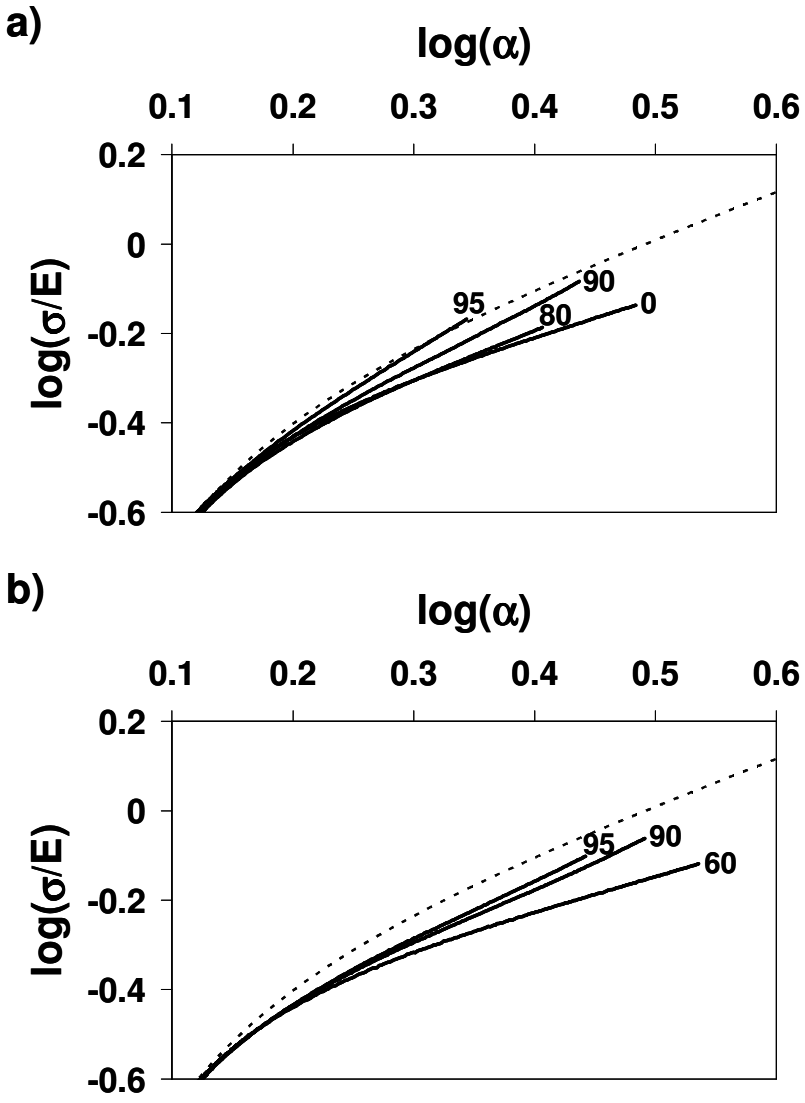

Figure 2.2. Logarithmic plot of engineering stress normalized by modulus vs. extension ratio for bimodal networks (a) 800-29,000 g/mol networks; (b) 4500-91,000 g/mol networks. Curves are labeled with mol% short chains. Dashed line represents ideal rubber elasticity (equation 3), which is based on the assumption of affine deformation.

appears to mitigate the effect of the "slippage" of entanglements on the stress-stretch curve as the strain increases.

Plotting the data in a Mooney-Rivlin representation is a better way to visualize the upturns in stress. This is done by dividing the engineering stress by $\alpha-\alpha^{-2}$ and plotting the results against α^{-1}. Some curves of interest are shown in Figure 2.3. The stress upturn for 85 and 90 mol% short chain networks is seen at inverse elongation values of less than about 0.4. The curve for the 60% short chain network, however, does not display an upturn.

In the bimodal network of 90 mol% short chains of 4500 g/mol with long chains of 91,000 g/mol, both chains are Gaussian in their unperturbed state. It may then be instructive to perform a simple calculation of the affine extension of both chains even though it has been established that deformation is not affine at the macromolecular scale in elastomers. The maximum extensibility of a PDMS chain r_m as a function of number of monomer units n has been shown to be:[10]

$$r_m = 1.34n = 1.34(2 \times M_n / 74) \tag{4}$$

The pre-factor, 1.34 Å, is the axial length of a PDMS bond projected along a straight line, and 74 g/mol is the molar mass of an $Si(CH_3)_2$-O unit. Additionally, the average chain extension r at elongation ratio α for a PDMS chain of a given M_n can be calculated based on affine deformation from the relation:[11]

$$r = < r_0^{\,2} >^{1/2} \alpha = 730 \times 10^{-3} \left(M_n\right)^{1/2} \alpha \tag{5}$$

Here, r_0 is the unperturbed end-to-end distance of a PDMS chain and the pre-factor 730 x 10^{-3} has units of Å $mol^{1/2}$ $g^{-1/2}$.

These relations provide a simple way to calculate the extension ratio of each chain compared to its maximum extension (r/r_m). Therefore, the normalized stress-

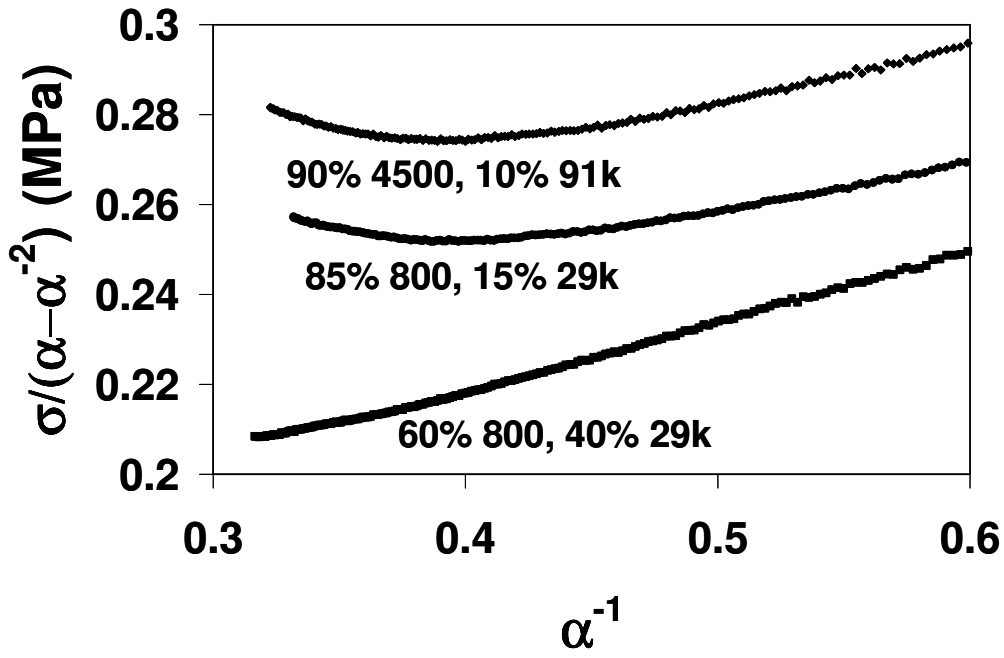

Figure 2.3. Normalized stress vs. inverse elongation for three bimodal networks. Those at 85-90 mol% short chains show a clear upturn in stress, while 60% does not. The curve for 60 mol% 4500, 40 mol% 91,000 shows a lineshape similar to the 60 mol% curve above.

inverse elongation plots in Figure 2.3 enable the determination of the elongation at which the stress rises for a given network. Calculations of the extension of each chain at both the stress upturn and the network rupture are given for some unimodal and bimodal networks in Table 2.2 assuming affine deformation.

The unimodal end-linked networks and the 60 mol% short chain 4500-91,000 M_n network lack an upturn in stress at high extension ratios. However, once the short chain mol% is increased to 90%, the stress does increase rapidly before fracture of the network. For the unimodal networks shown in Table 2.2, the affine deformation calculation of r/r_m predicts that the end-linked chains are at about 30-50% of their maximum extensibilities at fracture.

However, the bimodal networks stretch to much higher elongation ratios. According to this crude calculation, the synergistic effect of the two chain length distributions stretches the short (4500 g/mol) chains to their maximum lengths in the bimodal systems. More reliable estimates of r/r_m have been obtained from simulations and are reported in reference 1. One can also argue against affine deformation of the short chains in the case of low molar fractions of short chains in the bimodal networks because of strong evidence of short chain cluster formation. In these inhomogeneous bimodal networks, the load is not evenly distributed across the network.

It is also informative to take into account the physical phenomena that cause deviations from the ideal rubber elasticity results shown in Figure 2.2. At moderate extension, the deviation can be assumed to be due to the slippage of entanglements, which reduces the stress from its ideal rubber elasticity value. At higher elongation, limited extensibility takes over and the stress starts to increase again. A semi-empirical approach that accounts for both effects is to combine the Mooney-Rivlin representation[12,13] with the inverse Langevin expression for non-Gaussian chain

Table 2.2. Chain extensions for unimodal and bimodal networks

component	mol%	M_n	r_m	α upturn	r upturn	r/r_m upturn	α fracture	r fracture	r/r_m fracture
unimodal	unimodal	4500	163				1.73	85	0.52
		10,000	362				1.87	137	0.38
		21,000	761				2.01	213	0.28
		29,000	1050				3.05	379	0.36
short chain	60 mol%	4500	163				3.43	168	1.03
long chain	40 mol%	91,000	3296				3.43	756	0.23
short chain	90 mol%	4500	163	2.57	126	0.77	3.10	152	0.93
long chain	10 mol%	91,000	3296	2.57	566	0.17	3.10	683	0.21

deformation.[14] One can then write:

$$\sigma = \frac{2C_1}{3} n^{1/2} \left[\mathrm{L}^{-1}\left(\frac{\alpha}{n^{1/2}} \right) - \alpha^{-3/2} \mathrm{L}^{-1}\left(\frac{1}{\alpha^{1/2} n^{1/2}} \right) \right] + \frac{2C_2}{\alpha}\left(\alpha - \alpha^{-2} \right) \qquad (6)$$

where C_1 and C_2 are the Mooney-Rivlin coefficients and L^{-1} is the inverse Langevin expression. This combination would in principle make the equation applicable at low, medium, and high elongation ratios.[15] Equation 6 has been used previously by Meissner[16] on some of Mark et al.'s data on bimodal networks.[7,8] The parameters C_1 and C_2 can be determined from the data up to moderate extension ratios and the values for stress and elongation ratio at the upturn for can be used in equation 6 to determine n. This yields C_1 = 0.104 MPa, C_2 = 0.073 MPa, and n = 105 for 90 mol% short chains in the 4500-91,000 g/mol bimodal network, which corresponds to a PDMS molar mass of about 30,000 g/mol. Therefore, the characteristic elastic strand length at the upturn location is much longer than the short chain length, but much shorter than the long chain component. This supports the idea that at this high concentration of short chains, the network is more homogeneous and the load (stress) is more uniformly distributed.

The experimental data for this bimodal network are shown Figure 2.4 in comparison with the ideal rubber elasticity expression (equation 3), the Mooney-Rivlin equation with C_1 = 0.104 MPa and C_2 = 0.073 MPa , and equation 6 with n = 105. As expected, the ideal rubber elasticity (one parameter fit) gives a good fit only at low extension ratios. The Mooney-Rivlin equation (two parameter fit) gives a good fit up to moderate extension ratios but fails at high extension. Equation 6 with three parameters gives a good fit up to the point where the stress upturn occurs. However, at network rupture the maximum stress is about 5% higher than that predicted by equation 6. Therefore, the upturn itself is not completely described by this equivalent "unimodal" network of 30,000 g/mol elastic chains, but instead by a shorter length

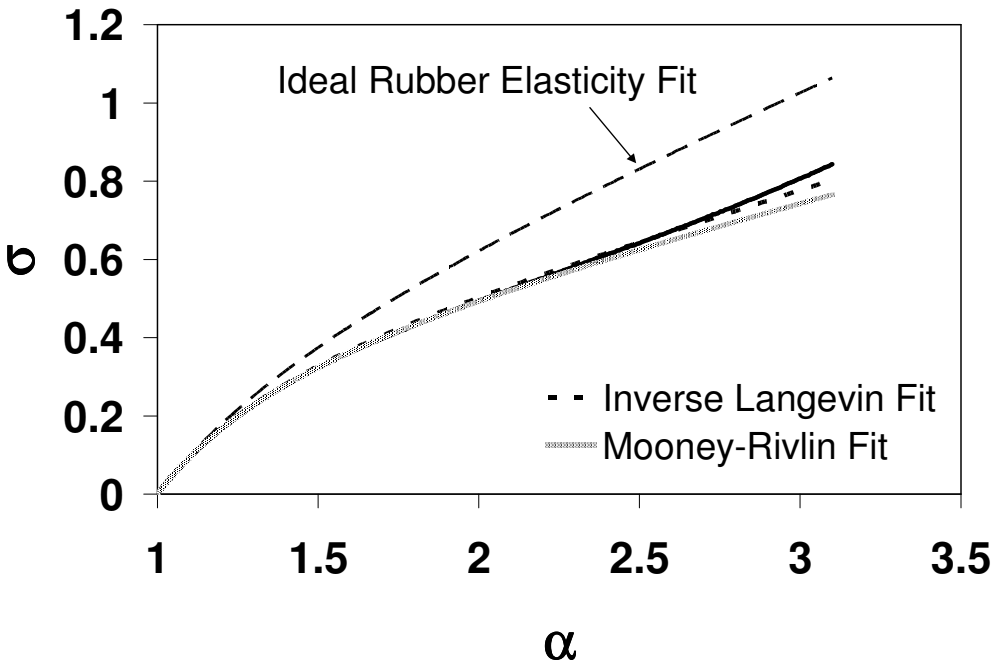

Figure 2.4. Ideal rubber elasticity, inverse Langevin, and Mooney-Rivlin fits to the stress-elongation ratio curve for the 90% 4500 – 10% 91,000 g/mol bimodal network. The experimental data are represented by the solid line. The inverse Langevin equation fit yields a characteristic strand length in between the long and short chain molecular weights.

scale. Nonetheless, as compared to the result of the 60 mol% short chains, this result indicates a better sharing of the load between the two chains of this bimodal network of 90 mol% short chains.

2.4 Comparison to Monte Carlo simulations

2.4.1 Stress-elongation and swelling results

Monte Carlo simulations[1] and experimental results can be compared by obtaining the equivalent molar mass of a simulation bead. This is done by comparing the entanglement molecular weight observed experimentally for PDMS[17] to the number of beads in chains that exhibit entanglements in simulation.[18] A conversion factor of 300 g/mol per LJ bead is obtained.

The short and long chains employed in Monte Carlo studies of bimodal networks were 4 and 69 LJ beads, and 15 and 300 LJ beads. Using the conversion above, these correspond to bimodal networks of 1200-20,700 g/mol and 4500-90,000 g/mol, respectively. The experiments have examined the properties of bimodal networks formed from chain mixtures of 800-21,000 g/mol and 4500-91,000 g/mol, which can be compared to the 4-69 and 15-300 bead simulated systems.

The equivalence between the non-dimensional simulated stress, σ_{sim}, and the experimental dimensional stress, σ_{exp}, is given by:

$$\sigma_{sim} k_b T / \sigma_{LJ}^{\ 3} = \sigma_{\exp} \tag{7}$$

where σ_{LJ} is the Lennard-Jones bead size, and $k_B T$ has its usual meaning. To compare experiments with simulations, the data from the 4500-91,000 g/mol bimodal networks were fit to the 15-300 bead data in the low strain region. After plugging in the pertinent values for k_b and room temperature, the fits yielded an average value of $\sigma_{LJ} \approx$ 7.15 Å. While the pervaded volume of a bead representing 4 PDMS repeat units is

difficult to predict, this value certainly seems reasonable, given that the Si-O bond length is approximately 1.63 Å.[19,20] Figure 2.5 shows the comparison between experimental and simulation results of the stress-elongation ratio data. Although there is some divergence as the networks are stretched to higher extensions, the simulations and experiments show rather good agreement. The largest deviations in the data result from a slight over-prediction of the stress upturn in bimodal networks by the Monte Carlo simulation. Note that while the end points of the experimental curves represent breakage points, the simulation does not have a bond-breaking mechanism. The stress-extension ratio curves for the 4-69 systems showed similar trends as in Figure 2.5 but the simulation data tended to deviate more from the experimental measurement for bimodals with high concentration of short chains. This is likely due to the stiffness of the 4-bead simulated chain and its inability to represent the flexibility of the experimental 800 g/mol chain. This discrepancy is also reflected in the extent of swelling of these networks discussed below.

An interesting result of Figure 2.5 is the similarity between the pure long chain (0% short chain) and 60 mol% short chain curves in the 15-300 bead simulated system. Note that the unimodal long chain network is not shown for the experimental series. At relatively high molecular weights like 91,000, it is impossible to end-link into unimodal networks of "model" quality because of the increased soluble fraction (and therefore increased network defects). However, Figures 2.1a and 2.1b demonstrate that a similar matching is observed in experimental systems as well. This similarity between the 0 and 60 mol% short chain networks is also reflected in the equilibrium swelling of the networks in a solvent.

The PDMS networks were swollen in toluene and the equilibrium volume fraction of the polymer Φ_0 determined using standard gravimetric procedures.[21] The equilibrium swelling calculations in simulation were done with an implicit solvent.

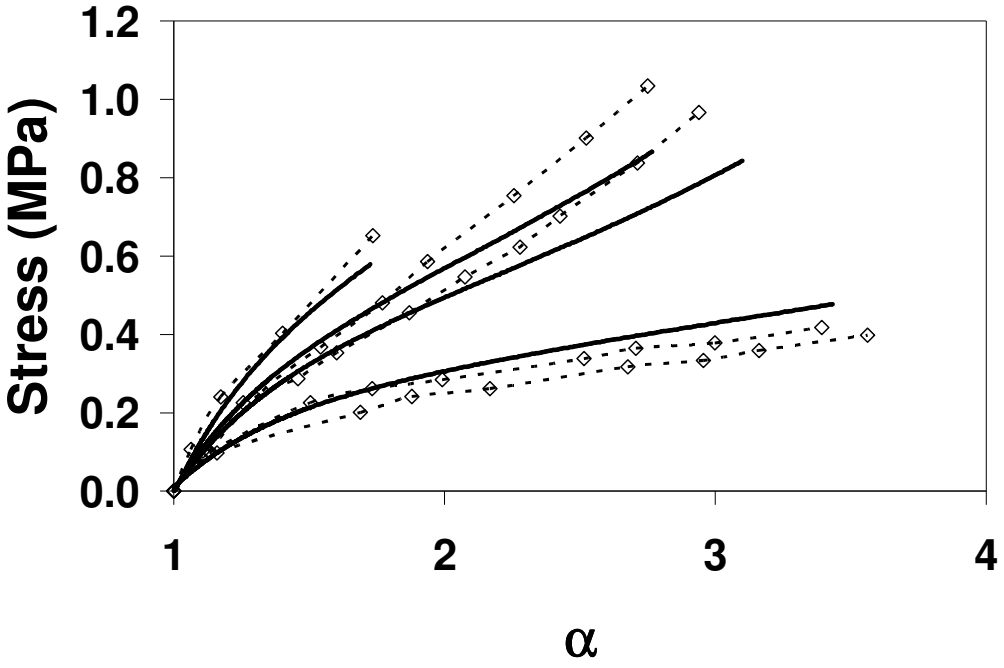

Figure 2.5. Comparison of 4500-91,000 g/mol experimental stress-elongation ratio curves (solid lines) with 15-300 bead networks from simulation (dashed lines). The curves correspond to 100, 95, 90, and 60 mol% short chain with decreasing modulus for both simulation and experiment. The lowest modulus dashed curve is a 300 bead unimodal network.

Since the simulations were not done with an interacting solvent, the simulated networks swell more than the corresponding experimental networks (leading to lower simulated Φ_0 values).[22] Therefore, the data of each simulated series are shifted upwards to match the corresponding experimental Φ_0 values of a unimodal network (4500 and 21,000 g/mol) to allow for simple comparison. The matches to unimodal 4500 and 21,000 g/mol networks were chosen because of limitations of the 4-bead representation of the 800 g/mol chains on one hand and the experimental difficulty of synthesizing low soluble fraction 91,000 g/mol networks on the other hand.

The most striking result of Figure 2.6 is the fact that the 0 and 60 mol% short chain networks have very similar Φ_0 values (i.e. very similar extent of swelling for both experimental data and simulation results). Thus, despite the addition of the short chains (and a cross-link density over 2 times greater in the 15-300 case), the overall response to swelling of each of these networks appears to be quite similar. The simulation data of the 15-300 series match with experimental results of the equivalent experimental bimodal networks quite well (just as for the stress in Figure 2.5). However, the 4-69 networks swell a lot less than the corresponding experimental bimodals at high concentration of short chains after normalizing the data to the experimental unimodal long chain network. This is consistent with the deviations between simulation results and experimental measurements of stress-strain data of these systems mentioned earlier.

2.4.2 Microstructure of bimodal networks

At 60 mol% short chains, the majority of the chain ends in the system come from the short chains, but due to the large difference in chain lengths most of the volume of the system is occupied by the long chains. At this volume fraction of short chains, their concentration is below their overlap concentration. One would then expect a heterogeneous distribution of short chains due to the faster curing kinetics of

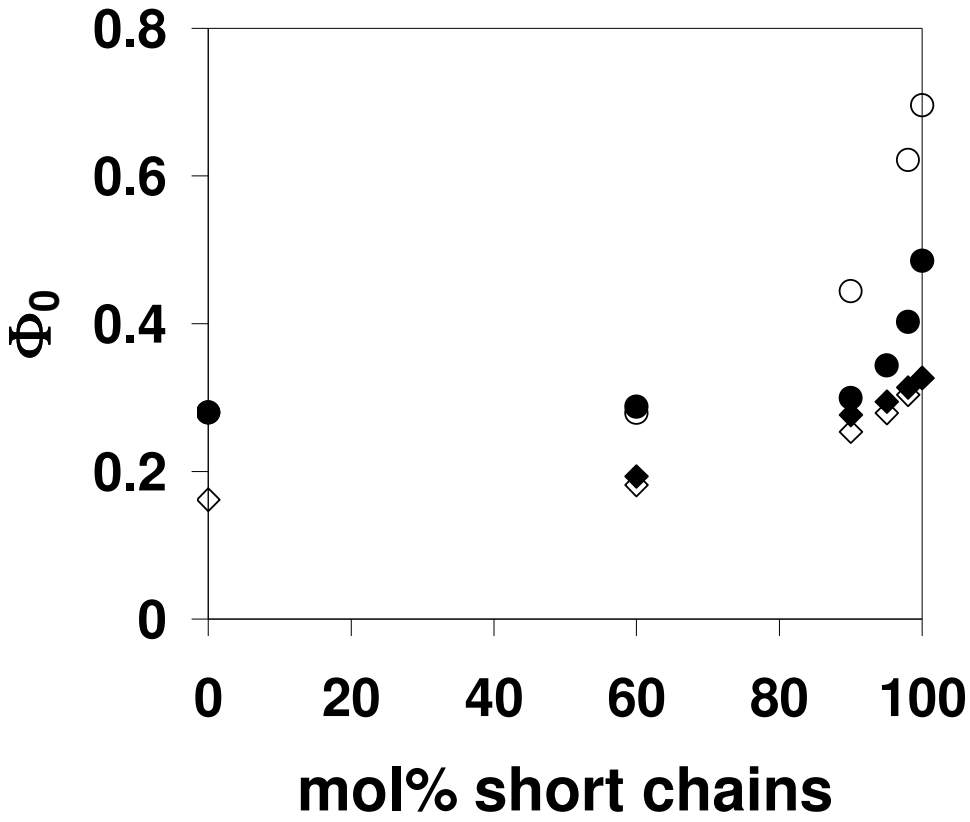

Figure 2.6. Polymer volume fraction when swollen (Φ_0) vs. mol% short chains for the experimental (filled symbols) and simulated (open symbols) networks. Circles represent 4-69 networks and their experimental analog, while diamonds correspond to 15-300. Note the similar degree of swelling for the 0 and 60 mol% short chain networks. The disparity in Φ_0 values is explained in the text.

the much smaller chains. When the short chain concentration is increased, there are many more chain ends available and a percolated network of short chains with interspersed long chains should result.

This phenomenon is illustrated by calculating the number of chains contained in the pervaded volume of one long chain. For a Gaussian PDMS chain, the radius of gyration R_g in Å is:

$$R_g = C_\infty nl^2/6 = 5.2\times(M_n/37)\times 1.64^2/6 = 0.251 M_n^{1/2} \quad (8)$$

The pervaded volume of a chain V_{chain} can be calculated from the chain R_g:

$$V_{chain} = 4/3\pi(R_g)^3 \quad (9)$$

Finally, the number of chains $\Re$ contained in the volume occupied by one long chain is calculated from:

$$\Re = (\rho A/M_n)\times V_{chain} = .0387 M_n^{1/2} \quad (10)$$

This equation uses Avagadro's number A and PDMS mass density $\rho = 0.97$ g/cm^3. Therefore, while a unimodal long chain network in the 4-69 series would contain approximately 5.5 total chains in its pervaded volume, it will clearly contain many more short chains in bimodal mixtures. This is illustrated in Figure 2.7 for a bimodal mixture of Gaussian chains with a molar mass ratio of 18. These cartoons show that the short chains begin to overlap as their concentration increases. The degree of clustering in the network is further demonstrated in computer simulation by comparing the computer-simulated intermolecular pair distribution function [g(r)] of the short chain centers of mass from before the cross-linking reaction to after the reaction is complete.[1] These simulations demonstrate that the 60 mol % short chains are

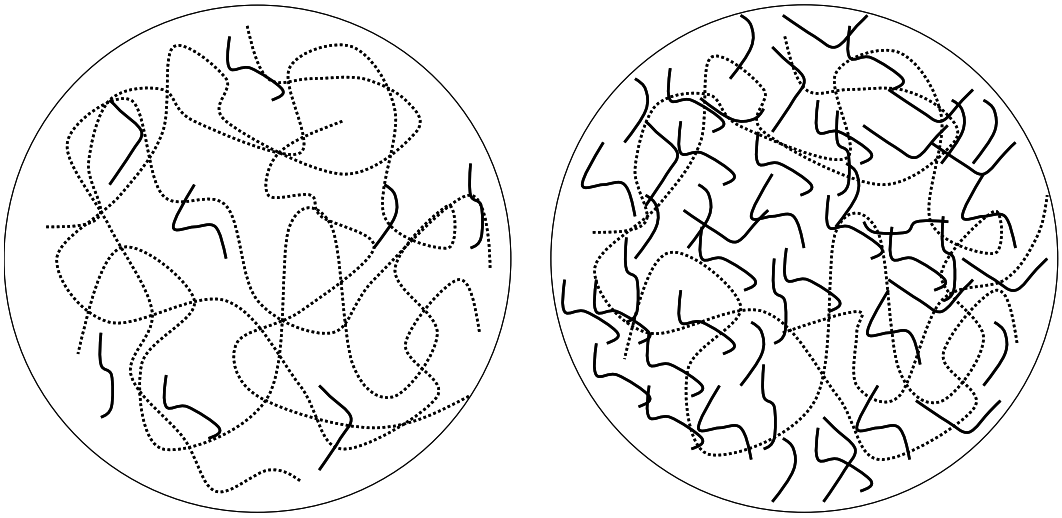

Figure 2.7. Sketches of short chains (solid) and long chains (dashed) contained in the pervaded volume of a long chain of a bimodal mixture with molar mass ratio of 18.

segregated into clusters, while the effect is much less pronounced for 90 and 95 mol % short chain networks. This supports the representation of a bimodal network with high short chain content as a network with a relatively homogeneous distribution of short chains throughout the network.

A microstructure of heterogeneous domains of the short chains at 60 mol% helps to explain the results of Figure 2.6. While the cross-link density is markedly increased when moving from 0 to 60 mol% short chains, macroscopic swelling of the networks in experiments and in simulations is similar. Swelling within these densely cross-linked clusters that occupy only 7% of the total volume (Table 2.1) is limited, and therefore the overall swelling is almost solely dictated by the changes in the microstructure of the long chains. This seems consistent with the results of Sommer and Lay,[23] who have simulated the swelling of bimodal networks using the bond-fluctuation model. They find that the global swelling ratio is caused by the unfolding of substructures of interconnected short chains linked by long chains that unfold in non-affine deformation.

As demonstrated by MC simulations,[1] the clustering phenomenon appears to be much more important at lower mol% short chains. Furthermore, as reported in Figures 2.5 and 2.6, there is little to no enhancement in the mechanical properties of these dilute short chain bimodal networks. Thus, it appears that these small, heterogeneous clusters of short chains do little to reinforce the elastomers. An examination of past experimental works that demonstrated heterogeneities and clustering of short chains shows that they were carried out at relatively low short chain concentrations. For instance, Stein et al.[24] performed SANS measurements on PTHF bimodal networks with 50 and 70 mol% deuterated short chains of molar mass 1000 g/mol with hydrogenated long chains of molar mass 10,000 g/mol. Hecht et al.[25] also reported short chain aggregation in a bimodal network of 68 mol% short chains.

Additionally, these authors did not report the mechanical properties of these networks. Given the findings reported here, it appears that these clustered short chain networks would not have demonstrated enhanced mechanical properties.

It is interesting to note that the bimodal networks with the best experimentally determined ultimate properties contain an amount of short chains around their overlap concentration. For example, one can calculate the point at which the short chains begin to overlap in the 15-300 series using the expression for the radius of gyration R_g of an ideal chain. For N = 15, overlap occurs at short chain volume fraction 0.47, which corresponds to 95 mol% in this system. Examination of Table 2.1 shows that for a corresponding 4500-91,000 M_n system, 90 and 95 mol% short chain networks give optimum toughness. Also note that the simulation results[1] suggest that some degree of clustering may be present even at these high concentrations of short chains. This is also supported by the presence of bimodality in the distribution of residual dipole-dipole coupling as measured by multiple-quantum NMR for bimodal systems of 780–47,200 g/mol.[26] It thus appears that this intermediate structure between prevalent cluster formation at low concentration of short chains and homogeneous distribution at very high concentration leads to the best ultimate mechanical properties of bimodal networks.

2.5 Comparison to "equivalent" unimodal networks

While Table 2.1 and Figure 2.1 show improved mechanical properties in bimodal networks when compared to the corresponding pure short chain and long chain networks, it is perhaps more appropriate to weigh their performance against more similar unimodal networks. Such a comparison requires unimodal and bimodal networks with similar cross-link densities. For networks with equivalent values of *r*, defined following equation 2, similar cross-link density also means similar average

molar mass. M_{avg} of a bimodal network is easily calculated from the molar fractions of the short and long chains and their respective molar masses:

$$M_{avg} = x_{short} \times M_{n,short} + x_{long} \times M_{n,long} \tag{11}$$

Comparisons of a unimodal network to a bimodal network of similar average molar mass and cross-link density are shown in Table 2.3 and Figure 2.8. From the figure, it is easily seen that the two networks have almost identical stress-strain behavior in the region $\alpha < 2$. However, whereas the unimodal network broke before it reached twice its initial length, the bimodal network stretched much farther before fracture, exhibits a stress upturn as discussed earlier, and shows greatly improved toughness and ultimate stress (Table 2.3). Thus, it is clear that the synergistic effect gained via bimodality manifests itself in improved high-strain properties rather than equilibrium modulus.

2.6 Conclusions

Mechanical and swelling properties of PDMS bimodal networks were obtained and compared with Monte Carlo simulations. While improvements in mechanical properties were previously demonstrated with non-Gaussian chains short chains on order of 1000 g/mol, it is demonstrated that networks with Gaussian short chains in their unperturbed states also show enhancement in properties. The two prevalent hypotheses for the nature of the improvement in ultimate mechanical properties were examined. While short chains will cluster at lower mol% of short chains (typically below their overlap concentration), these networks do not show increased toughness or upturns in stress. Instead, it appears that the finite extensibility of the short chains at high strain ratios plays a significant role in ultimate property improvement and occurs only at fairly high molar concentrations of short chains where the short chains are

Table 2.3. Bimodal vs. unimodal network properties

M_n of short chains	M_n of long chains	mol%, mass% of short chains	M_{avg}	E (MPa)	Q	Cross-link $\rho \times 10^3$ (mol xlink / g PDMS)	Toughness (MPa)	Ultimate Stress (MPa)
4500	91,000	95, 48	8,830	1.09 ± 0.03	3.40	0.034	0.79 ± 0.09	0.82 ± 0.04
10,000	(unimodal)	100	10,000	1.04 ± 0.03	3.16	0.030	0.20 ± 0.06	0.44 ± 0.06

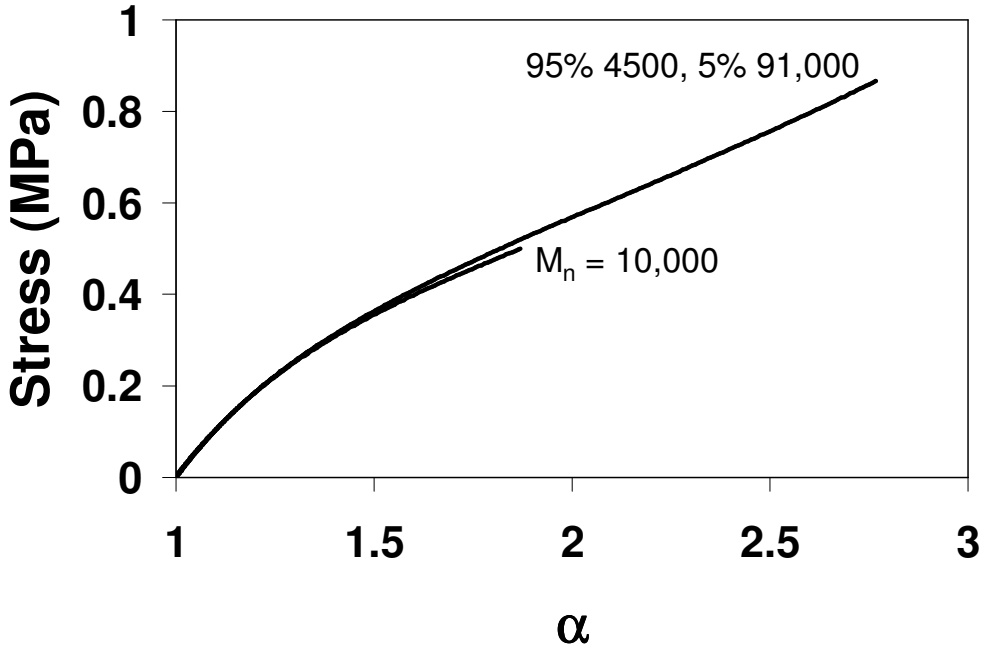

Figure 2.8. Stress-elongation ratio curves for a 4500-91,000 M_n bimodal network and an "equivalent" unimodal network of 10,000 g/mol.

intimately coupled to the long chains and the load is distributed among both types of chains. The best performing bimodals in terms of stored strain-energy at break may still have some residual short-chain clusters that are shielded by the long chains from stress overload. This allows the network to sustain high elongation before the short chains are stressed to their breaking point.

REFERENCES

1. Genesky, G. D.; Aguilera-Mercado, B. M.; Bhawe, D. M.; Escobedo, F. A.; Cohen, C. *Macromolecules* **2008**, *41*, 8231-8241.

2. Lee, C. L.; Johannson, O. K. *J. Polym. Sci. Pol. Chem.* **1976**, *14*, 729-742.

3. Lee, C. L.; Marko, O. W.; Johannson, O. K. *J. Polym. Sci. Pol. Chem.* **1976**, *14*, 743-758.

4. Lapp, A.; Herz, J.; Strazielle, C. *Makromolekul. Chem.* **1985**, *186*, 1919-1934.

5. Patel, S. K.; Malone, S.; Cohen, C.; Gillmor, J.; Colby, R. *Macromolecules* **1992**, *25*, 5241-5251.

6. Takahashi, H.; Shibyama, M.; Fujisawa, H.; Noruma, S. *Macromolecules* **1995**, *28*, 8824-8828.

7. Andrady, A. L.; Llorente, M. A.; Mark, J. E. *J. Chem. Phys.* **1980**, *72*, 2282-2290.

8. Llorente, M. A.; Andrady, A. L.; Mark, J. E. *J. Polym. Sci. Pol. Phys.* **1981**, *19*, 621-630.

9. Mark, J. E.; Tang, M. -Y. *J. Polym. Sci. Pol. Phys.* **1984**, *22*, 1849-1855.

10. Flory, P. J. *Statistical Mechanics of Chain Molecules*; Interscience: New York, 1969.

11. Flory, P. J. *Principles of Polymer Chemistry*; Cornell University Press: Ithaca, NY, 1953.

12. Mooney, M. *J. Appl. Phys.* **1940**, *11*, 582-592.

13. Rivlin, R. S. *Philos. Trans. R. Soc.* **1948**, *A241*, 379-397.

14. Treloar, L. R. G. *The Physics of Rubber Elasticity, 3rd Ed.*; Clarendon Press: Oxford, 2005.

15. Morris, M. C. *J. Appl. Polym. Sci.* **1964**, *8*, 545-553.

16. Meissner, B. *Polymer* **2000**, *41*, 7827-7841.

17. Mark, J. E. In *Physical Properties of Polymers, 2nd ed.;* American Chemical Society: Washington, DC, 1993.

18. Putz, M.; Kremer, K.; Grest, G. S. *Europhys. Lett.* **2000**, *49*, 735-741.

19. Sides, S. W.; Curro, J.; Grest, G. S.; Stevens, M. J.; Soddemann, T.; Habenschuss, A.; Londono, J. D. *Macromolecules* **2002**, *35*, 6455-6465.

20. Lide, D. R. In *CRC Handbook of Chemistry and Physics, 87th ed.*; CRC Press: Boca Raton, FL, 2006; p. **9**-46.

21. Weiss, P.; Herz, J.; Rempp, P. *Makromolekul. Chem.* **1970**, *135*, 249-261.

22. Chen, Z.; Cohen, C.; Escobedo, F. A. *Macromolecules* **2002**, *35*, 3296-3305.

23. Sommer, J. -U.; Lay, S. *Macromolecules* **2002**, *35*, 9832-9843.

24. Wu, W. L.; Jong, L.; Hanyu, A.; Coyne, L .D.; Stein, R. S. *Macromolecules* **1990**, *23*, 351-353.

25. Hecht, A. -M.; Horkay, F.; Geissler, E. *J. Phys. Chem. B* **2001**, *105*, 5637-5642.

26. Saalwächter, K.; Ziegler, P.; Spyckerelle, O.; Haidar, B.; Vidal, A.; Sommer, J. -U. *J. Chem. Phys.* **2003**, *119*, 3468-3482.

CHAPTER 3

MECHANICAL PROPERTIES OF TRIMODAL NETWORKS AND BIMODAL NETWORKS WITH WIDELY SEPARATED PRECURSOR MOLAR MASSES IN UNIAXIAL EXTENSION*

3.1 Introduction

As detailed in Chapter 2, the stress upturn at high elongations in bimodal networks has often been attributed to an increased loading on the short chains, whose stress increases as they approach their limited extensibilities.[1-4] Even though they can sustain high stresses, optimal bimodal networks can still be stretched to large elongations before fracture due to the ductility afforded by the long chains. This proposed mechanism for reinforcement suggests that elastomers with three distinct precursor molar mass distributions could provide a further advancement in mechanical properties. Such trimodal networks would have chemically-identical short, medium, and long chains cross-linked into the same structure. Addition of the medium precursor molar mass would add a more flexible component than the brittle short chains, while still contributing to the stress upturn as the network was stretched to increased elongation ratios.

Despite the potential of trimodal networks, very few studies of these types of materials have been published. Experimental investigations of trimodal polydimethylsiloxane (PDMS) networks revealed a disappointing stress-strain performance, but the elastomers studied were quite brittle since the long chain molar mass was only 18000 g/mol.[5] However, theoretical calculations have indicated that trimodal networks can outperform unimodal or bimodal elastomers since they can

store an increased amount of elastic free energy before the network chains are stretched to their maximum extensibilities.[6] These calculations revealed that trimodal networks would be particularly attractive if the long chain was quite long (~100,000 g/mol) and the three precursor molar masses were widely separated (each by at least a factor of 10). More recently, multiple quantum (MQ) NMR experiments have shown that filled trimodal PDMS networks can show three distributions of residual dipolar couplings when in the unstrained state,[7] indicating three domains of residual chain segment order. Although the authors attribute the highest frequency coupling to a fitting anomaly, these results appear to correspond to MQ-NMR studies of bimodal networks that found a distinct residual dipolar coupling from both the short chains and the long chains.[8-10] As multiple chain segment orientations in ^{2}H-NMR studies of bimodal networks can be related to their improved mechanical properties (Chapter 6), trimodal networks with two or three distributions of segment order should be capable of absorbing a high energy before fracture.

In this chapter, PDMS multimodal network properties are investigated through uniaxial extension (simple extension) testing. Mechanical properties for unimodal, bimodal, and trimodal networks with similar molar mass M_c between effective cross-links are compared to assess the degree of improvement brought about by increasing the number of molar mass distributions in the elastomers. A mechanism for reinforcement in bimodal and trimodal networks is proposed to link the network microstructure to the ultimate mechanical properties.

3.2 Experimental Procedures

3.2.1 Elastomer synthesis and characterization

All PDMS chains and networks were synthesized via methods detailed in Section 2.2. Gel permeation chromatography (GPC) was used to determine the

number-average molar mass of chains, whose polydispersity indices were found to be 1.43 or lower.

It is difficult to perform a systematic series of experiments on trimodal networks due to the large number of design variables to account for. Namely, three molar masses and two independent molar fractions can be adjusted. Therefore, trimodal networks with varying amounts of short-medium-long precursor chains of 800-8500-91,000 g/mol were synthesized since these precursor molar masses are similar to those predicted to have enhanced toughness by Erman and Mark.[6] Bimodal networks composed of 800-91,000 g/mol chains were also examined.

An optimal amount of tetrakis(dimethylsiloxy)silane cross-linker was used in each sample to produce networks with as few defects as possible. This is achieved in end-linked unimodal PDMS networks at a ratio of cross-linking arms to polymer chain ends r of 1.7 for M_n greater than about 10000 g/mol.[11] Since optimal r is smaller for networks of shorter precursor molar masses,[12] the ideal ratio is not obvious for bimodal or trimodal networks containing chains of widely varying precursor molar mass. Therefore, r was varied for selected 800-91000 g/mol bimodal and 800-8500-91000 g/mol trimodal networks. This revealed that $r = 1.7$ produced model networks with the lowest possible soluble fraction w_{sol} and mass swell in toluene Q.

3.2.2 Uniaxial extension tests

Samples of uniform width and thickness for simple extension tests were punched out of the cured PDMS networks. The procedures for uniaxial extension detailed in Section 2.2.3 were also utilized in these experiments. Average molar mass between effective cross-links M_c was determined from:

$$M_c = 3\rho RT/E \tag{1}$$

Here, ρ is the density of the polymer, R is the gas constant, and T is absolute

temperature. Young's modulus E, ultimate stress σ_{max}, elongation ratio at fracture α_c, and toughness were recorded on 4-6 samples for each network formulation tested.

3.3 Results and Discussion

Mechanical properties for all the networks tested are displayed in Table 3.1. While the shape of the stress-strain curve was reproducible from sample to sample, each test piece broke at a slightly different α. Therefore, the average and standard deviation for 4-6 test pieces on each composition studied are reported in Table 3.1. For clarity, full stress-strain curves (Figures 3.1a, 3.2a, 3.3a) are displayed for only the sample from each composition which reached the highest α before fracturing. Each series of networks has been assigned a name based on the number of molar mass distributions included and the mol % of short chains in the network. For instance, the 800-8500-91000 g/mol trimodal network with 45-45-10 mol % of each respective chain length will be referred to as T-45. Unimodal networks are distinguished by the molar mass of their precursor chains (i.e. U-4500), while the 4500-91000 g/mol bimodal series (see also Chapter 2) is referred to in the style B-4500-short chain mol%.

Stress-elongation ratio curves for a series of trimodal networks with increasing amounts of 91000 g/mol chains are displayed in Figure 3.1a. The concentration of the 8500 g/mol chains was held constant at 20 mol % in this series to assess the effect of adding long chains at the expense of 800 g/mol chains. Not surprisingly, the elastic modulus decreases a great deal as long chains are added. As demonstrated in Table 3.1, B-80 (a bimodal network containing only 800 and 8500 g/mol chains) has mechanical properties that are almost identical to the brittle 800 g/mol unimodal network. Addition of 91000 g/mol chains to the system greatly increases the ductility of the trimodal networks, such that T-70 can be stretched to α_c nearly three times that

Table 3.1 – Network properties - uniaxial extension

Unimodal networks

g/mol precursor chains	Nomenclature	E (MPa)	Q	w_{sol} (mass %)	Toughness (MPa)	σ_{max} (MPa)	α_c	M_c (g/mol)
800+	U-800	2.72 ± 0.11	2.06	0.90	0.09 ± 0.02	0.59 ± 0.10	1.21 ± 0.09	2700
4500+	U-4500	1.34 ± 0.06	3.06	0.93	0.24 ± 0.01	0.57 ± 0.02	1.71 ± 0.02	5400
10000+	U-10000	1.04 ± 0.03	3.16	0.34	0.20 ± 0.06	0.44 ± 0.06	1.74 ± 0.13	6900
16500	U-16500	0.83 ± 0.02	3.94	1.01	0.39 ± 0.06	0.48 ± 0.01	2.27 ± 0.18	8700
29000+	U-29000	0.74 ± 0.04	3.75	0.78	0.53 ± 0.12	0.48 ± 0.04	2.71 ± 0.24	9700
45000	U-45000	0.57 ± 0.05	4.87	0.81	0.58 ± 0.31	0.34 ± 0.05	3.41 ± 0.93	12700

Bimodal networks 800-91000 g/mol

mol % short chains (mass%)	Nomenclature	E (MPa)	Q	w_{sol} (mass %)	Toughness (MPa)	σ_{max} (MPa)	α_c	M_c (g/mol)
60 (1)	B-60	0.70 ± 0.01	4.49	0.64	0.42 ± 0.20	0.40 ± 0.06	2.56 ± 0.52	10300
95 (14)	B-95	0.72 ± 0.01	4.14	1.99	0.77 ± 0.23	0.68 ± 0.15	3.09 ± 0.32	10000
98 (30)	B-98	1.45 ± 0.02	2.63	0.48	0.89 ± 0.12	1.69 ± 0.15	2.21 ± 0.07	5000

Bimodal networks 4500-91000 g/mol+

mol % short chains (mass%)	Nomenclature	E (MPa)	Q	w_{sol} (mass %)	Toughness (MPa)	σ_{max} (MPa)	α_c	M_c (g/mol)
60 (7)	B-4500-60	0.64 ± 0.03	5.17	3.74	0.64 ± 0.10	0.45 ± 0.02	3.13 ± 0.23	11300
90 (31)	B-4500-90	0.94 ± 0.01	3.62	0.26	0.90 ± 0.09	0.79 ± 0.04	2.93 ± 0.12	7700
95 (48)	B-4500-95	1.09 ± 0.03	3.40	0.22	0.79 ± 0.09	0.82 ± 0.04	2.64 ± 0.11	6600
98 (71)	B-4500-98	1.24 ± 0.04	3.06	1.00	0.28 ± 0.09	0.57 ± 0.07	1.80 ± 0.16	5800

+ Reported in Chapter 2

Table 3.1 (Continued)
Trimodal networks 800-8500-91000 g/mol

mol % short, medium chains (mass %)	Nomenclature	E (MPa)	Q	w_{sol} (mass %)	Toughness (MPa)	σ_{max} (MPa)	α_c	M_c (g/mol)
80,20 (27,73)	B-80	2.75 ± 0.02	2.26	0.12	0.09 ± 0.03	0.60 ± 0.09	1.27 ± 0.05	2600
79,20 (19,53)	T-79	1.08 ± 0.02	3.35	0.81	0.41 ± 0.13	0.65 ± 0.10	2.09 ± 0.18	6700
78,20 (15,41)	T-78	0.89 ± 0.01	3.64	1.82	0.49 ± 0.16	0.61 ± 0.10	2.37 ± 0.28	8100
77,20 (12,34)	T-77	0.79 ± 0.01	3.81	0.98	0.75 ± 0.28	0.63 ± 0.14	2.92 ± 0.44	9200
70,20 (5,15)	T-70	0.60 ± 0.01	4.70	1.69	1.00 ± 0.29	0.56 ± 0.08	3.89 ± 0.53	12000
80,10 (6,8)	T-80	0.60 ± 0.03	4.67	1.11	0.82 ± 0.43	0.52 ± 0.14	3.48 ± 0.76	12100
65-25 (4,18)	T-65	0.77 ± 0.05	4.12	0.93	1.34 ± 0.56	0.79 ± 0.19	3.88 ± 0.84	9400
45,45 (3,29)	T-45	0.95 ± 0.02	3.70	0.18	1.62 ± 0.47	1.11 ± 0.25	3.74 ± 0.37	7600

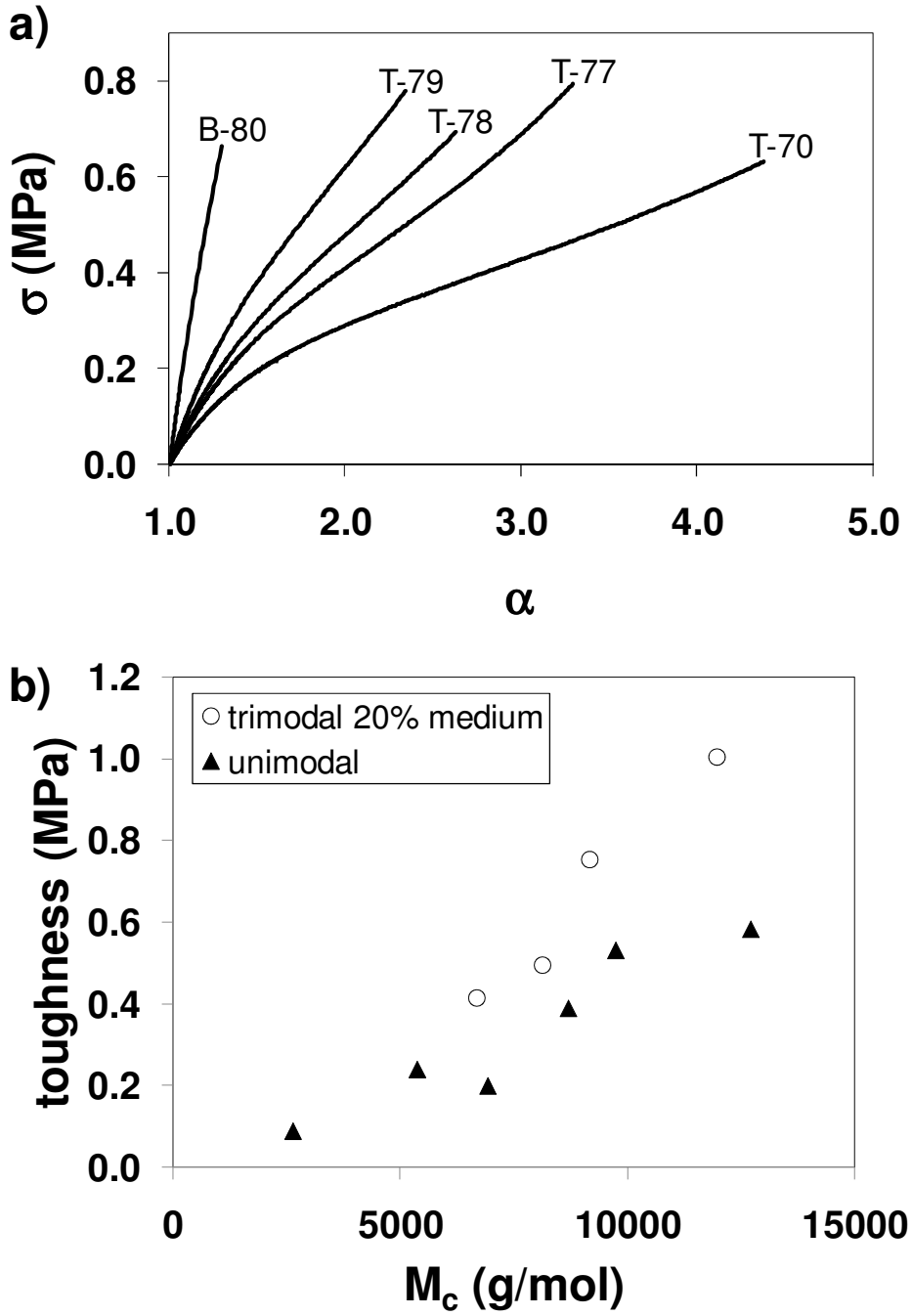

Figure 3.1. a) Stress-elongation ratio curves and b) average toughness vs. M_c plots for trimodal networks with 20 mol % medium (8500 g/mol) chains. The networks are more extensible and show a stress upturn at high strain as the long chain content is increased. The toughness value of B-80 is coincident with U-800 at M_c ~ 2700 g/mol.

of T-79. The networks with higher long chain content also show an upturn in stress at high α. Figure 3.1a and Table 3.1 reveal that each of these trimodal elastomers break at σ_{max} values that are essentially identical. Since it breaks at similar σ_{max} as the other trimodal networks but can be extended to higher α_c, T-70 will absorb the most energy before rupture. Average toughness vs. M_c data are displayed in Figure 3.1b for this trimodal series and unimodal networks of varying precursor M_n. The lower M_c trimodal networks only show a moderate increase in toughness over unimodal networks with similar low-strain elastic modulus (or similar M_c, equation 1). However, the toughness values for each series begin to diverge in the more ductile networks – T-70 (M_c = 12000) is clearly superior to U-45000 (M_c = 12700). Therefore, networks with higher long chain content appear to be more likely to display improved ultimate properties, showing qualitative agreement with the predictions of reference 6.

Taking a cue from T-70, the next series of trimodal networks was synthesized with a constant 10 mol % of 91000 g/mol chains and varying short and medium chain contributions. Since each molar mass is so widely separated in these trimodal networks, 10 mol % long chains equates to 68-86 mass % in the compositions tested (Table 3.1). Therefore, these networks can be classified as high long-chain content systems. Representative stress-strain curves are shown in Figure 3.2a. The networks display a relatively high elastic modulus while still maintaining extraordinary ductility. T-45 (M_c = 7600) in particular exhibits a noticeable upturn in stress that persists for quite some time before fracture. Therefore, it is not surprising that the toughness values for this trimodal system are far superior to the end-linked unimodal networks (Figure 3.2b). In contrast to Figure 3.1b, the higher toughness values for the 10 mol % 91000 g/mol systems are found for networks with lower M_c. This is likely due to the fact that each of the trimodal networks in Figure 3.2 contains a high mass

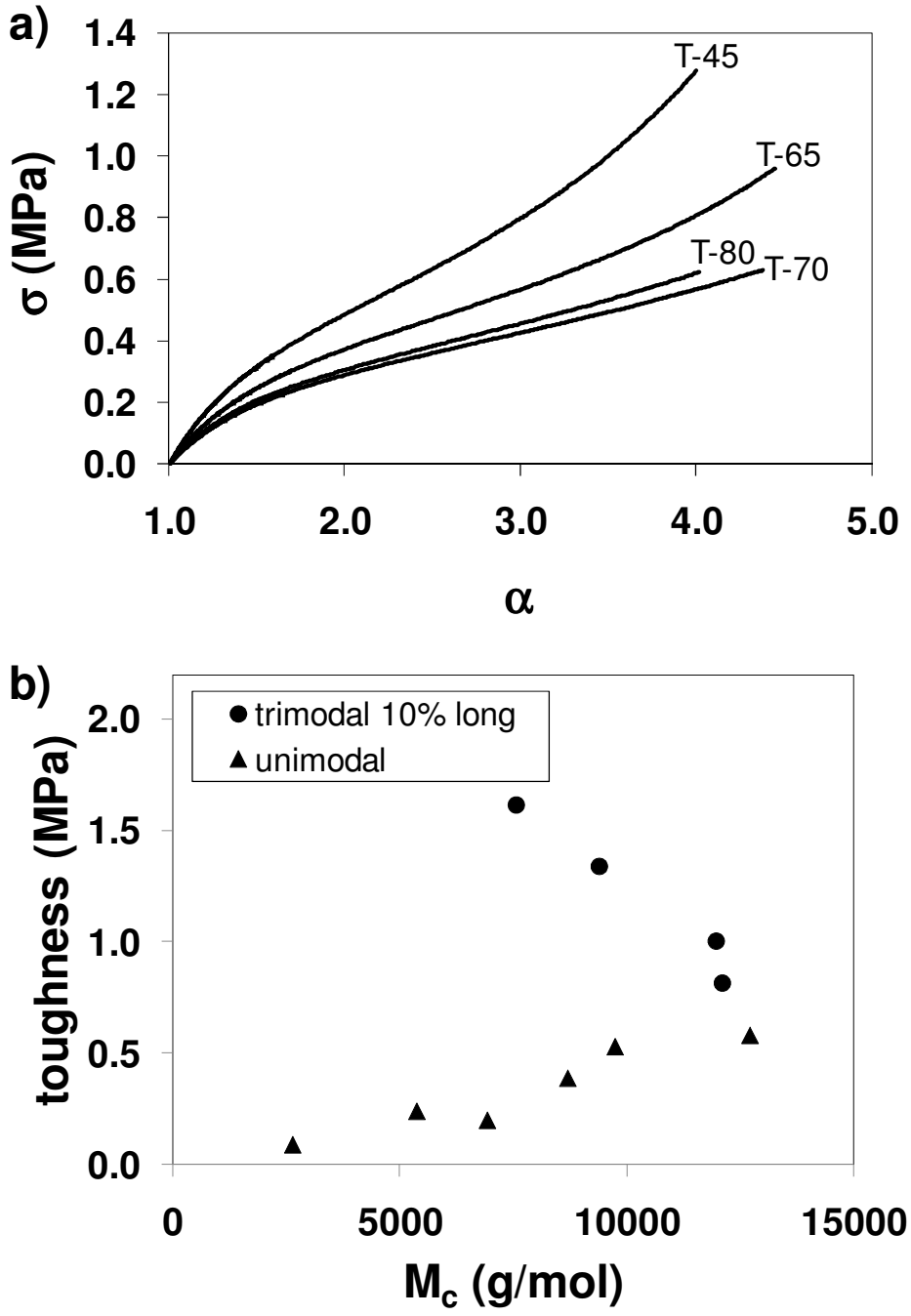

Figure 3.2. a) Stress-elongation ratio curves and b) average toughness vs. M_c plots for trimodal networks with 10 mol % long (91000 g/mol) chains. T-45 and T-65 in particulary show outstanding mechanical properties when compared to unimodal networks.

fraction of long chains. Therefore, all these networks are very ductile and have similar α_c, but the varying relative contributions from the short and medium molar mass chains cause σ_{max} and toughness to be greatest for T-45.

To establish that these trimodal networks show enhanced mechanical properties, they must also be compared to analogous bimodal networks. The properties of a bimodal 4500-91000 g/mol system were reported in Chapter 2. These networks contain short chains that have essentially the average molar mass of the short and medium chains employed in the trimodal networks. While this bimodal system showed improvement over unimodal networks, Table 3.1 reveals trimodal networks with 10 mol % long chains to have superior toughness. Bimodal networks with very widely separated molar mass distributions were also tested (800-91000 g/mol). The stress-elongation ratio curves and toughness vs. M_c results are shown in Figure 3.3. B-60 and B-95 have a very similar elastic modulus, which is likely a consequence of the extreme separation in precursor M_n used to prepare each network. B-60 and B-95 contain only 1 and 14 mass % of the short chain, respectively, so the elastic response is dominated by the long chains. B-95 does receive enough of a contribution from the 800 g/mol chains at high elongation to show an upturn in stress, however. The Young's modulus E increases as the networks are further loaded with short chains, as the B-98 results demonstrate. This network is not as ductile as B-60 or B-95, but it shows an exceptional stress upturn and thus reaches a higher σ_{max} than any other sample examined in this study (Table 3.1). As seen in Figure 3.3b, B-98 absorbs a large amount of energy before fracture for an end-linked PDMS network with a relatively high modulus.

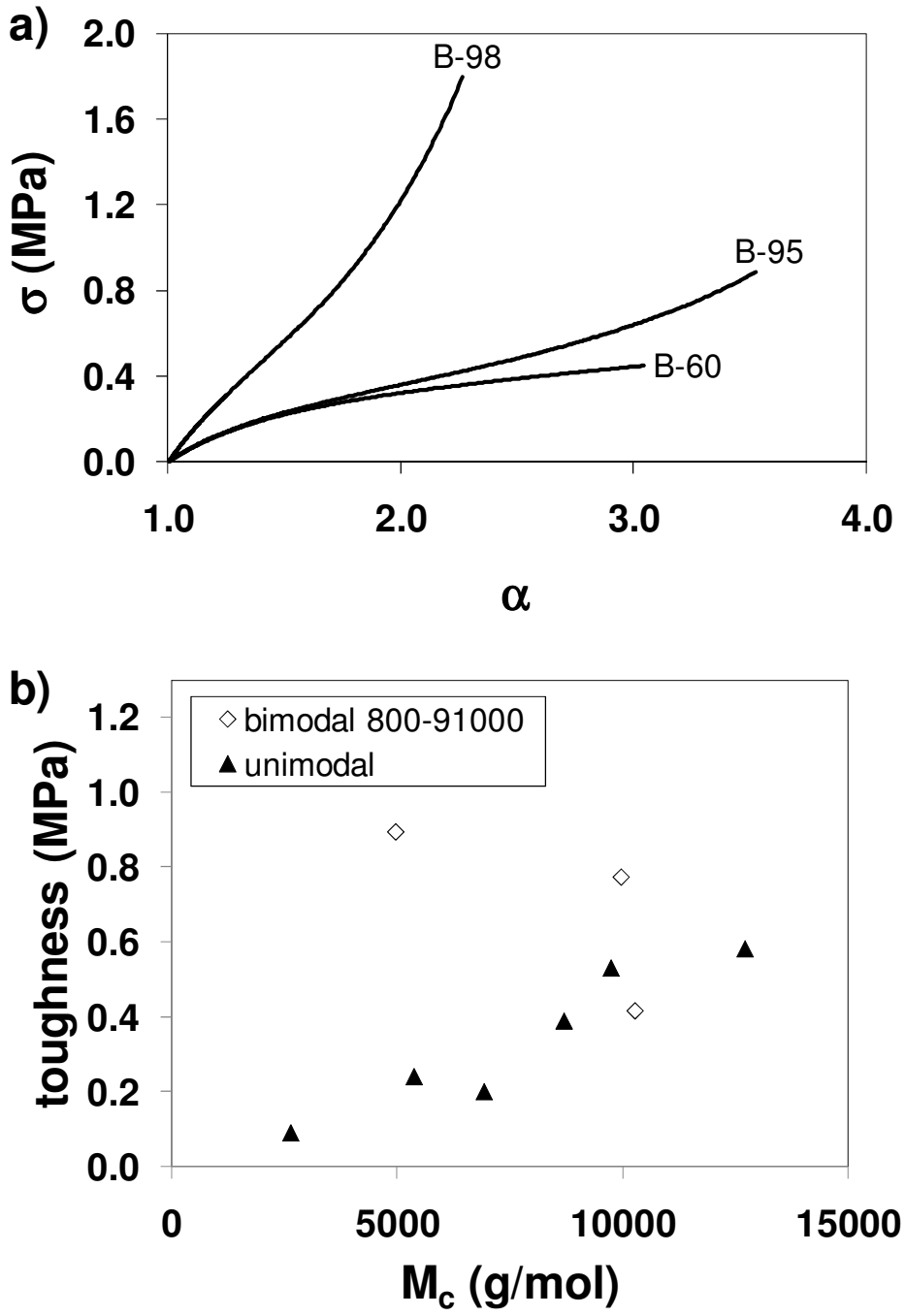

Figure 3.3. a) Stress-elongation ratio curves and b) average toughness vs. M_c plots for bimodal networks with very widely separated precursor chains (800-91000 g/mol). B-98 shows a huge stress upturn and sustains a high stress before fracture.

Stress data for B-98, T-45, and U-29000 are each normalized by E and plotted on a log-log plot vs. α in Figure 3.4. This allows for comparison to the model of ideal rubber elasticity, which can be written as:

$$\sigma/E = \left(\alpha - \alpha^{-2}\right)/3 \tag{2}$$

While each curve follows the ideal model at low strains, T-45 and U-29000 drop below this prediction at moderate elongation ratios. This typical behavior is attributed to "slippage" in chain interactions (entanglements) as the network is deformed (modeled by the C_2 term in the Mooney-Rivlin equation). At high strains, limited extensibility of the shorter chains in T-45 leads to an upturn in stress and the curve again reaches the ideal rubber prediction before fracture. B-98 is an interesting case since it never falls below the theoretical prediction, such that its stress-strain performance is devoid of a C_2 term. This might suggest that this network has very few chain entanglements; however, this seems impossible since 70 mass % of the chains in the system are of the "very long" 91000 g/mol variety (Table 3.1). Therefore, it appears that the 800 g/mol chains approach the limit of their extensibility at low α. The increase in stress resulting from deformation of the short chains is strong enough to offset the C_2 damping of the stress-strain curve due to the long chain entanglements.

Examination of Table 3.1 makes obvious the importance of the ductility provided by the long chains on the mechanical properties of B-98. U-800 has a high modulus but is very brittle (α_c = 1.21 +/- 0.09), while B-98 can be stretched to about 6 times further on average (α_c = 2.21 +/- 0.07). As detailed in Chapter 2, bimodal networks have optimal ultimate properties when the short chains are approaching their overlap concentration. At such concentrations, the short chains can form an interconnected matrix that spans the entire network, but the long chains are still concentrated enough such that there are "pockets" of long chains that provide

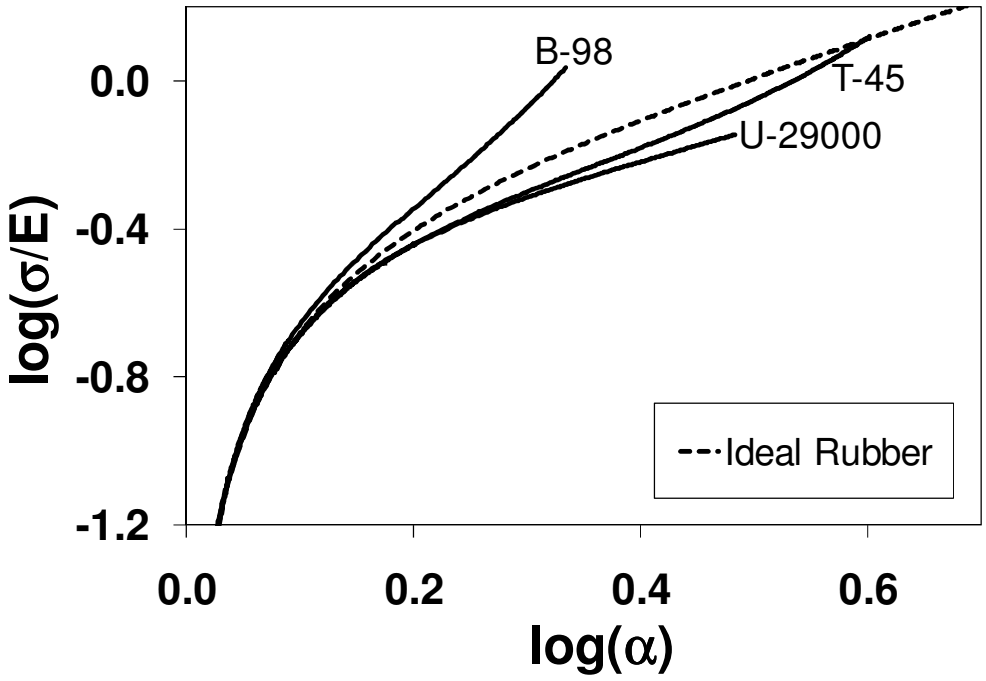

Figure 3.4. Unimodal and multiomodal networks compared to ideal rubber elasticity. Bimodal network B-98 does not show Mooney-Rivlin behavior since it never dips below the ideal rubber prediction.

ductility.[13,14] For a given applied strain, the short chains are more aligned than the long chains, causing the increase in σ before fracture. While there is no clear-cut way to calculate overlap concentration for the very short and non-Gaussian 800 g/mol chains, a similar microstructure appears likely for B-98 given its mechanical properties.

However, it can be instructive to calculate overlap concentrations using the R_g of an ideal linear chain in other bimodal and trimodal networks. For instance, the overlap concentration of 4500 g/mol chains is 0.47, which is almost identical to the mass % of short chains in B-4500-95 (Chapter 2). In the 4500-91000 g/mol bimodal series, B-4500-90 and B-4500-95 have the highest toughness values. The overlap concentration for the medium (8500 g/mol) chains in the trimodal networks studied here is 0.35. The trimodal network with the best mechanical properties, T-45, incorporates medium chains at a mass fraction of 0.29. This is the highest concentration of 8500 g/mol chains used and the closest to their overlap concentration. Thus, it appears that the medium chains in T-45 act similarly to the short chains in B-4500-90 – they form a connected skeleton that spans the network structure. However, the trimodal networks are more ductile since these medium chains have twice the backbone length of the short chains in 4500-91000 g/mol bimodal networks. The trimodals also contain a small amount of 800 g/mol chains, so the sweeping upturn in stress in T-45 is likely a result of the short and medium molar mass chains becoming highly stressed at high elongation ratios. The 800 g/mol chains may initially be protected from excessive deformation since they are expected to cluster into heterogeneous domains when incorporated at such low concentrations.[13] Therefore, the stress likely starts to increase at moderate strain when the medium chain matrix is

highly stretched but the long chains are still able to provide ductility and resist fracture. Since these trimodal networks can be stretched to such large elongations, the short chains may eventually contribute to this stress upturn even if they are initially protected.

3.4 Conclusions

Unimodal, bimodal, and trimodal networks are investigated using uniaxial extension. Trimodal networks can show outstanding mechanical properties when the majority of the volume fraction of the networks is taken up by long chains. Such elastomers can be extended to a large elongation ratio before fracture and have a large upturn in stress at high elongation, resulting in toughness values that are much higher than unimodal networks with similar elastic modulus. Bimodal networks with widely separated chain lengths are not quite as tough as trimodal networks, but can sustain high stress before fracture when the short chains reach 98 mol % in the system. The enhanced mechanical properties in multimodal networks are attributed to the ability of the shorter chains to sustain most of the applied stress, while the more flexible long chains provide ductility. These properties are maximized when the short or medium chains are near their overlap concentration, such that the resulting microstructure consists of an interconnected skeleton of the shorter chains with intermittent regions heavily populated by the long chains.

REFERENCES

1. Andrady, A. L.; Llorente, M. A.; Mark, J. E. *J. Chem. Phys.* **1980**, *72*, 2282-2290.

2. Llorente, M. A.; Andrady, A. L.; Mark, J. E. *J. Polym. Sci. Pol. Phys.* **1981**, *19*, 621-630.

3. Mark, J. E.; Tang, M. -Y. *J. Polym. Sci. Pol. Phys.* **1984**, *22*, 1849-1855.

4. Mark, J. E. *Acc. Chem. Res.* **1994**, *27*, 271-278.

5. Madkour, T.; Mark, J. E. *J. Macromol. Sci. Macromol. Reports* **1994**, *A31*, 153-160.

6. Erman, B.; Mark, J. E. *Macromolecules* **1998**, *31*, 3099-3103.

7. Giuliani, J. R.; Gjersing, E. L.; Chinn, S. C.; Jones, T. V.; Wilson, T. S.; Alviso, C. T.; Herberg, J. L.; Pearson, M. A.; Maxwell, R. S. *J. Phys. Chem. B* **2007**, *111*, 12977-12984.

8. Saalwächter, K.; Ziegler, P.; Spyckerelle, O.; Haidar, B.; Vidal, A.; Sommer, J. -U. *J. Chem. Phys.* **2003**, *119*, 3468-3482.

9. Saalwächter, K. *J. Am. Chem. Soc.* **2003**, *125*, 14684-14685.

10. Saalwächter, K.; Sommer, J. -U. *Macromol. Rapid Commun.* **2007**, *28*, 1455-1465.

11. Patel, S. K.; Malone, S.; Cohen, C.; Gillmor, J.; Colby, R. *Macromolecules* **1992**, *25*, 5241-5251.

12. Takahashi, H.; Shibyama, M.; Fujisawa, H.; Noruma, S. *Macromolecules* **1995**, *28*, 8824-8828.

13. Genesky, G. D.; Aguilera-Mercado, B. M.; Bhawe, D. M.; Escobedo, F. A.; Cohen, C. *Macromolecules* **2008**, *41*, 8231-8241.

14. Genesky, G. D.; Duncan, T. M.; Cohen, C. submitted to *Macromolecules*.

CHAPTER 4

FRACTURE ENERGY OF UNIMODAL AND MULTIMODAL NETWORKS IN PURE SHEAR CUT GROWTH EXTENSION*

4.1 Introduction

The classic Lake-Thomas theory[1] directly correlates the threshold fracture energy of an elastomer with the length of the elastic strands making up the polymer network and the dissociation energy of the main-chain chemical bonds comprising these strands. This simple theory has predicted threshold strength to reasonable accuracy for a number of different elastomers.[2,3] According to Lake and Thomas, the fracture energy expressed as the energy to tear through a unit area can be calculated from:[1]

$$G_c = KM^{1/2} \tag{1}$$

In this equation, M is the molar mass of the elastic strand that is to be ruptured and K is a prefactor calculated from the polymer chain properties:

$$K = (3/8)^{1/2}\, \rho A U q^{1/2} l \Big/ M_0^{3/2} \tag{2}$$

Here, ρ is the mass density of the polymer (0.97 g/cm^3), U is the dissociation energy of a bond along the polymer chain (6.1 x 10^{-19} J), q is the chain stiffness (6.25), l is the bond length (0.143 nm), M_0 is the molecular weight of the repeat unit (37 g/mol), and A is Avogadro's number. All reported values are for PDMS. Equations 1 and 2 were developed by considering ideal chains with Gaussian distributions of displacement lengths. The derivation of this theory is available in a number of publications.[1,3,4,5] It is

worth noting that nearly identical equations can be derived by considering the size of the tip diameter to be on the order of the distance between adjacent cross-links.[1] The only difference found from this treatment is that the $(3/8)^{1/2}$ prefactor in equation 2 increases to $(8/3\pi)^{1/2}$, leading to approximately a 50 % increase in the prediction for the fracture energy.

Cut growth tests yield fracture energies that are an intrinsic material property and can be compared to the Lake-Thomas theory. While materials tested in simple uniaxial extension (Chapters 2 and 3) fail due to natural flaws, the elongation at failure is controlled in cut growth testing by introducing a long pre-cut in the samples. The fracture energy measured by the cut growth tests in this chapter is sometimes referred to as fracture toughness. Since this terminology may cause confusion with uniaxial extension results, a consistent notation is adopted in this thesis. The area under the stress-elongation ratio curve in uniaxial extension (Chapters 2 and 3) is termed toughness, while the energy per unit area for fracture in the cut growth tests (this chapter) is termed fracture energy.

In this chapter, unimodal network fracture energies are compared to the Lake-Thomas theory to assess relative contributions from the chemical cross-links and inter-chain entanglements to the fracture process. Fracture energy results for bimodal and trimodal networks are contrasted with the toughness values measured via the simple extension experiments.

4.2 Experimental Procedures

4.2.1 Elastomer synthesis and characterization

PDMS precursor chains and networks were synthesized following the methods from Sections 2.2.1-2.2.2. New networks were synthesized for cut growth testing because the samples prepared for uniaxial extension tests (Chapters 2 and 3) were

exhausted in those experiments. Unimodal networks sweeping a wide range of precursor M_n were tested, along with 800-26000 g/mol bimodal networks similar to those previously shown to have enhanced mechanical properties (Chapter 2) and 800-8500-97000 g/mol trimodal networks. These trimodal networks are very similar to those tested in Chapter 3, except that the long chain M_n is slightly higher. The network properties are listed in Table 4.1 and an analogous naming convention to Chapter 3 is adopted, except for the additional prefix CG to denote cut growth samples. Model networks were produced at a ratio of cross-linking arms to polymer chain ends $r = 1.7$ for trimodal networks and $r = 1.1$ for the 800-26000 g/mol bimodal series.

4.2.2 Cut growth tests

Fracture energy G_c was determined using samples with geometry for pure shear extension,[6,7] where the width of the test piece must be at least 4 times the thickness and initial length.[8] Thus, the tested samples were 25 mm wide and 0.5-1 mm thick, and the initial distance between the clamps l_0 was 3-4 mm. The Instron 1125 was outfitted with a wide set of clamps that could hold such a sample. For the cut growth experiments, a 6 mm edge cut was made along the width of the test pieces (perpendicular to the loading direction).

G_c was determined following procedures adapted from those originally developed by Rivlin and Thomas.[8] First, the stress-elongation ratio data were recorded on uncut samples of each type of network in pure shear. Each pre-cut sample was then extended at a constant crosshead speed until the crack had propagated through its entire width. The elongation ratio at which the crack began to grow in these samples α_{cg} was determined from the maximum of the force-displacement curve measured by the Instron, since the force immediately began to drop when the crack began to move. The accuracy of this method to determine α_{cg} was verified by taking video footage of the crack propagation for selected samples. The elastically stored energy per unit

Table 4.1 – Network properties – cut growth
Unimodal networks

g/mol precursor chains	Nomenclature	G_c (J/m^2)	α_{cg}	Q	w_{sol} (mass %)	M_c (g/mol)
4500	U-CG-4500	34 ± 8	1.13 ± 0.02	2.52	0.32	4000
8000	U-CG-8000	34 ± 7	1.14 ± 0.01	2.96	0.30	5400
16500	U-CG-16500	65 ± 13	1.24 ± 0.02	3.64	0.71	7900
26000	U-CG-26000	65 ± 8	1.26 ± 0.02	3.92	1.68	9200
29000	U-CG-29000	82 ± 21	1.45 ± 0.08	4.57	0.82	12000
45000	U-CG-45000	105 ± 25	1.40 ± 0.06	4.87	0.81	12700

Bimodal networks 800-26000 g/mol

mol % short chains (mass%)	Nomenclature	G_c (J/m^2)	α_{cg}	Q	w_{sol} (mass %)	M_c (g/mol)
60 (4)	B-CG-60	67 ± 18	1.28 ± 0.04	3.94	0.86	8800
85 (15)	B-CG-85	65 ± 9	1.23 ± 0.02	3.40	2.23	7300
90 (22)	B-CG-90	65 ± 9	1.23 ± 0.01	3.49	2.28	7000

Trimodal networks 800-8500-97000 g/mol

mol % short, medium chains (mass%)	Nomenclature	G_c (J/m^2)	α_{cg}	Q	w_{sol} (mass %)	M_c (g/mol)
45,45 (3,28)	T-CG-45	125 ± 19	1.36 ± 0.03	3.74	0.23	8400
65,25 (4,17)	T-CG-65	127 ± 12	1.42 ± 0.03	4.74	0.58	11100
80,10 (6,8)	T-CG-80	122 ± 5	1.49 ± 0.03	5.36	2.63	13600

volume required to initiate fracture (W_0) was calculated by integrating under the *uncut* stress-elongation ratio curve up to α_{cg} from the corresponding *pre-cut* samples. Finally, G_c was calculated from:[8]

$$G_c = W_0 l_0 \tag{3}$$

The threshold fracture energy of these materials has been measured through careful experimental methods. Additional contributions to G_c can come from viscous dissipation, strain-induced crystallization, and deviation of the tear path in reinforced materials.[4,9] Crystallization and deviation of the tear path are not factors in these unfilled PDMS networks. Viscous dissipation is already minimized in model networks, since they contain relatively few dangling ends and defects[10] and room temperature is far above the glass transition temperature for PDMS (T_g = -127°C). Any remaining viscous contribution to the measured G_c has been eliminated by performing experiments at a extension speed of 0.5 mm/min, after verifying that the stress-elongation data were identical to those taken on the same sample tested at 0.05 mm/min. At these low extension speeds, the propagating crack speed was slow and relatively constant instead of accelerating (as can occur when elastomers are rapidly loaded).[11,12]

The Young's Modulus E and Mooney-Rivlin constants C_1 and C_2 were determined using simple extension tests on small pieces cut from the pure shear samples. Each of these samples was extended to α = 1.5. These data were fit to the Mooney-Rivlin equation:[13,14]

$$\sigma/\left(\alpha - 1/\alpha^2\right) = 2\left(C_1 + C_2/\alpha\right) \tag{4}$$

Average molar mass between effective cross-links M_c was determined from:

$$M_c = 3\rho RT/E \tag{5}$$

where ρ is the mass density of the polymer, R is the gas constant, and T is absolute temperature. The Young's modulus E was determined using stress-elongation ratio data from $\alpha = 1.00$ to 1.05.

4.3 Results and Discussion

4.3.1 Comparison of unimodal end-linked networks to the Lake-Thomas theory

As detailed in the Introduction, the Lake-Thomas theory[1] (equations 1 and 2) correlates the threshold fracture energy of a polymer network with molecular properties of its elastic chains. Threshold fracture energy tests on randomly cross-linked PDMS networks by Gent and Tobias showed good agreement with equations 1 and 2.[3] Far fewer results on end-linked PDMS are available in the literature, but tests by Yanyo and Kelley on a single end-linked unimodal network also appeared to match the theory relatively well.[15] All these tests employed $M = M_c$ in equation 1, where M_c is the molar mass between effective cross-links calculated from equation 5. Calculation of M_c via equation 5 uses the low-strain modulus, where both chemical cross-link constraints and inter-chain entanglements (modeled by the C_1 and C_2 terms in the Mooney-Rivlin equation, respectively) are significant. While the Lake-Thomas model ignores entanglements, their possible effect on G_c can be introduced in an empirical manner by taking $M = M_c$ in equation 1.

Fracture energy vs. M_c is plotted for end-linked unimodal networks and for networks from references 3 and 15 in Figure 4.1a. Also plotted is the Lake-Thomas prediction for PDMS given by equations 1 and 2. The previously reported results from randomly cross-linked networks are much better represented by the model. While the

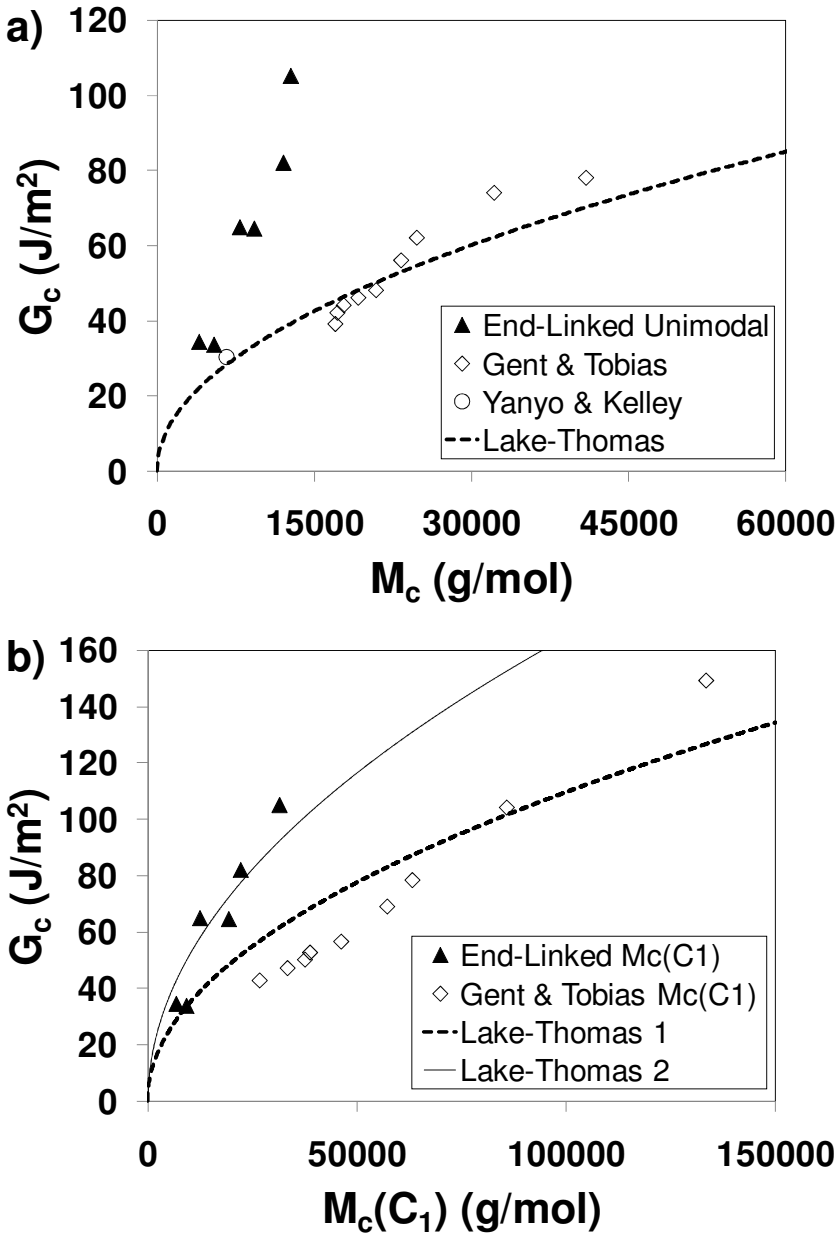

Figure 4.1. Threshold fracture energy of end-linked model networks, along with results from an end-linked network (Yanyo & Kelley[15]) and randomly cross-linked networks (Gent & Tobias[3]). a) $M = M_c$ in equation 1 and b) $M = M_c(C_1)$ in equation 1. The first Lake-Thomas prediction (dashed line) uses the prefactor $(3/8)^{1/2}$, while the second (solid line) uses $(8/3\pi)^{1/2}$.

fracture energies for the end-linked networks increase with M_c as expected, the experimental energies become significantly higher than the theoretical prediction with increasing M_c. The Lake-Thomas theory is meant to be a scaling theory, and correspondence with experimental data may not be exact. However, the different G_c vs. M_c trends followed by end-linked and randomly cross-linked networks suggest that the fracture process may be different in each type of network. Thus, an alternative approach for evaluating M in equation 1 is taken to provide further insight into these results. Here, M is assumed to represent the molar mass between actual covalent cross-links (as originally assumed by Lake & Thomas). This value is calculated by using only the Mooney-Rivlin $2C_1$ contribution to the modulus because it represents the effect of chemical cross-links:[16]

$$M = M_c(C_1) = \rho RT / 2C_1 \tag{6}$$

Figure 4.1b displays G_c vs. $M_c(C_1)$ results compared with the same theoretical prediction. The unimodal end-linked network data have now shifted closer to the dashed line generated by equations 1 and 2. Also plotted as a solid line is the Lake-Thomas prediction with the alternative prefactor of $(8/3\pi)^{1/2}$, to which the end-linked data are a good fit.

The closer correspondence of the $M_c(C_1)$ data to the theory for the end-linked elastomers suggests that the chemical constraints are the most important factor in the fracture process of such networks. In this point of view, "slippage" of trapped entanglements at high strains causes the elastic strand length to be governed primarily by the chemical cross-links. Of course, the crack begins to propagate in the end-linked unimodal networks at moderate strains ($\alpha_{cg} \leq 1.45$ – Table 4.1). The effect of chain entanglements is just beginning to decrease in magnitude at such bulk elongation ratios but is certainly still important. However, in cut growth tests the stress is

concentrated at the crack tip and the material in its immediate vicinity is in a highly stretched and complicated state.[17] Thus, the stretched chains that are ruptured once threshold fracture begins (those just ahead of the crack tip) have a local α that is likely much greater than α_{cg}. Once the material is in this highly strained state, there should be a significant decrease in the contribution to the material properties from entanglements.

Of course, the fact that the randomly cross-linked networks closely follow the theory when M_c is calculated from the elastic modulus that includes the effect of entanglements (equation 5, Figure 4.1a) cannot be ignored. Additional threshold fracture energy experiments on randomly cross-linked PDMS by Mazich et al. have correlated the characteristic elastic strand length for fracture with the entanglement spacing for PDMS.[5,18] The G_c results of Gent & Tobias can also be plotted against $M_c(C_1)$ to isolate the effect of the chemical cross-links on fracture energy. However, the influence of pendant chains on the effective density of elastic chains in each network must now be considered. The Lake-Thomas theory assumes all chains to be elastically active, which is a reasonable approximation for the model end-linked networks but not for randomly cross-linked networks, particularly at low cross-linking densities. The fraction of elastic chains in randomly cross-linked networks can be estimated from the initial molar mass in the melt state $M_{n,init}$ and the molar mass between chemical cross-links $M_c(C_1)$ upon network formation (equation 6). The ratio of $M_{n,init}$ to $M_c(C_1)$ is the average number of sections between cross-links into which each initial chain will be partitioned. Therefore, the fraction of elastically active chains f_{el} in randomly cross-linked networks can be calculated from:

$$f_{el} = \frac{M_{n,init}/M_c(C_1) - 2}{M_{n,init}/M_c(C_1)} = 1 - \frac{2}{M_{n,init}/M_c(C_1)} \qquad (7)$$

The subtracted term in the equation accounts for the two ends of the initial strand that become pendant chains upon cross-linking. The measured fracture energy $G_{c,meas}$ for the randomly cross-linked networks can be compared to the Lake-Thomas theory by adjusting the raw data to account for the fewer number of elastic chains actually crossing the fracture plane. Since the fracture plane is two-dimensional but f_{el} is a volume term, the adjustment factor must be raised to the 2/3 power:

$$G_c = (1/f_{el})^{2/3} G_{c,meas} \tag{8}$$

Note that this is adjustment is not required for G_c vs. M_c plots (as shown in Figure 4.1a) since M_c represents the molar mass of *effective* elastic strands calculated from the elastic modulus E.

G_c values from equation 8 are plotted for the Gent & Tobias data against $M_c(C_1)$ in Figure 4.1b. The Lake-Thomas model with the $(3/8)^{1/2}$ prefactor provides a good fit to these data. Since the analogous G_c vs. M_c results in Figure 4.1a are also a good match to this same prediction, it is difficult to determine whether the elastic molar mass associated with fracture in randomly cross-linked networks is related to the distance between chemical cross-links or between "effective" cross-links that include entanglements. The fracture energy of end-linked networks appears to be associated with the molar mass between chemical cross-links. However, it correlates with $M_c(C_1)$ according to the Lake-Thomas theory with a different prefactor than the randomly cross-linked networks. This apparent discrepancy may be due to the relative contributions of the cross-linking reaction and the trapped entanglements in each type of network. As shown in the inset of Figure 4.2, C_2 is considerably larger than C_1 for the majority of the randomly cross-linked networks and thus the elastic response at

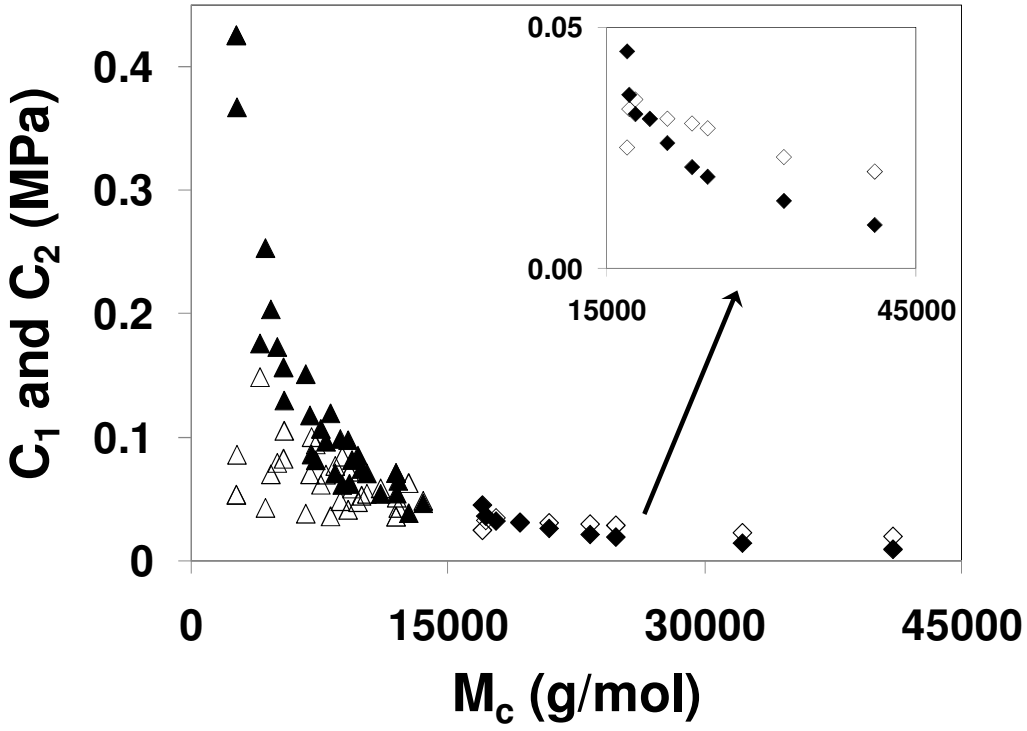

Figure 4.2. Mooney-Rivlin parameters C_1 and C_2 vs. M_c for end-linked networks reported here (triangles) and randomly cross-linked networks from Gent & Tobias[3] (diamonds). Values of C_1 are represented by filled symbols and those of C_2 by open symbols.

low strain is dominated by trapped entanglements. On the other hand, the end-linked networks are much more highly cross-linked and C_2 is less than C_1 for most of these samples (Figure 4.2).

4.3.2 Comparison of unimodal and multimodal results

Values of the fracture energy G_c are plotted against M_c for unimodal, bimodal, and trimodal networks in Figure 4.3. It is immediately apparent than any enhancement in G_c for multimodal networks is much milder than that seen in toughness measured by uniaxial extension (Chapters 2 and 3). In fact, the bimodal networks show almost identical fracture energy to unimodal networks of similar M_c, while similar networks to B-CG-85 and B-CG-90 have shown enhanced toughness in simple extension (Chapter 2). These results are somewhat at odds with some previously reported studies. For instance, Yanyo and Kelley found increased fracture energy in a bimodal network as compared to unimodal, but this was only for a single sample of each and the networks were of relatively poor quality (w_{sol} ~ 5 %).[15] Other researchers have found the fracture energy of bimodal networks to peak at certain short chain compositions,[19,20] but these experiments did not compare to equivalent unimodal networks and the network qualities were not reported. The trimodal networks studied here fared slightly better than the unimodal networks, but only T-CG-45 (and perhaps T-CG-65) has a G_c value that is distinctly higher than the unimodal networks.

Elongation ratios at fracture α_c for the uniaxial extension tests (Chapter 3) are plotted against M_c in Figure 4.4a, while average elongation ratios at the moment when crack growth began in cut growth testing α_{cg} are displayed in Figure 4.4b. In simple extension, the bimodal and trimodal networks usually reach higher α_c before fracture than unimodal networks with similar values of elastic modulus. These results reiterate that enhanced mechanical properties in multimodal networks are manifested at high strains.[21] The long chains provide ductility that allows the networks to be stretched to

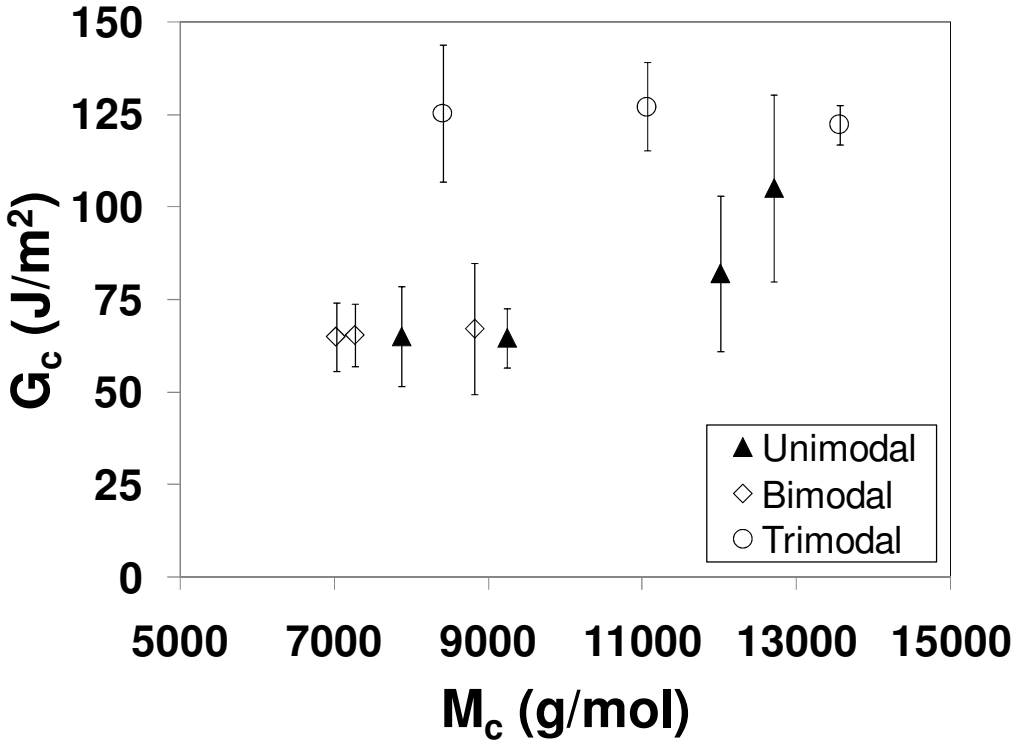

Figure 4.3. Fracture energy vs. M_c for unimodal and multimodal networks. Enhancement in G_c for trimodal networks is much milder than enhancement in toughness measured by uniaxial extension.

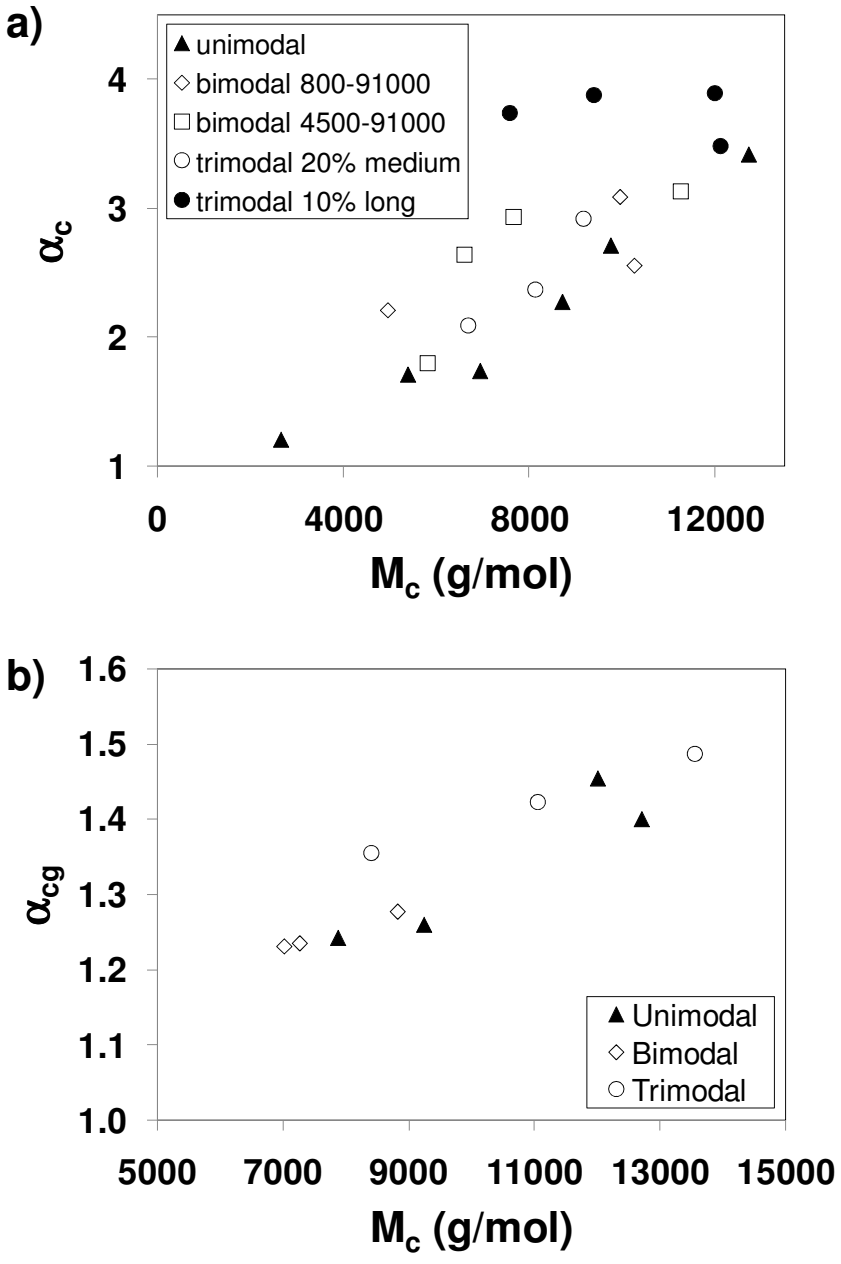

Figure 4.4. Average elongation ratio at fracture for a) uniaxial extension (Chapter 3) and b) cut growth experiments. Multimodal networks can usually be stretched farther than unimodal networks with similar M_c in uniaxial extension. Note the different scales on each ordinate.

high strains, which along with the upturn in stress due to the limited extensibility of the short chains leads to high toughness values. When a pre-cut sample is prepared, network fracture begins at a much lower elongation ratio since the stress is concentrated at the crack tip. Since the pre-cut samples in the tests reported here always utilize edge cuts and the crack tip is sharp, it is not surprising that the α_{cg} values shown in Figure 4.4b are much lower than the α_c values reported in Figure 4.4a. In the cut growth tests, α_{cg} follows roughly the same trend with M_c whether the networks are unimodal or multimodal. Therefore, the resulting G_c values are similar for most networks with similar M_c.

The reason the fracture energies are not always improved for the multimodal networks despite the large enhancement exhibited in their toughness may be the energy needed to generate a nucleating crack in the bulk. In the pre-cut samples this energy has already been supplied, but in toughness measurements of uncut samples the energy necessary depends on the microstructure for networks with the same macroscopic modulus (i.e. M_c). Bimodal networks have been demonstrated to have a heterogeneous microstructure[21-25] and heterogeneities are also expected in the structure of trimodal networks (Chapter 3). Therefore, micro-cracks that develop in multimodal networks tested in uniaxial extension will require more energy to propagate if they occur in a softer, long chain-heavy region of the elastomer. This will lead to higher elongation ratios before fracture than for homogeneous networks with the same bulk M_c value. In the pre-cut networks, the applied cut is macroscopic. Thus, the crack that dictates the fracture process accesses each of the effective elastic chain lengths included in the multimodal networks, and the fracture energies more universally correlate with average M_c.

4.4 Conclusions

Multimodal networks do not show the same degree of improvement in threshold fracture energy as is found for their toughness values. This is a consequence of the inability of the bimodal or trimodal elastomers to reach higher elongation ratios at crack growth onset than unimodal networks with similar low-strain properties. These results are likely due to the large stress concentration at the tip of the macroscopic pre-cut in the cut growth experiments, where the fracture process is dictated by the average molar mass of the effective elastic strands. Unimodal network fracture energies more closely correlate to predictions from the Lake-Thomas theory[1] when the pertinent elastic chain length is taken to be the distance between chemical cross-links. Therefore, inter-chain entanglements appear to have much less influence on the fracture process in these end-linked model networks.

REFERENCES

1. Lake, G. J.; Thomas, A. G. *P. R. Soc. Lond. A Mat.* **1967**, *300*, 108-119.

2. Ahagon, A.; Gent, A. N. *J. Polym. Sci. Pol. Phys.* **1975**, *13*, 1903-1911.

3. Gent, A. N.; Tobias, R. H. *J. Polym. Sci. Pol. Phys.* **1982**, *20*, 2051-2058.

4. Bhowmick, K. *J. Macromol. Sci. R. M. C.* **1998**, *C28*, 339-370.

5. Mazich, K. A.; Samus, M. A. *Macromolecules* **1990**, *23*, 2478-2483.

6. Takigawa, T.; Yamasaki, S.; Urayama, K.; Takahashi, M.; Masuda, T. *Rheol. Acta* **1996**, *35*, 288–295.

7. Urayama, K.; Ogasawara, S.; Takigawa, T. *Polymer* **2006**, *47*, 6868-6873.

8. Rivlin, R. S.; Thomas, A. G. *J. Polym. Sci.* **1953**, *10*, 291–318.

9. Lake, G. J. *Rubber Chem. Technol.* **1995**, *68*, 435-460.

10. Patel, S. K.; Malone, S.; Cohen, C.; Gillmor, J.; Colby, R. *Macromolecules* **1992**, *25*, 5241-5251.

11. Baumberger, T.; Caroli, C.; Martina, D. *Eur. Phys. J. E* **2006**, *21*, 81-89.

12. Baumberger, T.; Caroli, C.; Martina, D. *Nat. Mater.* **2006**, *5*, 552-555.

13. Mooney, M. *J. Appl. Phys.* **1940**, *11*, 582-592.

14. Rivlin, R. S. *Philos. Trans. R. Soc.* **1948**, *A241*, 379-397.

15. Yanyo, L. C.; Kelley, F. N. *Rubber Chem. Technol.* **1987**, *60*, 78-88.

16. Yoo, S. H.; Yee, L.; Cohen, C. manuscript in preparation.

17. Hui, C. -Y.; Jagota, A.; Bennison, S. J.; Londono, J. D. *P. R. Soc. Lond. A Mat.* **2003**, *459*, 1489-1516.

18. Mazich, K. A.; Samus, M. A. *Macromolecules* **1990**, *23*, 2478-2483.

19. Smith, T. L.; Haidar, B.; Hedrick, J. L. *Rubber. Chem. Technol.* **1990**, *63*, 256-264.

20. Shah, G. B.; Winter, R. W. *Macromol. Chem. Physic.* **1996**, *197*, 2201-2208.

21. Genesky, G. D.; Aguilera-Mercado, B. M.; Bhawe, D. M.; Escobedo, F. A.; Cohen, C. *Macromolecules* **2008**, *41*, 8231-8241.

22. Wu, W. L.; Jong, L.; Hanyu, A.; Coyne, L .D.; Stein, R. S. *Macromolecules* **1990**, *23*, 351-353.

23. Hecht, A. -M.; Horkay, F.; Geissler, E. *J. Phys. Chem. B* **2001**, *105*, 5637-5642.

24. Saalwächter, K.; Ziegler, P.; Spyckerelle, O.; Haidar, B.; Vidal, A.; Sommer, J. -U. *J. Chem. Phys.* **2003**, *119*, 3468-3482.

25. Genesky, G. D.; Duncan, T. M.; Cohen, C. submitted to *Macromolecules.*

CHAPTER 5

THE EFFECT OF PRECURSOR MOLAR MASS ON THE ^{2}H-NMR LINESHAPES OF PDMS UNIMODAL NETWORKS*

5.1 Introduction

5.1.1 ^{2}H-NMR background

To understand molecular-level structure in elastomers, it is important to directly probe the network properties at local scales. ^{2}H-NMR has been utilized for this purpose because it allows for examination of chain segment orientation through the deuterium quadrupole interaction.[1] In polymers, deuterium nuclei are typically covalently bonded to carbon atoms. Each deuterium has a quadrupolar moment that interacts with the component of the electric field gradient directed along the C-^{2}H bond. The distribution of C-^{2}H orientations is controlled by the distribution of orientations of the polymer backbone. Therefore, since ^{2}H-NMR measures the quadrupolar interaction at each C-^{2}H bond, it is a tool to directly examine the orientations of polymer chain segments.[2] When segments are randomly oriented and their motion is fixed on the time scale of the NMR experiment, a Pake pattern is observed.[3] This well known lineshape, which is found for rigid solids, has an overall linewidth on order 100 kHz. When segmental motion increases and the motion is isotropic, like in the case of low molar mass polymer melts, significant averaging of the quadrupolar interaction occurs and the spectrum narrows into a sharp peak.

Elastic chains cross-linked into a network structure are an intermediate case. While the motion of the segments is fast and the linewidth is orders of magnitude narrower than the Pake pattern, the spectra are still significantly broader than those of

* Reproduced in part with permission from *Macromolecules*, submitted for publication.

uncross-linked melts. Past experiments[4,5] have demonstrated "wings" in the spectra which correspond to a super-Lorentzian lineshape (Figure 5.1). Therefore, the constraints imposed by the cross-links cause non-isotropic motion corresponding to a residual quadrupolar frequency distribution when compared to the melt state. For any single, fixed orientation of a C-^{2}H bond, the resulting NMR spectrum is two lines spaced equally about zero frequency. The magnitude of this separation $\delta\nu_Q$ is given by:[3]

$$\delta\nu_Q = 3/4\ \delta_Q\ (3\cos^2\theta - 1) \qquad (1)$$

where δ_Q is the quadrupolar coupling constant and θ is the angle between the C-^{2}H bond and the magnetic field B_0. In a labeled elastic network, however, C-^{2}H bonds are oriented at all possible angles with the magnetic field, and these orientations are constantly fluctuating due to segmental motion. Therefore, the NMR spectrum of an undeformed elastomer is a time-averaged sum of the pair of lines corresponding to each C-^{2}H bond.

When a deuterium-labeled network is deformed uniaxially, more elastic chain segments are aligned with the strain axis. Therefore, the motional averaging of the quadrupolar interaction is no longer spatially isotropic, and the NMR spectrum broadens inhomogeneously. When the applied stress becomes high enough, the time-averaged sums of the pairs of lines described by equation 1 become disparate enough such that two peaks become visible. The distance between these two peaks is termed the splitting $\Delta\nu$ (Figure 5.1). As the spectrum broadens with increasing elongation ratio α, the distance between the peaks also increases.

The instantaneous contribution to the lineshape for any given segment of an

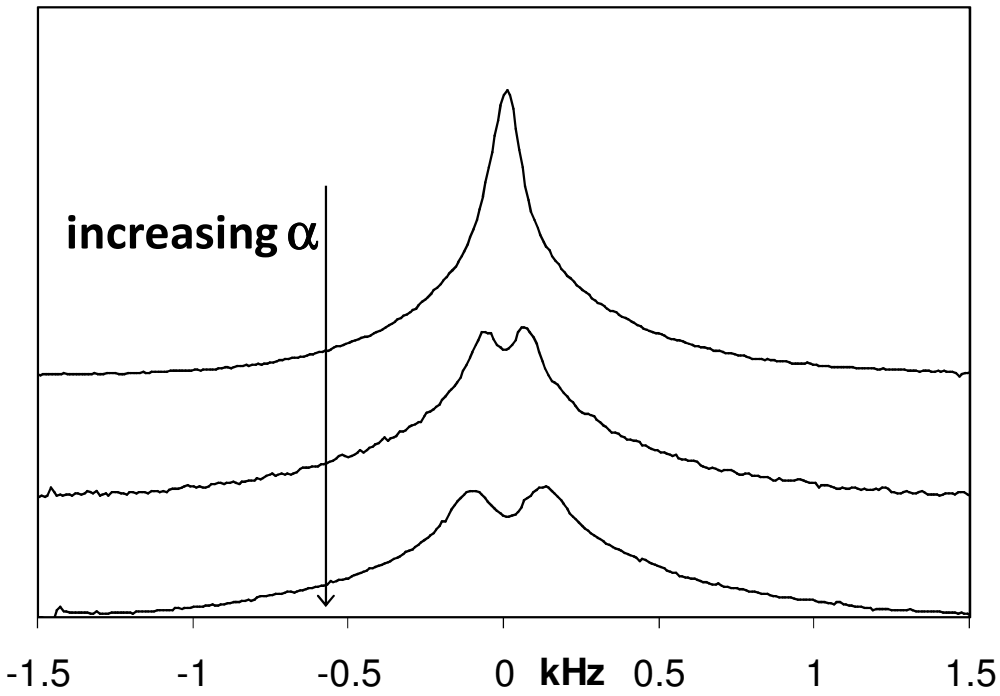

Figure 5.1. The "super-Lorentzian" lineshape of an undeformed elastomer splits into two peaks equidistant from zero frequency with increasing elongation ratio α.

elastomer strained perpendicular to the external magnetic field is given by:[6]

$$\delta\nu = 3/4\ \delta_Q\ P_2(\cos\phi)\ P_2(\cos\psi) \qquad (2)$$

where $\delta\nu$ is the doublet separation, ϕ is the angle between the chain segment vector and the C-^{2}H bond, ψ is the angle between the segment vector and the applied strain, and $P_2(\cos x)$ is the second Legendre polynomial of cos x.

The order parameter used to quantify segment anisotropy, S, is defined as:

$$S = \langle P_2(\cos\psi)\rangle \qquad (3)$$

where the brackets indicate an average over all chain segments. Comparison with equation 2 reveals that $\delta\nu$ is directly proportional to S. Classical elastic theories[7,8] predict a direct dependence of S on α^2-1/α, and thus the distance between the peaks $\Delta\nu$ is often correlated with this elongation ratio-dependent term. However, just as in the undeformed case, the total spectrum of a strained elastomer is the sum of the contributions from each labeled bond, averaged over time. Therefore, the locations of the peaks represent the most frequently accessed degree of segment orientation and not the average segment orientation ($\Delta\nu$ does not correspond to the average $\delta\nu$). To obtain the average segmental orientation, one needs to consider the entire lineshape of the ^{2}H-NMR spectrum.

5.1.2 ^{2}H-NMR analysis of elastomers

The earliest work in the field[9] employed sulfur-cured polyisoprene swollen in a series of perdeuterated solvents. The observed split $\Delta\nu$ was attributed to the nonzero average orientational order of the solvent when diffusing through the deformed network. The authors attributed the separation of the spectral peaks to nematic-like short-range interactions between partially aligned chain segments. Subsequent studies began to explore the spectra of elastomers with deuterium-labeled elastic chains.

Deloche et al.[4] mixed perdeuterated polydimethylsiloxane chains with unlabeled precursors. The resulting network spectra were qualitatively similar to that of deformed networks swollen in deuterated solvents. However, the labeled network lineshapes included spectral wings that were not observed in previous experiments. The same researchers later demonstrated that the rate of change of $\Delta\nu$ with increasing α followed a straight line when plotted against polymer fraction at equilibrium swelling Φ_0.[10] This result reinforced the importance of segment-segment interactions on induced order.

In an attempt to explain the lineshape in addition to the strain-induced frequency split $\Delta\nu$, Gronski et al.[5,6] studied randomly cross-linked polybutadiene networks that were either homogeneously deuterated or selectively labeled at network junctions. These authors attributed the NMR signal near the peak maxima to longer chain segments and proposed that the wings resulted from larger segmental orientation of shorter chains. Additionally, they found a larger quadrupolar splitting for segments selectively deuterated near the cross-links, but this effect appeared to be rather small. Since segment-segment interactions play an important role in the anisotropic order measured by NMR, several researchers compared the results from labeled elastic chains to labeled solvents or probe chains. For instance, deuterated PDMS elastomers were found to show similar $\Delta\nu$ upon extension to protonated networks in dissolved deuterated benzene[11] or labeled non-reactive PDMS.[12,13] Other experimentalists speculated that the increased mobility of dangling chains caused their contributions to dominate the center portion of the spectra from which the splitting is measured.[14] McLoughlin et al. systematically investigated PDMS networks with deuterated elastic, probe, or pendant chains.[15] They found a universal correspondence between the strain efficiency $\Delta\nu/(\alpha^2-1/\alpha)$ upon compression and the elastic modulus, no matter which type of chains was labeled.

A uniaxial mean field model was used to replicate the orientational coupling between chain segments.[16] Results of this treatment indicate that the doublet disappears when the field is absent and the network chains thus become non-interacting ("phantom" chains). Alternatively, the splitting has been reproduced by introducing a term that creates an anisotropic attractive potential upon strain to mimic the screening of excluded volume interactions between segments.[17,18] This theoretical model shows reasonable agreement with polybutadiene network lineshapes at low strain.[19] These observations have been corroborated by Monte Carlo (MC) simulations of rubbery networks, where the mean field was introduced as an excluded volume effect between chain segments.[20,21] Further MC work demonstrated identical $\Delta\nu$ values upon stretching for both elastic chains and free chains dissolved in a network, but a higher average total order for the elastic chains.[22] These analyses and experimental results led to several models that attempted to describe the entire spectrum in terms of contributions from two different segment populations.[23-26] In their computer simulation study of NMR lineshapes with increasing strain, Yong and Higgs observed that the center portion of the spectra correlates with chain interaction and packing whereas the outer wings result from highly extended chains with large end-to-end distances.[27] Additionally, the authors found that proximity to cross-link points had very little effect on the lineshape contribution.

In this Chapter, the evolution of the ^{2}H-NMR spectra is obtained and described for elastic chains as a function of the precursor chain length (or cross-link density). Such a study of model end-linked unimodal networks with a systematic variation of the precursor chain molar mass has not been performed and reveals the role of the cross-link constraint on the NMR spectra. Lineshape analysis of the end-linked PDMS networks probes the segment orientation of the elastic chains of different chain sizes in the undeformed state. Stretched networks are also examined, where a shoulder appears

in the spectra at high strain. This may indicate two characteristic populations, which are empirically fit to two pairs of curves. To compare the spectra of elastic chains which are constrained on both ends to those of unconstrained free chains of the same size, deuterated free chains are dissolved into unlabeled PDMS networks to examine the lineshapes at high extension.

5.2 Procedures

5.2.1 Elastomer synthesis and characterization

PDMS chains were synthesized via anionic ring-opening of hexamethylcyclotrisiloxane.[28-30] Deuterated hexamethylcyclotrisiloxane monomer was produced using a reaction sequence adapted from Beltzung et al.[31] To conserve valuable deuterated material, these monomer crystals were mixed with hydrogenated hexamethylcyclotrisiloxane (Gelest, Inc.) before polymerization to yield randomly-deuterated polymer chains.

PDMS chains were characterized using gel permeation chromatography (GPC) with polystyrene-calibrated columns. Equivalent PDMS molar masses were obtained by implementing an established conversion.[32] Partially-deuterated chains with number-average molar mass of 5000, 11000, 36000, and 90000 g/mol and low polydispersity (≤ 1.32) were end-capped with vinyl termination. These chains were cured into elastic networks by performing a hydrosilylation reaction with tetrakis(dimethylsiloxy)silane cross-linker and *cis*-dichlorobis(diethylsulfide)platinum(II) catalyst. The parameter r is defined as the ratio of cross-linker arms to polymer chain ends. In accordance with past work[33], $r = 1.7$ was used to create the highest quality networks for precursors of 11000 g/mol and above. The optimal ratio is smaller for shorter precursor chains[34], so r was reduced to 1.5 for the 5000 g/mol sample. The networks were cured in Teflon molds at 35°C for 3 days. One unlabeled network with number-average molar mass of

30000 g/mol (PDI = 1.27) was synthesized via the same methods with monomer purchased from Gelest.

The networks were characterized by standard swelling and extraction techniques using toluene.[35] Equilibrium mass swell ratios Q were calculated using the dry and swollen network masses. Soluble fractions w_{sol} were determined by comparison of the sample masses before and after toluene extraction. The network characteristics are summarized in Table 5.1. All networks were extracted before the NMR experiments were performed. Therefore, the tested samples contained no free chains, except for the unlabeled network with dissolved probe chains. The deuterated polymer chains used as a non-elastic probe chains were trimethylsiloxy end-capped and un-reactive. A small amount of these chains, with M_n = 30000 g/mol and PDI = 1.41, was spread onto the surface of the 30000 g/mol unlabeled network. To dissolve the probe chains into the network, the sample was covered with a glass vial and placed into an oven at 65^{o}C for one week, by which time the network surfaces were completely dry. The concentration of free chains dissolved in the network was 9 wt%. After the NMR experiments were performed, a second toluene extraction was carried out to remove the deuterated probes. The network did not display a ^{2}H-NMR signal after this extraction.

Samples for ^{2}H-NMR measurements were cut with a razor blade into rectangular strips of approximate dimensions 32 x 2 x 1 mm. Dynamic mechanical testing on these relatively small samples yielded inconsistent values for the low-strain elastic modulus E. Therefore, an empirical correlation between Q and E using unlabeled PDMS networks[33] was used to obtain E values for the deuterated networks .

5.2.2 ^{2}H-NMR methods

^{2}H-NMR data were measured on a Tecmag Apollo HF spectrometer operating at 30.72 MHz for deuterium. The NMR spectra were obtained by Fourier transforming

Table 5.1. ^{2}H-network compositions and properties

M_n (g/mol)	Q	E (MPa)	w_{sol} (mass%)
5000	3.02	1.30	0.59
11000	3.39	1.06	0.80
36000	4.64	0.61	1.45
90000	7.31	0.27	5.48
30000*	4.55	0.63	2.36

*Consists of unlabeled elastic chains and labeled probe chains, both with M_n = 30000 g/mol. Unlabeled soluble material was extracted before dissolution of labeled free chains.

the quadrature-detected free-induction decay after a 90^{o} pulse of 5 μs. Each sample was centered in an 8.5 mm long RF coil at room temperature. The number of scans was increased (up to 100000 in some cases) with increasing extension of the sample to achieve reasonable signal-to-noise ratio. The repetition delay between each scan was 1s. A gentle line-broadening of 10 Hz was applied to the time-domain data before Fourier transformation to improve the apparent signal-to-noise ratio. Since the ^{1}H-^{2}H dipolar coupling is very weak compared to the ^{2}H quadrupolar coupling, proton decoupling was not necessary and therefore was not applied. All test pieces had uniform width and thickness to ensure uniform stretching. Stretched samples were oriented perpendicular to the 4.7T external magnetic field and deformed using a device described in reference 36. Approximately 8 mm of material on each end of the sample were clamped into the stretching device, leaving a gauge length of about 16 mm. This was sufficient to ensure that the inner uniformly-stretched portion of the sample was surrounded by the RF coil; the clamped ends were outside of the RF coil. To monitor the local extension ratio, each sample was marked with ink dots in the unstretched state. High-resolution photographs of the marked samples were taken at the rest state and for each elongation ratio once the length had stabilized. The distance between the dots was measured from each photograph, and the elongation ratio calculated by dividing the stretched distance by the unstretched distance.

5.3 Results and Discussion

5.3.1 Data analysis: empirical fitting procedure for ^{2}H-NMR spectra

As discussed in the Introduction, the incomplete averaging of the quadrupolar interaction in ^{2}H-labeled elastomers leads to non-Lorentzian lineshapes. Even the spectral lineshapes of samples in the unstretched state cannot be fitted to a single

curve. They can, on the other hand, be well represented by a sum of two curves, each centered at zero frequency. A representative example is shown in Figure 5.2. The Solver tool in Microsoft Excel was implemented to fit the spectra, iterating on the height and width of each peak. Depending on the sample, the lineshape was best fit by either a pair of Lorentzian curves, or one Lorentzian and one Gaussian curve. For each network studied, a narrow and a wide curve were required to obtain a good fit. The widths at half-height for each of these curves are denoted as γ_n and γ_w, respectively. Even though the procedure is empirical, the fitting parameters for the narrow and wide curves yielded interesting information concerning the effect of the precursor molar mass on the lineshape. When the samples were deformed and the spectra broadened, the fitting procedure was adjusted. Here, each spectrum was modeled by the sum of two pairs of curves, and the program also iterated on the peak distance from $\nu = 0$ for each pair of curves. Each coupled pair was constrained to have the same peak height, width, and distance from zero frequency.

5.3.2 Evolving lineshape in unstretched networks

^{2}H-NMR spectra for unstretched end-linked networks with varying precursor M_n are presented in Figure 5.3. The peak heights are normalized such that the area under each spectrum is identical. Each spectrum was fit to the sum of two curves using the procedures outlined in section 5.3.1. These fitting parameters are displayed in Table 5.2. The widths at half-height for the chains in the *melt state* before cross-linking are reported as γ_{melt}. The spectra for these melts showed rather sharp Lorentzian peaks, as expected. Note the increase in γ_{melt} with increasing M_n. This reflects the higher viscosity of the longer chains, where random segment motion is slightly slower and the spectra are thus a bit broader. The observed lineshape shows clear changes with the precursor molar mass, M_n. The 5000 g/mol network is best represented by the typical super-Lorentzian curve (the sum of a narrow and a wide

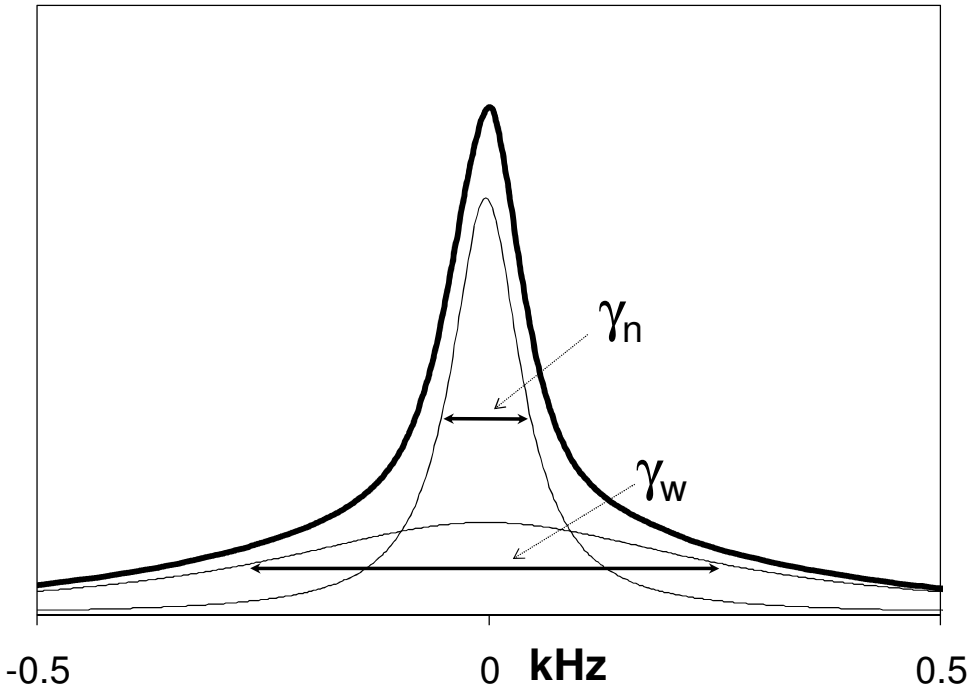

Figure 5.2. Empirical decomposition of the spectral lineshape of an undeformed PDMS network (bold line). The experimental spectrum is well represented by the sum of a narrow curve and a wide curve (thin lines) with widths at half-height γ_n and γ_w.

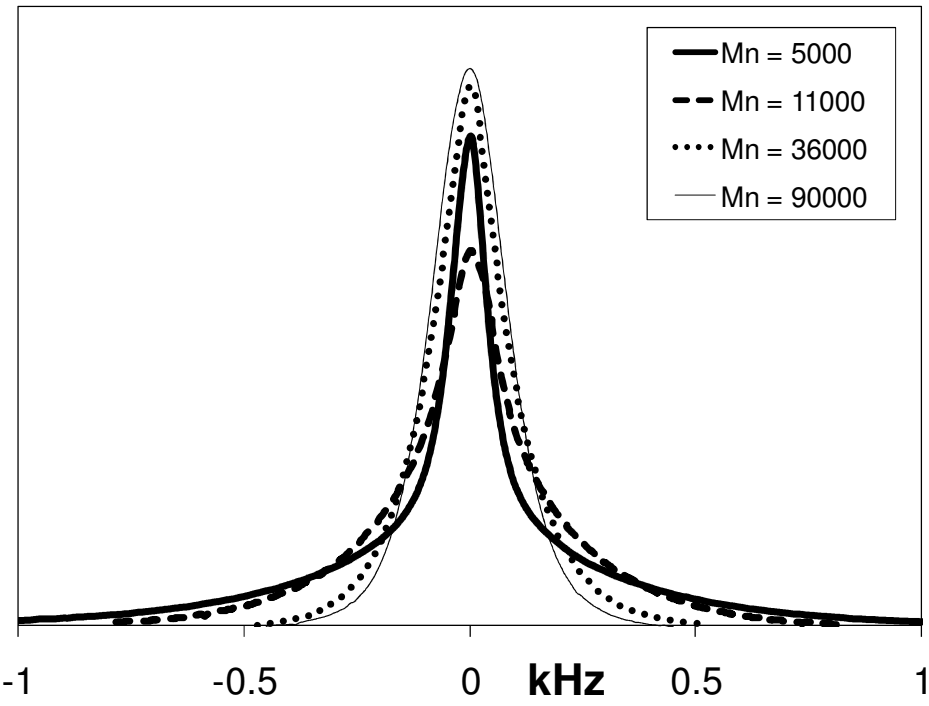

Figure 5.3. ^{2}H-NMR spectra for undeformed 5000 (thick line), 11000 (dashed line), 36000 (dots), and 90000 (thin line) g/mol networks. The lineshapes are normalized by the area under each spectrum.

Table 5.2. Fitting parameters for melt and network spectra and estimated fraction of elastic chains in each network

M_n	linewidth (kHz)			f_{el}
(g/mol)	γ_{melt}	γ_n	γ_w	
5000	0.054	0.047	0.289	0.86
11000	0.061	0.077	0.245	0.84
36000	0.069	0.065	0.121	0.79
90000	0.077	0.075	0.090	0.62

Lorentzian curve) previously reported for PDMS networks.[4] However, the form of the spectra, particularly in the wings, differs with increasing M_n. The spectra in Figure 5.3 demonstrate that the spectral wings are most important for networks synthesized from low molar mass precursors. For networks synthesized from precursors with M_n = 11000 g/mol and above, the spectra were better modeled by a Lorentzian with narrow linewidth and a Gaussian with larger linewidth. This is a consequence of the decreasing importance of the wings of the spectra, since Gaussian functions have a sharper cut-off than the wide wings of a Lorentzian. This is also captured by the value of γ_w, which decreases steadily with increasing M_n.

To interpret these results, it is instructive to think of the spectra as the sum of time-averaged pairs of lines, as outlined in the Introduction. Therefore, each spectrum is the sum of the chain segment order parameter distribution and its image reflected across $\nu = 0$. The outer portion of the distribution, which is represented by the wings in the full spectrum of the 5000 g/mol elastomer, corresponds to segments with a high degree of order. Computer simulations have demonstrated that these outer portions of the spectra result from chains with especially high end-to-end distances.[27] Thus, it appears that some amount of short chains cross-link when in an extended state. These chains are more motionally constrained than those that attach to a constraint while still in a more coiled state. Since the wings decrease progressively with increasing precursor M_n, the distribution of segment orientations is narrower for higher molar mass elastic chains. Longer chains, then, are less perturbed from their initial, random conformations when changing from the melt state to the elastic state. This interpretation is consistent with recently reported MQ NMR experiments[37-39] that demonstrated wider order parameter distributions for shorter elastic chain networks.

Using the natural ^2H abundance in a 47000 g/mol end-linked network, Saalwächter and Sommer observed that the spectrum was not Lorentzian and did not

show long spectral wings.[39] The authors used this example to assert that the super-Lorentzian lineshape is not universal for PDMS elastomers. They attributed the sharp center of this frequently observed shape to high numbers of mobile defects (sol, dangling chains, loops) in previous studies. The lineshape reported for this 47000 g/mol specimen appears qualitatively similar to the 36000 and 90000 g/mol spectra presented in Figure 5.3. Therefore, comparison with the lower M_n samples seems to indicate that the transition from super-Lorentzian to this unexpected spectral form must be a result of the length of the elastic chains and not just the presence of inelastic defects.

The networks synthesized from precursors with M_n up to 36000 g/mol were high quality and had low soluble fractions upon extraction, but the soluble fraction for the 90000 g/mol network was 5.5% (Table 5.1). Even though these free chains were removed before the NMR experiment, one would expect a relatively large fraction of isotropically mobile pendant chains in this network. The Macosko-Miller model for nonlinear polymerization[40-42] estimates the fraction of elastic chains f_{el} in each network (Table 5.2). This analysis predicts that 38% of the chains remaining in the 90000 g/mol network after extraction are tethered only at one end. But this high fraction of non-elastic material in the 90000 g/mol network did not lead to a sharp central peak. The relatively broad center in this case appears to be a consequence of the reduced mobility of the chain segments with increasing viscosity (note that the network fitting parameters γ_n and γ_{melt} are essentially equal). Furthermore, the constraints in this poor quality network do not restrict isotropic segment motion much, since γ_w is less than 20% larger than the melt value. Contrast this with the higher quality 36000 g/mol network where γ_w is nearly twice γ_{melt}, indicating a significant restriction due to the cross-links. Network quality aside, this general trend should be expected since the cross-link density is higher for lower M_n networks.

Despite the wide spectral wings, the spectrum for the 5000 g/mol network is much thinner in the center portion ($\gamma_n = 0.047$) than any of the higher M_n shapes. Here, the soluble fraction is well below 1% and relatively few pendant chains are expected. On the other hand, the number of non-elastic loops for these short chain precursors is large and will influence the center of the spectrum. Increased loop formation in end-linked networks as the molar mass of the precursor chains decreases has been demonstrated by Monte Carlo simulations.[30,43]

5.3.3 Stretched networks: two doublets emerge at high extension

End-linked networks synthesized from low M_n precursor chains are brittle and thus difficult to stretch to high extension before fracture. The 36000 and 90000 g/mol networks proved compliant, however, and could be stretched to more than twice their initial lengths. A doublet in the NMR spectrum emerges with uniaxial extension, as depicted in Figure 5.1. This expected pattern was observed upon slight extension of the 5000 and 11000 g/mol samples. The 36000 g/mol network, meanwhile, began to show a more complex lineshape at high extension. Spectra for this network at $\alpha = 1.98$ and 2.56 are displayed in Figure 5.4. At these high states of strain, a shoulder appears on the outer edge of each doublet.

To analyze this spectral shape, the lineshape was fit to two pairs of peaks. The peak splitting for the wide and narrow doublet are termed $\Delta\nu_w$ and $\Delta\nu_n$, respectively. The outer shoulders are better fit to Gaussian curves, while the inner splitting is modeled by a pair of narrow Lorentzians. The observed shape is consistent with the spectral shape of the unstretched network depicted in Figure 5.3 (a single wider Gaussian and a single narrower Lorentzian). This suggests that the initial undeformed conformation of the cross-linked chains has some effect on the segment alignment at high strain. The outer doublet must result from more highly aligned chain segments. While the lineshape for the 36000 g/mol network (Figure 5.3) lacks wide spectral

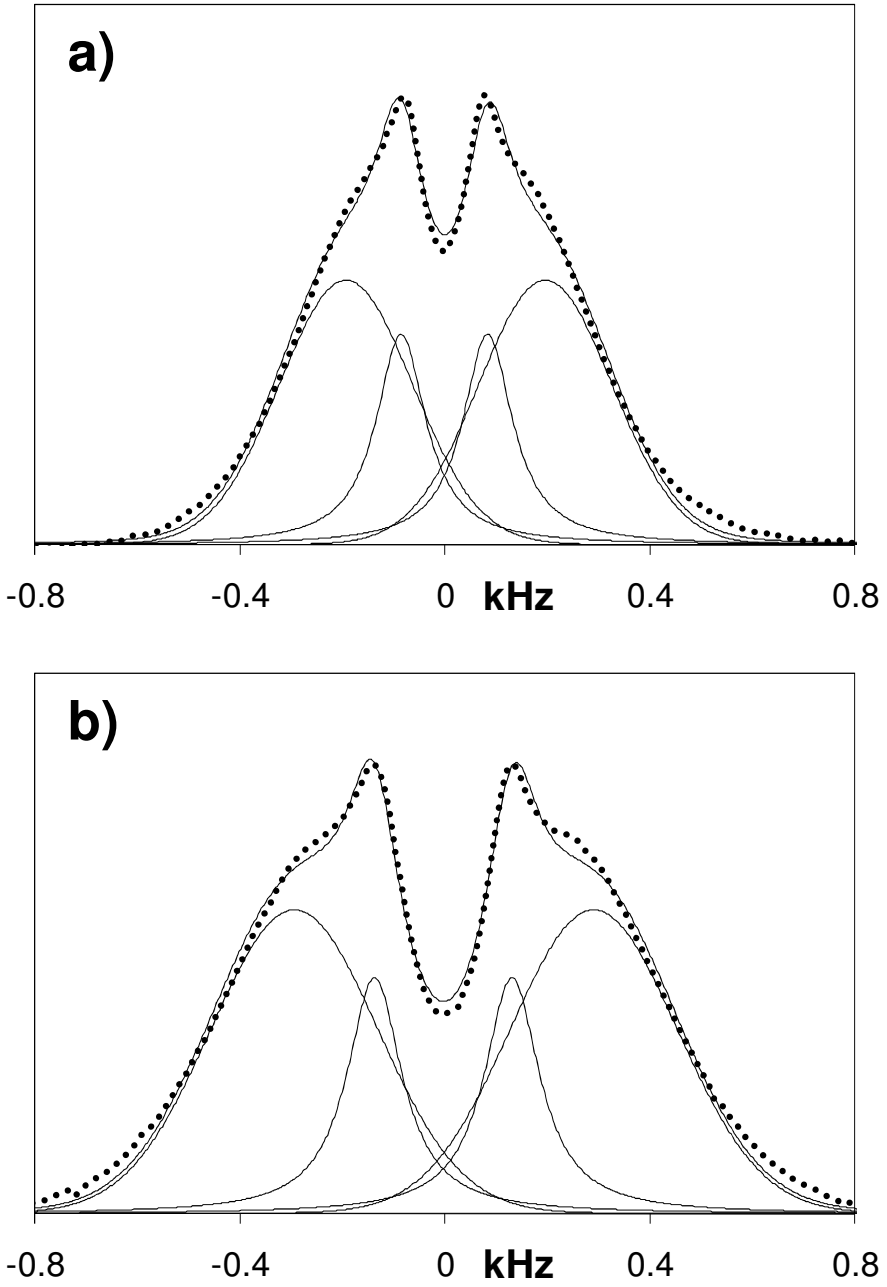

Figure 5.4. ^{2}H-NMR spectra for 36000 g/mol end-linked networks at a) $\alpha = 1.98$ and b) $\alpha = 2.56$. The experimental spectra (dots), doublet fits to each spectrum (lines) and the sum of the doublet pairs (line) are depicted. Note the appearance of a shoulder in the lineshape.

wings and the distribution of segment orientations appears relatively uniform in the unstrained state, a significant fraction of the chains must have their segment orientation constrained by the cross-links.

To attempt to identify the contributions to the outer and inner peaks, the spectra of dissolved free chain samples with increasing extension were examined. Any anisotropic ordering of the segments of these chains can only result from interchain couplings between elastic chains and free chains. A comparison of the spectra of a labeled network and labeled free chains at similar elongation is shown in Figure 5.5. Both the labeled network and the host network for the free chains have similar values of the elastic modulus (Table 5.1). From Figure 5.5, it is clear that the probe chain spectrum shows a single doublet when highly strained. This pair of peaks with separation $\Delta\nu_p$ roughly corresponds to the inner doublet pair $\Delta\nu_n$ displayed by the ^{2}H-labeled network. The outer shoulders from the network spectrum are absent for the free chains. Thus, the wider pair of peaks with splitting $\Delta\nu_w$ must result from the cross-link constraints placed on the elastic chains. The outer tails of these spectra correspond to chains whose segments are quite aligned along the end-to-end distance. A comparison of both $\Delta\nu_n$ and $\Delta\nu_w$ for the cross-linked network with the single peak splitting $\Delta\nu_p$ displayed by the probe chains vs. α^2-1/α is presented in Figure 5.6. Note the close correspondence of the probe chain splitting with the narrower splitting of the elastomer.

The previously unreported lineshape observed here supports the models detailed in the Introduction. Specifically, these models have divided the lineshape into contributions from network constraints and chain interaction.[16-19] As demonstrated in previous experiments[15] and analytical studies[44] and shown in Figure 5.6, there is a correlation between the classically reported $\Delta\nu_n$ values of network chains and unattached free chains. This anisotropic ordering, which is easily monitored by the

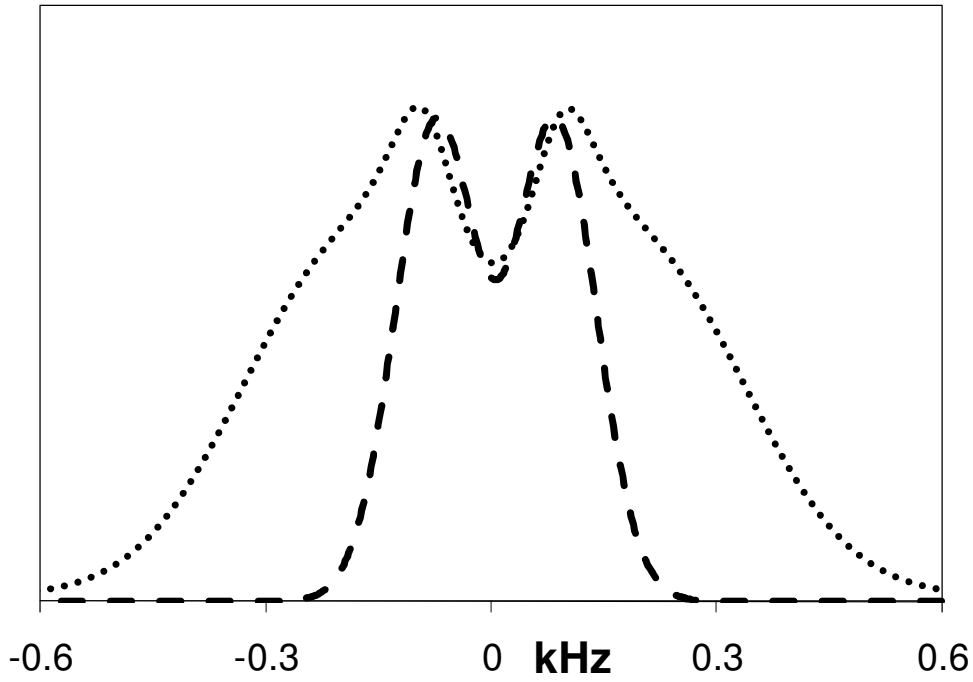

Figure 5.5. Comparison of the ^{2}H-NMR spectra of a 36000 g/mol labeled network at α = 2.03 (dots) and 30000 g/mol labeled free chains dissolved in a 30000 g/mol unlabeled network at α = 2.05 (dashed line). The PDMS networks have similar values of the elastic modulus E. The peak separation for the probe chains is similar to the inner doublet displayed by the network spectrum.

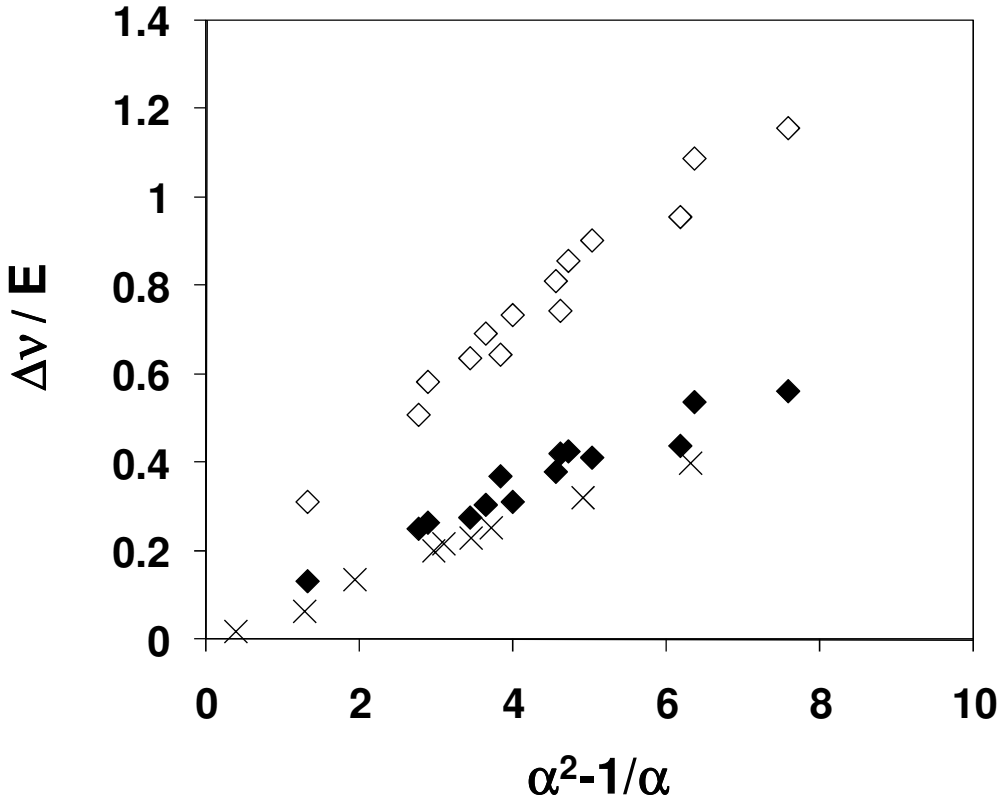

Figure 5.6. Peak separations normalized by elastic modulus vs. α^2-1/α. Diamonds represent splitting of the outer doublet ($\Delta\nu_w$, open symbols) and inner doublet ($\Delta\nu_n$, filled symbols) for the 36000 g/mol labeled network. X corresponds to labeled free chains dissolved in an unlabeled 30000 g/mol network ($\Delta\nu_p$). Note the close match of the $\Delta\nu_n$ and $\Delta\nu_p$ data.

splitting displayed in ^{2}H-NMR spectra upon strain, results from excluded volume interactions. The results presented here show that the contribution to the ^{2}H-NMR signal from the network constraints can become observable separately from the purely excluded volume effect at high extension. The models[16-19] predict that the lineshape for non-interacting phantom networks will simply broaden without splitting upon increasing strain. Therefore, the wider spectral splitting $\Delta\nu_w$ should not imply a splitting independent of the effect of excluded volume interactions. The highly stretched network chains that contribute to the outer shoulder in the spectra must (rather obviously) interact with other chain segments while preferentially orienting along the strain axis. Thus, it appears that this population of ordered segments is subject to an additional inherent potential imposed by the cross-linking that leads to chains with extended end-to-end distances.

To connect to the theoretical models, one can compare the slopes of the $\Delta\nu_n$ and $\Delta\nu_w$ data shown in Figure 5.6. For the outer doublet $(\Delta\nu/E)/(\alpha^2\text{-}1/\alpha) = 0.104$ kHz/MPa, vs. 0.050 for the narrow doublet. This yields a $\Delta\nu_w/\Delta\nu_n$ ratio of 2.08.

In reference 19, the average segment alignment due to the constraints and mean field (i.e. the excluded volume interaction) are termed $P_2(\cos\theta)_{\mathbf{R}}$ and $P_2(\cos\theta)_{\mathbf{V}}$, respectively. According to this model, these can be calculated by:

$$P_2(\cos\theta)_{\mathbf{R}} = \frac{1}{3N}\left(\alpha^2 - \frac{1}{\alpha}\right) \tag{4}$$

$$P_2(\cos\theta)_{\mathbf{V}} = \frac{1}{15N\pi}\frac{b}{\xi}\left(\alpha^2 - \frac{1}{\alpha}\right) \tag{5}$$

where N is the number of statistical segments of size b between each junction, and ξ is the Edwards screening length. For PDMS, the ratio b/ξ has been estimated to be 4.[44] Thus, the model predicts $P_2(\cos\theta)_{\mathbf{R}}/P_2(\cos\theta)_{\mathbf{V}} = 3.9$, almost twice the experimental $\Delta\nu_w/\Delta\nu_n$ ratio. The primary reason for the discrepancy is likely the model's

assumption of affine deformation at the molecular scale. Since the actual chain deformation is sub-affine, less segmental alignment should result than predicted by the above model. Another factor that may contribute to this discrepancy is the empirical fitting procedure used on the experimental spectra. While $\Delta\nu_w$ and $\Delta\nu_n$ were calculated from the peak locations of the curves used to fit the data, the average degree of order of a distribution does not always correspond with the peak position. The spectral wings resulting from the network constraints might lead to higher average values of segmental order than measured by the peak locations.

5.4 Conclusions

^{2}H-NMR lineshapes of end-linked networks evolve with precursor chain molar mass. These spectra were analyzed for unstretched and stretched elastomers to elucidate information about ordering of chain segments. Shorter elastic chains must extend to cross-link, which causes spectral wings in the ^{2}H-NMR lineshape. These wings form the super-Lorentzian lineshape commonly reported for PDMS elastomers in the unstrained state. This residual segmental orientation is quantified by the larger peak width at half-height of the short chain networks as compared to the uncross-linked precursors. The distribution of order parameters in longer network chains is more uniform. Thus, the lineshape of the labeled networks made from larger molar mass precursors is pseudo-Gaussian, exhibiting a broader center and a less prominent contribution from the high frequency wings. This indicates that the longer chains are less perturbed from their random melt conformations upon cross-linking than the network chains cross-linked from smaller precursors.

When long-chain elastomer samples are highly stretched, the lineshape can show two populations of segmental order. Both populations become more ordered with increasing strain. Since the distribution with smaller average order can be

mimicked by labeled free chains dissolved in an unlabeled network, the more highly ordered chain segments are shown to result from the elastic constraints induced during the cross-linking. This high degree of order is attributed to segments on chains that are stretched to a large end-to-end distance. The distance between the peaks in the narrower splitting are due to excluded volume interactions between neighboring chains. These peaks correspond to the quadrupolar splittings $\Delta\nu$ measured in previous experimental studies.

The lower molar mass networks, meanwhile, could not be deformed to high extension. In the limited elongation ratios accessible for the 5000 and 11000 g/mol networks, it was not possible to observe a clear outer doublet. It appears that the chain segment orientations that are highly influenced by the cross-linking contribute to the long spectral wings here, which widen further upon deformation but cannot be separated into a second doublet at the elongation ratios accessible before fracture.

These changes in lineshape with molar mass in both the stretched and unstrained state demonstrate the wealth of information contained in the entire spectrum. While the fitting procedure detailed here has proven useful to analyze the entire ^{2}H-NMR spectrum of an elastomer, it is desirable to measure the average segmental alignment and generate the full probability distribution. In the following chapter, an approach that allows for estimation of these properties directly from each spectrum[45] is applied to unimodal and bimodal networks.

REFERENCES

1. Abragam, A. *The Principles of Nuclear Magnetism*; Clarendon Press: Oxford, 1961.

2. Mark J. E.; Erman, B. *Rubberlike Elasticity: A Molecular Primer*; Wiley-Interscience: New York, 1988.

3. Jelinski, L. *Annu. Rev. Mater. Sci.* **1985**, *15*, 359-377.

4. Deloche, B.; Beltzung, M.; Herz, J. *J. Phys. (Paris), Lett.* **1982**, *43*, 763-769.

5. Gronski, W.; Stadler, R.; Jacobi M. M. *Macromolecules* **1984**, *17*, 741-748.

6. Gronski, W.; Emeis, D.; Brüderlin, A.; Jacobi, M. M.; Stadler, R. *Br. Polym. J.* **1985**, *17*, 103-110.

7. Flory, P. J. *Principles of Polymer Chemistry*; Cornell University Press: Ithaca, NY, 1953.

8. Kuhn, W.; Grün, F. *Kolloid Z.* **1942**, *101*, 248-271.

9. Deloche, B.; Samulski, E. T. *Macromolecules* **1981**, *14*, 575-581.

10. Dubault, A.; Deloche, B.; Herz, J. *Polymer* **1984**, *25*, 1405-1410.

11. Toriumi, H.; Deloche, B.; Herz, J.; Samulski, E.T. *Macromolecules* **1985**, *18*, 304-305.

12. Deloche, B.; Dubault, A.; Herz, J.; Lapp, A. *Europhys. Lett.* **1986**, *1*, 629-635.

13. Sotta, P.; Deloche, B.; Herz, J.; Lapp, A.; Durand, D.; Rabadeux, J. C. *Macromolecules* **1987**, *20*, 2769-2774.

14. Kornfield, J. A.; Chung, G.; Smith, S. *Macromolecules* **1992**, *25*, 4442-4444.

15. McLoughlin, K.; Waldbieser, J. K.; Cohen, C.; Duncan, T.M. *Macromolecules* **1997**, *30*, 1044-1052.

16. Sotta, P.; Deloche, B. *Macromolecules* **1990**, *23*, 1999-2007.

17. Brereton, M. G. *Macromolecules* **1993**, *26*, 1152-1157.

18. Warner, M.; Callaghan, P. T.; Samulski, E. T.; *Macromolecules* **1997**, *30*, 4733-4736.

19. Ries, M. E.; Brereton, M. G.; Klein, P. G.; Ward, I. M.; Ekanayake, P.; Menge, H.; Schneider, H. *Macromolecules* **1999**, *32*, 4961-4968.

20. Depner, M.; Deloche, B.; Sotta, P. *Macromolecules* **1994**, *27*, 5192-5199.

21. Sotta, P.; Higgs, P. G.; Depner, M.; Deloche, B. *Macromolecules* **1995**, *28*, 7208-7214.

22. Sotta, P. *Macromolecules* **1998**, *31*, 8417-8422.

23. Poon, C.; Samulski, E. T. *Makromol. Chem.-M. Symp.* **1990**, *40*, 109-120.

24. Poon, C.; Samulski, E. T. *J. Non-Cryst. Solids* **1991**, *131*, 509-515.

25. Gronski, W.; Forster, F.; Pyckhout-Hintzen, W.; Springer, T. *Makromol. Chem.-M. Symp.* **1990**, *40*, 121-137.

26. Sotta, P. *Macromolecules* **1998**, *31*, 3872-3879.

27. Yong, C. W.; Higgs, P. G. *Macromolecules* **1999**, *32*, 5062-5071.

28. Lee, C. L.; Johannson, O. K. *J. Polym. Sci., Polym. Chem.* **1976**, *14*, 729-742.

29. Lee, C. L.; Marko, O. W.; Johannson, O. K. *J. Polym. Sci., Polym. Chem.* **1976**, *14*, 743-758.

30. Genesky, G. D.; Aguilera-Mercado, B. M.; Bhawe, D. M.; Escobedo, F. A.; Cohen, C. *Macromolecules* **2008**, *41*, 8231-8241.

31. Beltzung, M.; Picot, C.; Rempp, P.; Herz, J. *Macromolecules* **1982**, *15*, 1594-1600.

32. Lapp, A.; Herz, J.; Strazielle, C. *Makromol. Chem.* **1985**, *186*, 1919-1934.

33. Patel, S. K.; Malone, S.; Cohen, C.; Gillmor, J.; Colby, R. *Macromolecules* **1992**, *25*, 5241–5251.

34. Takahashi, H.; Shibyama, M.; Fujisawa, H.; Noruma, S. *Macromolecules* **1995**, *28*, 8824–8828.

35. Weiss, P.; Herz, J.; Rempp, P. *Makromol. Chem.* **1970**, *135*, 249-261.

36. Hedden, R. C.; Tachibana, H.; Duncan, T. M.; Cohen, C. *Macromolecules* **2001**, *34*, 5540-5546.

37. Saalwächter, K.; Ziegler, P.; Spyckerelle, O.; Haidar, B.; Vidal, A.; Sommer, J.-U. *J. Chem. Phys.* **2003**, *119*, 3468–3482.

38. Saalwächter, K.; Kleinschmidt, F.; Sommer, J.-U. *Macromolecules* **2004**, *37*, 8556-8568.

39. Saalwächter, K.; Sommer, J.-U. *Macromol. Rapid Comm.* **2007**, *28*, 1455-1465.

40. Macosko, C. W.; Miller, D. R. *Macromolecules* **1976**, *9*, 199-206.

41. Miller, D. R.; Macosko, C. W. *Macromolecules* **1976**, 9, 206-211.

42. Miller, D. R.; Valles, E. M.; Macosko, C. W. *Polym. Eng. Sci.* **1979**, *19*, 272-283.

43. Gilra, N.; Cohen, C.; Panagiotopoulos, A. Z. *J. Chem. Phys.* **2000**, *112*, 6910-6916.

44. Brereton, M. G.; Ries, M. E. *Macromolecules* **1996**, *29*, 2644-2651.

45. Aguilera-Mercado, B. M.; Cohen, C.; Escobedo, F.A. submitted to *Macromolecules*.

CHAPTER 6

^{2}H-NMR STUDIES OF CHAIN SEGMENT ORIENTATION IN PDMS BIMODAL NETWORKS*

6.1 Introduction

Given the great interest in the structure and properties of bimodal networks and the ability of ^{2}H-NMR experiments to monitor either the short or long chains through selective labeling, relatively few ^{2}H-NMR studies have been performed on this type of elastomer. Chapellier et al.[1,2] and Sotta[3] selectively labeled 3000 and 25000 g/mol PDMS chains and monitored the peak splittings $\Delta\nu$, concluding that the short and long chain segments experienced a similar degree of orientation with increasing strain. However, bimodal networks have been found to display enhanced mechanical properties only when the precursor molar masses differ by at least a factor of 10.[4,5] The relatively small (~8x) difference in molar masses employed by these authors was not an appropriate case to correlate segmental orientation with macroscopic properties in bimodal elastomers.

Other experimental methods have also been used to probe chain segment orientation in bimodal networks. Stress-optical studies have noted non-linearity in plots of birefringence vs. true stress.[6-8] This effect becomes more pronounced with increasing short chain concentration, suggesting changes in spatial heterogeneity with composition.[7] Infrared dichromism studies have found a similar degree of segment orientation for the short and long chains in polytetrahydrofuran networks,[9] but an increased ordering for the short chains when they occupy a majority of the volume of a

bimodal PDMS network.[10] A higher degree of segmental order has also been found for the short chains using Monte Carlo (MC) simulations.[11] More recently, multiple quantum (MQ) NMR has been utilized to elucidate the distribution function of local chain order in elastomers.[12] This method reveals that the distribution has two components for bimodal networks in the unstretched state,[13,14] suggesting a heterogeneous structure brought about by the differences in precursor chain lengths. However, MQ-NMR spectroscopy has yet to be applied to uniaxially stretched bimodal networks to monitor chain segment orientation of each component with strain.

In this chapter, a systematic ^{2}H-NMR study of model PDMS bimodal networks is presented. These well characterized elastomers contain selectively deuterated short or long chains to monitor the degree of chain segment orientation of each component in both the unstrained and highly stretched states. Although the spectra for stretched networks split into two peaks symmetric about $\nu = 0$, the segment orientation is not well described by these peak locations. The average absolute value of the complete spectrum $\langle|\nu|\rangle$ is computed since it better represents the ordering of all PDMS chain segments. Then, a recent method based on the maximum entropy method (MEM) allows for the calculation of the average segmental alignment $\langle\nu\rangle$ of both short and long chains and the full probability distribution of each.[15] This $\langle\nu\rangle$ describes the widening of the lineshape due to one of the two NMR transitions for ^{2}H, a spin-1 nucleus. These results are compared to previously reported MC simulations of average segmental order $\langle S\rangle$ in PDMS elastomers.[16] Variations in the ^{2}H-NMR response at different bimodal compositions are related to changes in the network microstructure and the resulting macroscopic properties.

6.2 Procedures

6.2.1 Experimental Procedures

Both hydrogenated and randomly deuterated PDMS precursor chains were synthesized using methods detailed in Section 2.2.1. Number average molar masses were determined to be 5500 (^{1}H), 80000 (^{1}H), 5000 (^{2}H), and 90000 (^{2}H) g/mol by gel permeation chromatography (GPC). These chains were measured and combined into 5000-80000 and 5500-90000 g/mol selectively labeled bimodal blends at the desired compositions (60-98 mol % short chains). To synthesize unimodal networks, 11000 (^{2}H), 30000 (^{1}H, ^{2}H), and 36000 (^{2}H) g/mol chains were used. The polydispersity index of all chains was 1.32 or lower. For both unimodal and bimodal networks, tetrakis(dimethylsiloxy)silane cross-linker was added such that the ratio of cross-linking arms to polymer chain ends was 1.7 to form networks of the highest possible quality.[17] Since this optimal ratio is smaller for shorter precursor chains,[18] it was reduced to 1.5 for the 5000 g/mol unimodal sample only. In one network, 36000 g/mol chains were mixed with non-reactive 2000 g/mol chains at a 70/30 mass % ratio before cross-linking. This network was tested in the preparation state (36000p) and in the dry state after extraction of the free chains (36000d). The PDMS/crosslinker mixtures were well-stirred with a spatula and mixed on a rotator overnight for homogeneous distribution of the components. Network formation was carried out upon addition of cis-dichlorobis(diethylsulfide)platinum(II) using the methods detailed in Section 2.2.2. Equilibrium mass swell Q, soluble fraction w_{sol}, and elastic modulus E of the fully cured elastomers were all determined by following previously reported techniques.[16] The E value for 36000p was calculated from that of 36000d by multiplying the latter by the polymer volume fraction in the prepared state raised to

the 1/3 power.[19] These bimodal and unimodal network properties are reported in Table 6.1. ^{2}H-NMR data were obtained on a Tecmag Apollo HF spectrometer operating at 30.72 MHz for deuterium by employing a 5μs 90^o pulse. Methods for processing these data are described in Section 5.2.2.

6.2.2 Calculation of the average chain segment order <ν>

A recently reported method allows for the calculation of <ν> for chain segments in a polymer network.[15] <ν> is valuable to understand chain segment alignment since the quadrupolar splitting Δν induced at high elongation has been shown to result from excluded volume interactions between interacting chains.[20-23] This new methodology accounts for both excluded volume and constraints imposed by the cross-links within a given network. The method considers the full observed ^{2}H-NMR lineshape, including the wide spectral wings often observed for PDMS elastomers.[24,25] To calculate <ν>, the first step is to compute the average absolute value <|ν|> from the spectrum using the relation:[15]

$$\langle|\upsilon|\rangle = \frac{\sum f(\upsilon)|\upsilon|}{\sum f(\upsilon)} \tag{1}$$

where f(ν) is the ^{2}H-NMR signal at frequency ν, and the sum is over the entire spectrum. Then, the average chain segment order <ν> is calculated from[15]

$$\langle|\upsilon|\rangle / \langle|\upsilon|\rangle_0 \cong \langle\upsilon\rangle / \langle|\upsilon|\rangle_0 + \exp\left(-\langle\upsilon\rangle / \langle|\upsilon|\rangle_0\right) \tag{2}$$

where $<|\nu|>_0$ is the average absolute value of the unstrained sample.

Table 6.1. ^{2}H-network compositions and properties

5000(^{2}H)-80000 g/mol bimodal networks

mol % short chains	Q	E(MPa)	w_{sol} (mass %)	$\langle\|\nu\|\rangle_0$ (Hz)	q* (Hz/MPa)
60	4.76	0.59	1.72	193	31.1
70	4.53	0.64	1.49	205	66.6
80	4.21	0.73	1.61	209	56.3
90	3.65	0.93	0.88	260	81.5
95	3.26	1.14	1.13	282	112.0
98	3.17	1.20	1.92	230	-

5500-90000(^{2}H) g/mol bimodal networks

mol % short chains	Q	E(MPa)	w_{sol} (mass %)	$\langle\|\nu\|\rangle_0$ (Hz)	q* (Hz/MPa)
60	5.24	0.49	2.18	81	71.6
70	4.68	0.60	1.82	89	72.0
80	4.09	0.76	1.01	85	71.9
90	3.99	0.80	2.31	84	65.2
95	3.78	0.88	2.46	87	49.9

Table 6.1 (Continued)
unimodal networks

M_n (g/mol)	Q	E(MPa)	w_{sol} (mass %)	$\langle\|\nu\|\rangle_0$ (Hz)	q* (Hz/MPa)
5000	3.02	1.30	0.59	181	54.5
11000	3.39	1.06	0.80	169	93.3
36000	4.64	0.61	1.45	96	65.0
90000	7.31	0.27	5.48	77	106.5
30000**	4.55	0.63	2.36	47	26.3
36000d***	5.98	0.39	1.46	107	73.3
36000p***	-	0.35****	-	103	80.6

*q = slope of best fit line through $(\langle\nu\rangle/E)/(\alpha^2-1/\alpha)$
**Consists of unlabeled elastic chains and ^{2}H-labeled probe chains, both with M_n = 30000 g/mol. Unlabeled soluble material was extracted before dissolution of labeled free chains.
***Unimodal network made with 70 mass % 36000 g/mol ^{2}H-labeled precursor chains and 30 % 2000 g/mol non-reactive and unlabeled "solvent" chains. ^{2}H-NMR experiments were performed on networks in the prepared state (p) and in the dry state after extraction of the solvent chains (d).
****Elastic modulus of network in the prepared state calculated from E of the dry network as detailed in the text.

6.3 Results and Discussion

6.3.1 Unstrained bimodal networks

^{2}H-NMR spectra for undeformed bimodal networks with selectively labeled short and long chains are shown in Figures 6.1a and 6.1b, respectively. All spectra are plotted with equal peak heights to emphasize the relative contributions from the center portion of the lineshape and the high frequency spectral wings. Comparison of Figures 6.1a and 6.1b demonstrates the different lineshape characteristics for the 5000 and 90000 g/mol chains. While the short-chain spectra have wide wings that form the "super-Lorentzian" shape typically observed for PDMS networks,[24,25] the long-chain lineshapes are relatively broad in the center but tail off rather quickly. Since the spectral wings correspond to the portion of the segment order distribution that is associated with more highly stretched chains, the 5000 g/mol lineshape is attributed to a higher proportion of these chains cross-linking while they are in a conformation with relatively high end-to-end distance. The long network chains, meanwhile, appear to be less perturbed from their melt configurations. Figure 6.1 reveals that these general lineshapes persist for 5000 and 90000 g/mol chains when they are incorporated into bimodal networks.

However, it is immediately clear from these figures that the lineshape of the short chain segments evolves with network composition, while the lineshapes of the long chains appear unchanged as their concentration is varied. Closer inspection of Figure 6.1a reveals that the prominence of the spectral wings for short chain segments in bimodal networks does not vary with the percentage of short chains in the network. Instead, the wings increasingly contribute to the spectra as the short chain content is increased from 60 to 90 mol %, then shrink at 98 mol % and for the unimodal short chain network (100 mol %). This trend also holds for the labeled short chain networks

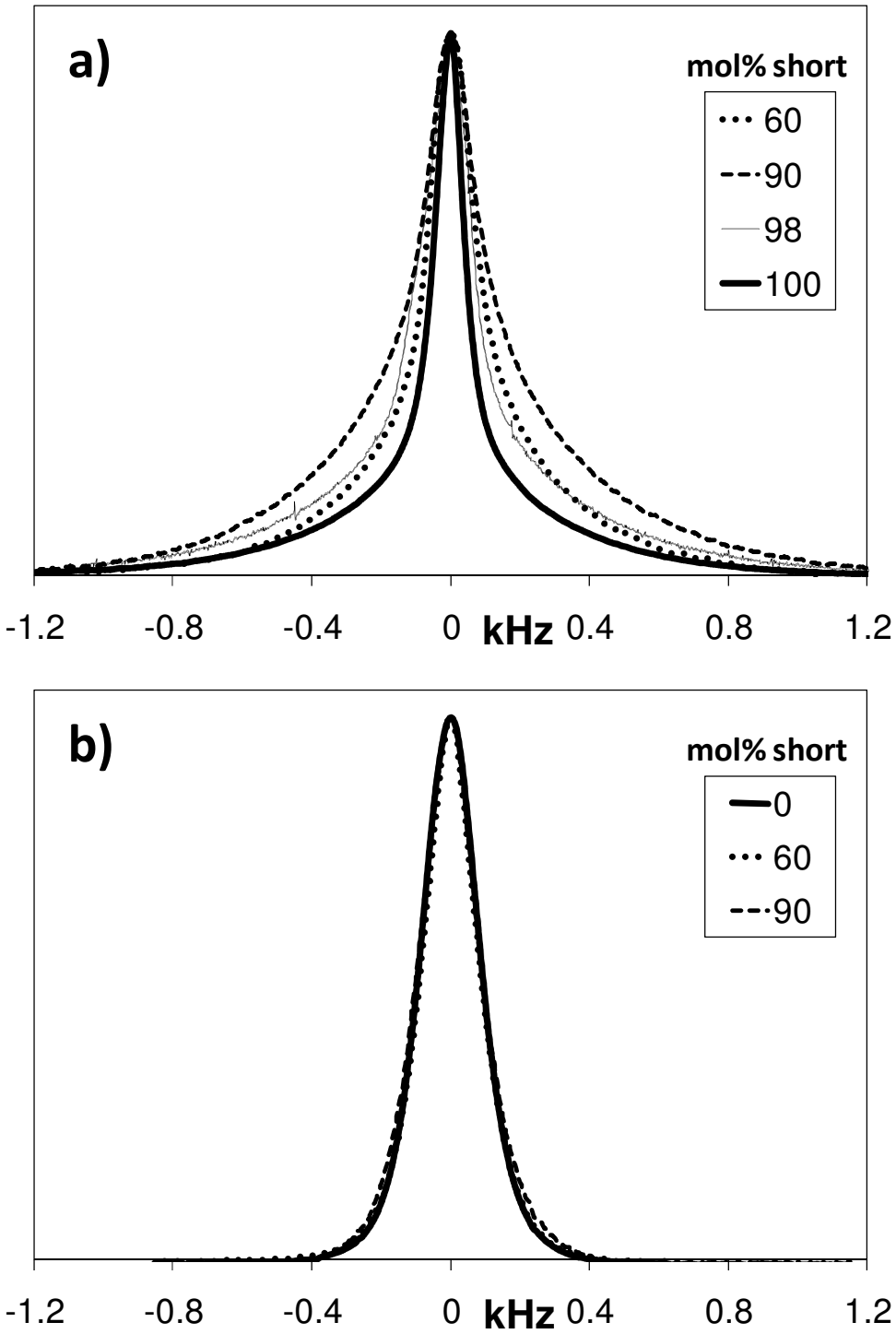

Figure 6.1. ^{2}H-NMR spectra for a) short (5000 g/mol) and b) long (90000 g/mol) chain segments in bimodal networks. Spectra are measured on samples in the unstrained state and are normalized by peak height.

(70, 80, 95 mol %) that were omitted from the figure for clarity. These results are quantified in Figure 6.2, where the average absolute values $\langle|\nu|\rangle_0$ (equation 1) for short and long chains in the network are plotted against mol % of short chains.

The nearly constant lineshape for the long chains in Figure 6.1b is well described by the constant value of $\langle|\nu|\rangle_0$ across all concentrations in Figure 6.2. Thus, the residual segmental order imposed on the long chains during cross-linking is not affected by the introduction of a bimodal distribution of chain lengths. Long chains also showed similar segmental order parameter distributions across a variety of bimodal network compositions in recent MQ-NMR studies of 800-47000 g/mol PDMS elastomers.[13,14] In unimodal 90000 g/mol networks, the lineshape broadens only slightly upon network formation since the cross-link concentration is low, and the network chains are perturbed negligibly from their random coiled states (Chapter 5). This persists in bimodal networks even with the increase in cross-linking density caused by the introduction of short chains. The 90000 g/mol chains likely react with the nearest cross-linker without much change in their melt state segmental order or end-to-end distance.

The short chains, on the other hand, are clearly affected by incorporation into the bimodal network. The variation in the spectral wings appears to be a consequence of changes in the network topology with short chain concentration. MC simulations have demonstrated an increased intermolecular pair distribution function g(r) upon cross-linking for 60 mol % short chain bimodal networks with similar molar masses to those employed in these experiments.[16] Therefore, the short chains can aggregate into heterogeneous domains when their concentrations are relatively low due to the faster diffusion of the mobile chains and cross-linkers in mixture. Clustering has also been observed for networks with low short chain concentrations via SANS[26,27] and light scattering.[28] Therefore, it is not surprising that the lineshapes for the 60 and 100 mol

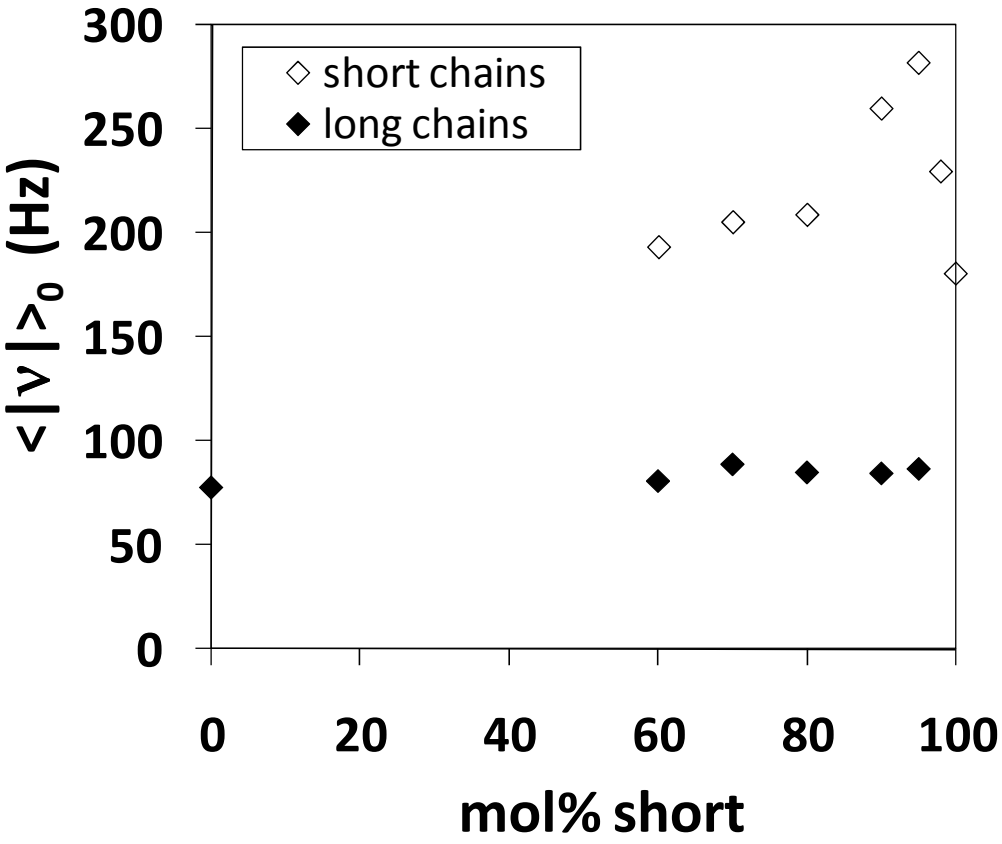

Figure 6.2. Average absolute value for unstretched bimodal networks $\langle|\nu|\rangle_0$ with varying short chain concentration.

% short chain networks are similar ($<|\nu|>_0$ = 193 and 181 Hz) even though the network compositions are very different. Since the short chains form clusters in the 60 mol % network, most of a given short chain's neighbors are other short chains and the cross-link density in their vicinity is quite high. Thus, the segmental order of these chains is affected negligibly by the presence of the long chains, and the microstructure can be pictured as small domains of 5000 g/mol unimodal network dispersed in a unimodal network of long chains. The similarity of 98 and 100 mol % short chain spectra, meanwhile, is expected given the similar number of the 5000 g/mol chains in each system. The smaller chains dominate the volume of the network in this bimodal system. Consequently, one would suspect the long chains to be intermittently woven into an interconnected skeleton of short chains that spans the whole network. The 90 and 95 mol % networks have the most prominent spectral wings in Figures 6.1a and 6.2, indicating a greater degree of motional restriction on their short chain segments. At these concentrations the short chains are near their overlap concentrations in a 5000-80000 g/mol system. Thus, it appears that the lower molar mass chains in these networks do not form small clusters, but instead reach cross-linker arms when they are slightly elongated from their random states. Here, the difference in residual segmental order between the short and long chain segments is at a maximum (Figure 6.2).

6.3.2 Stretched bimodal networks

Both experiments[22] and mathematical models[20,21,23] have established that the quadrupolar splitting $\Delta\nu$ induced at high extension is the result of excluded volume interactions between chain segments. When normalized by the elastic modulus E, $\Delta\nu$ has been shown to follow a universal relationship with α^2-1/α.[22] The close match of all $\Delta\nu$/E data with increasing strain between short, long and unimodal chain segments (Section 6.3.3) demonstrates that this universal correlation persists for bimodal networks. However, additional details of the ^{2}H-NMR lineshape describe network

chains that are greatly affected by the network constraints.[29,30] Specifically, the outer frequency portions of the lineshape have been associated with more ordered chain segments with less motionally averaged orientations since these wings represent the tail of the order parameter probability distribution.

Figure 6.3 further illustrates why the peak frequency split $\Delta\nu$ is not useful as a measure of the average segmental order. While the short chains in the 60 and 90 mol % networks each have a similar $\Delta\nu$ value in the plotted spectra, the wings are noticeably more prominent in the latter. Therefore, the higher proportion of ordered chain segments found in the rest state for the 90 mol % short chain elastomer (Figure 6.1a) continues as the network is extended. Clearly, the initial chain conformations have a significant effect on the segmental order induced upon loading. Due to these differences in lineshape, equation 2 was used to calculate the average segmental order $\langle\nu\rangle$ for the 60 and 90 mol % short chain bimodal networks at various elongation ratios. The results are normalized by the corresponding elastic modulus and displayed in Figure 6.4 against the average segmental order resulting from intersegmental interactions (section 6.3.3). These data are compared to $\frac{1}{2}\Delta\nu/E$ here since the two peaks in a ^{2}H-NMR spectrum are the result of the order parameter distribution and its mirror image reflected about $\nu = 0$.[30] While the trend for the 60 mol % short chain sample is noisy due to the lower ^{2}H content in this network, it follows the $\frac{1}{2}\Delta\nu/E$ trend more closely than the 90 mol % network. Consequently, the segmental order of short chains in the 60 mol % network is less influenced by chains with large end-to-end distances, but is instead dominated by excluded volume interactions between segments.

Since either the short or long chains have been selectively labeled in these bimodal networks, it is instructive to compare the segmental order of each with increasing sample elongation. These plots of $\langle\nu\rangle/E$ vs. α^2-1/α are displayed for 60,

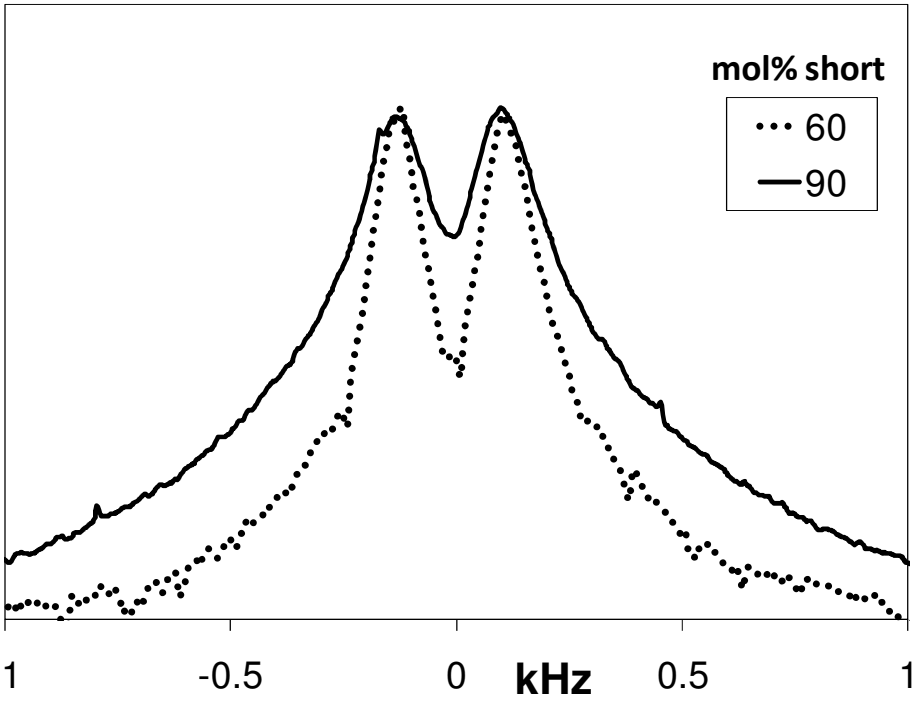

Figure 6.3. Bimodal networks at 60 and 90 mol % ^{2}H-labeled short chains (α = 2.43 and 1.81, respectively) have similar spectral splitting $\Delta\nu$ but different overall lineshapes. The wide spectral wings in the 90 mol % network are indicative of a large contribution from highly stretched chains.

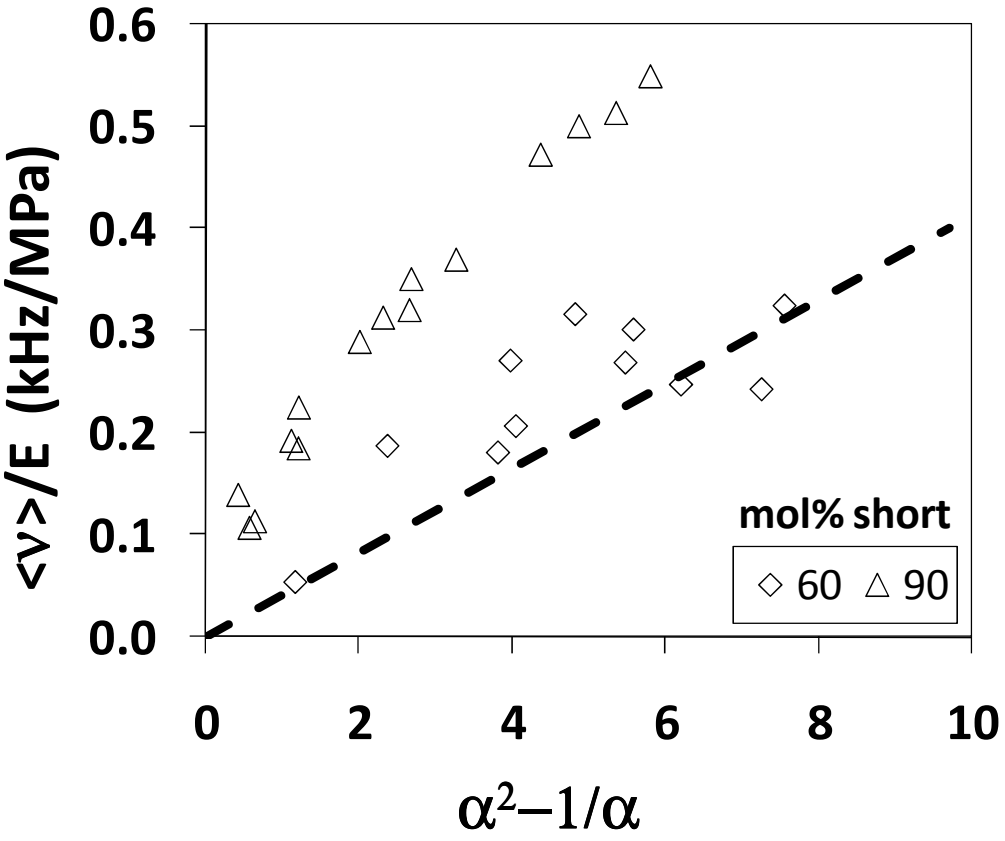

Figure 6.4. Average segmental order <ν> normalized by elastic modulus E for bimodal networks at 60 and 90 mol % ^{2}H-labeled short chains at increasing extension. The 60 mol % short chain segments follow approximately the universal curve for excluded volume interactions between chain segments ½Δν/E (dashed line). The average order is much higher for the short chains in the 90 mol % network due to its wide spectral wings.

70, 90 and 95 mol % short chain networks in Figure 6.5. The segmental orientation of the short chains gains on and surpasses that of the long chains as the short-chain concentration increases. At 60 mol % short chains, the clustered chains appear to be shielded from order by the more compliant long chain matrix. As detailed in Chapter 2, such highly heterogeneous networks do not show enhanced macroscopic properties, and the results of Figure 6.5a reinforce this view. If short chain clusters were to aid in the toughening of these elastomers, they would have to sustain a significant portion of the applied load. Instead, the ordering of these segments appears to primarily result from interchain segmental interactions (Figure 6.4). Previous MC simulations have predicted an identical order parameter S for both chains upon uniaxial deformation of a 60 mol % network.[16] In these experiments, this equivalence is achieved at 70 mol % short chains (Figure 6.5b), so the agreement with simulation results is quite reasonable. Beyond this point, segments on the smaller chains are more aligned than those from the long chains. The results for the 90 mol % short chain networks (Figure 6.5c) also follow the trends observed in the aforementioned simulations.

Networks at 90-95 mol % short chains display the greatest enhancement in mechanical properties[4,5,16,31] because further addition of short chains leads to very brittle samples. Note that even the 95 mol % short chain network breaks at a small value of α (Figure 6.5d). Increased ordering of the short chain segments appears to play a role in generating the stress upturn at high strain and increased toughness of these networks. Thus, the limited extensibility of the 90-95 mol % short chains must be the primary cause of the improved mechanical properties. While $\langle v \rangle$ is not a direct measure of end-to-end distance, the prominent spectral wings in the 90 mol % network (Figure 6.3) suggest that a significant portion of the orientation is due to segments on chains that are highly stretched by the movement of the cross-links. In fact, MC

Figure 6.5. Average segmental order <v> normalized by elastic modulus E for short (open squares) and long (filled squares) chain segments in a) 60 b) 70 c) 90 and d) 95 mol % short chain bimodal networks. The segment orientation of the short chains increases relative to the long chains as their concentration is increased.

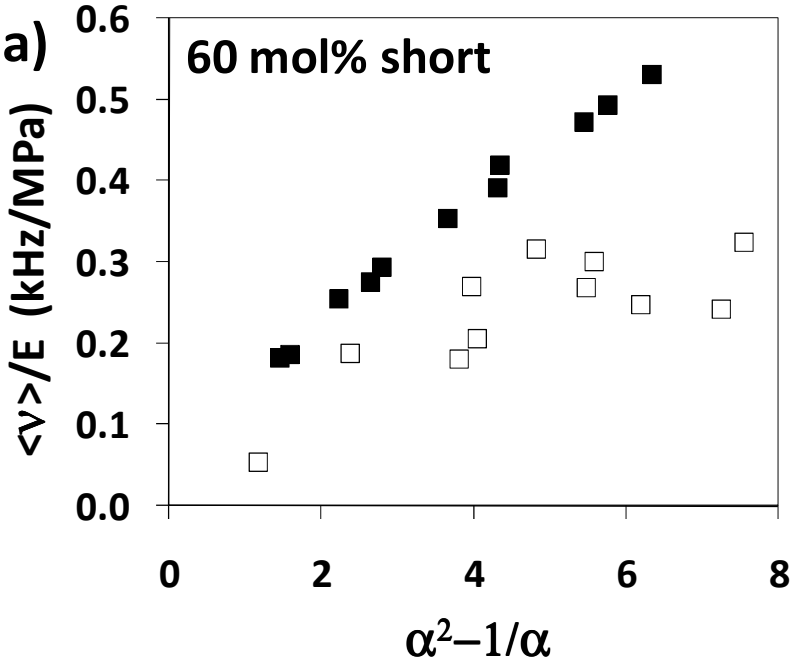
a)
60 mol% short
<ν>/E (kHz/MPa)
0.6
0.5
0.4
0.3
0.2
0.1
0.0
0
2
4
6
8
α²–1/α

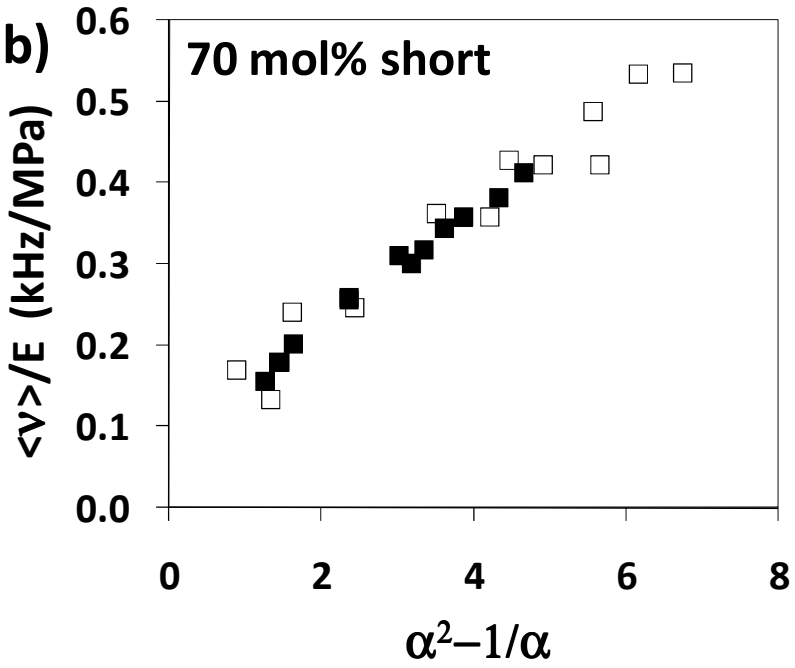
b)
70 mol% short
<ν>/E (kHz/MPa)
0.6
0.5
0.4
0.3
0.2
0.1
0.0
0
2
4
6
8
α²–1/α

Figure 6.5 (Continued)

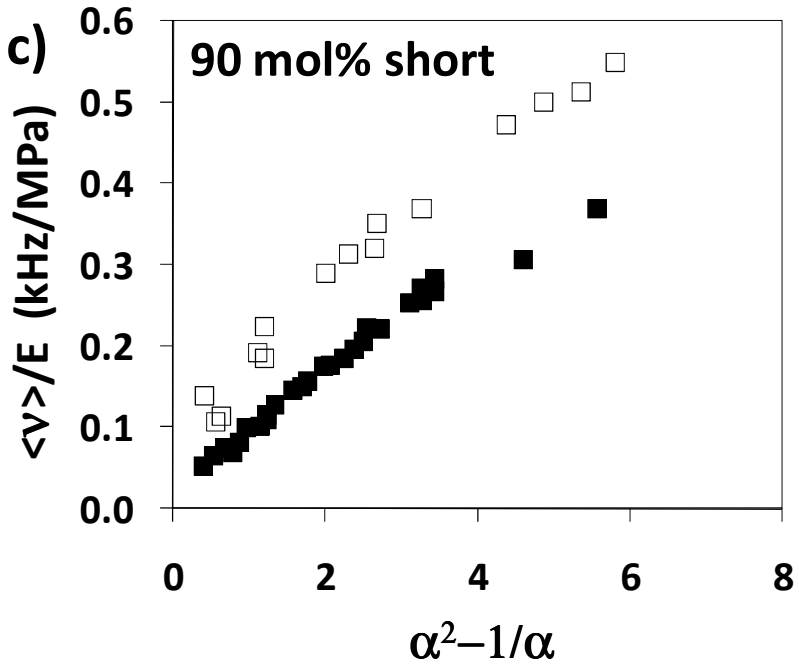

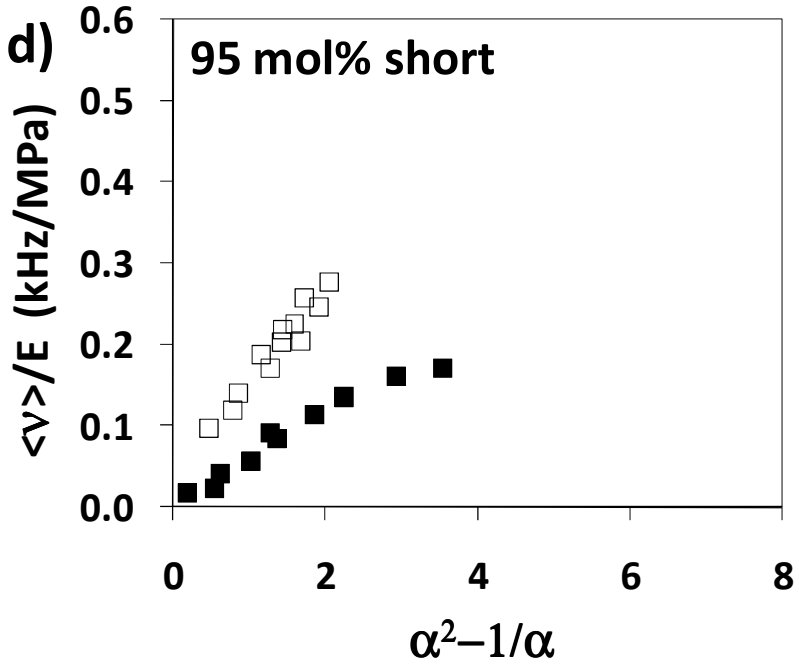

simulations have indicated that short-chain end-to-end distances in 90 mol % networks increase markedly with uniaxial elongation as compared to those in 60 mol % short chain networks.[16] Increased residual order upon cross-linking for the short chains in the 90 and 95 mol % networks (Figures 6.1a, 6.2) predisposes some of these chain segments to such a highly aligned state upon stretching.

While these results suggest that the extensibility of the short chains is a key factor in the enhanced mechanical properties of bimodal networks, note that MC simulations have predicted that some degree of topological heterogeneity is likely at compositions around 90 mol % short chains.[16] Additionally, the overall order parameter distribution in 800-47000 g/mol networks measured by MQ-NMR has a bimodal character up to relatively high short chain concentrations, suggesting a slightly heterogeneous structure.[13,14] Thus, while relatively concentrated short chains in a 90 mol % network will not form small clusters, there are likely regions within such networks with higher cross-link densities. At this bimodal network composition, pockets with larger concentrations of long chains interspersed amongst the overall stiffer matrix would likely provide ductility. Such a structure might explain why the 90 mol % short chain network (Figure 6.5c) could be stretched to nearly the same elongation at fracture as the 60 or 70 mol % networks (Figures 6.5a, 6.5b) even with the associated increase in cross-link density.

Given both the wide disparity in chain lengths and the changes in microstructure argued for here, it seems unlikely that classical elasticity theories could effectively describe these bimodal networks. These theories[19,32] predict that the average order parameter $\langle S \rangle$ is directly proportional to $E(\alpha^2 - 1/\alpha)$. Since $\langle \nu \rangle$ is a measure of $\langle S \rangle$, plots of $\langle \nu \rangle / E$ vs. $\alpha^2 - 1/\alpha$ should follow a universal trend. Defining the slope of this line to be q and taking the best fit line through the data, it is clear

from Table 6.1 that this relationship does not hold even for unimodal networks. This is unlike the case of previously reported $\Delta\nu/E$ vs. α^2-1/α data that follow the expected trend rather well.[22] Nonetheless, the average q for unimodal networks listed in Table 6.1 is calculated to be 80 +/- 24 Hz/MPa. While many of the q values for both short and long chains in bimodal networks fall within this standard deviation, there is a clear redistribution of chain segment orientation with short chain concentration as detailed in Figure 6.5. This effect is nicely quantified by the plot of q vs. mol % short chains displayed in Figure 6.6. Computation of the overall average q for each bimodal network is then performed by weighing the slopes for both the short and long chains (Figure 6.5) by their respective mass fractions within each network. These weighted averages yield a consistent average value of $(\langle\nu\rangle/E)/(\alpha^2-1/\alpha)$ = 73 +/- 6 Hz/MPa. Thus, the overall average segmental alignment in bimodal networks appears to follow a similar trend as the unimodal networks.

6.3.3 ^{2}H-NMR lineshapes of stretched networks

^{2}H-NMR lineshapes for a series of unimodal networks are detailed in Chapter 5. At high extension, the 36000 g/mol network spectra displayed a prominent shoulder in addition to the expected spectral splitting (Figure 6.7b). The lineshapes were empirically fit to two pairs of doublets with splittings $\Delta\nu_w$ and $\Delta\nu_n$ to describe the separation between the shoulders and the peak maxima, respectively. This $\Delta\nu_n$ is equivalent to the $\Delta\nu$ reported in all previous ^{2}H-NMR studies. The wide splitting is attributed to the alignment of chain segments that are highly influenced by the cross-link constraints, while the narrow splitting was shown to result from excluded volume interactions between chain segments (Chapter 5). Two populations are also observed in the ^{2}H-NMR spectra for labeled 90000 g/mol chains in highly extended bimodal networks (Figure 6.7a). While the shoulders are not always as pronounced in these systems as in the 36000 g/mol unimodal network, all of the bimodal long chain

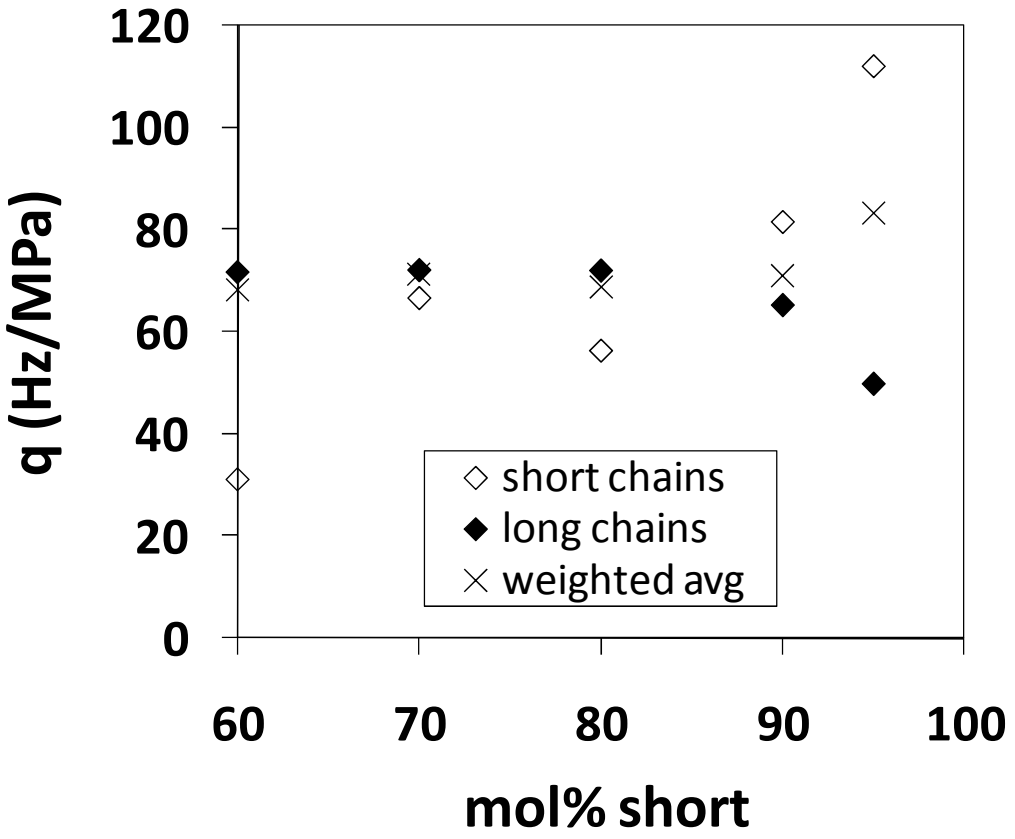

Figure 6.6. Slopes of <v>/E vs. α^2-1/α = q for short (open diamonds) and long (filled diamonds) chain segments at various bimodal compositions. The mass % weighted average at each composition (x) is relatively consistent across all short chain concentrations and shows good agreement with the average q found for unimodal networks of various precursor molar masses.

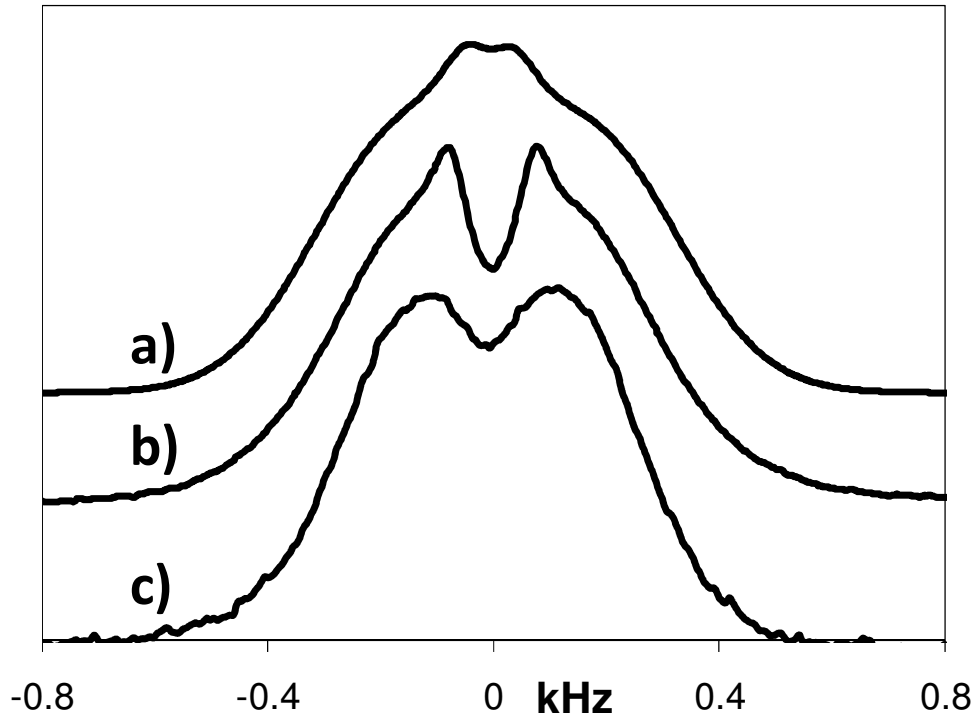

Figure 6.7. ^{2}H-NMR lineshapes for a) 60 mol % short chain bimodal network with ^{2}H-labeled long chains (α = 2.04) b) 36000 g/mol unimodal network (α = 1.98) and c) 90000 g/mol unimodal network (α = 2.26). Only the 90000 g/mol unimodal network does not show a "two doublet" spectrum that would be reflected in a shoulder.

lineshapes were successfully fit to doublets with peak separation $\Delta\nu_w$ and $\Delta\nu_n$. These data are normalized by the elastic modulus and plotted vs. α^2-1/α in Figure 6.8a.

The $\Delta\nu_w$/E and $\Delta\nu_n$/E data follow universal trends for both unimodal and bimodal networks across different precursor chain lengths and compositions. This correspondence indicates that the effects of the excluded volume interactions and the constraints on segmental alignment are each linked to the average mesh size (modulus) of the bulk network. Therefore, it is surprising that the 90000 g/mol unimodal network lineshape does not display an outer shoulder (Figure 6.7c), even though the long chains in bimodal networks employed in this study (depicted in Figure 6.7a) are of the same precursor molar mass. The splitting between the peak maxima for the 90000 g/mol unimodal network are plotted in Figure 6.8b against best-fit lines generated from the unimodal and bimodal network data in Figure 6.8a. Also included are data from Chapter 5 for ^{2}H-labeled 30000 g/mol non-reactive chains dissolved in a protonated host network. Since these probe chains are not chemically attached to the network, their segments only align through excluded volume interactions with neighboring chains. These data follow the $\Delta\nu_n$/E trend line as expected. Meanwhile, the $\Delta\nu$ values for the 90000 g/mol network closely follow the $\Delta\nu_w$/E relationship associated with segment alignment due to the effect of constraints. Upon first glance this result seems odd since the excluded volume interactions cannot be avoided. It thus appears that this effect is obscured in the spectrum of Figure 6.7c by the large signal from chain segments that are aligned due to the effect of cross-links. This lineshape characteristic is a result of the structure of the 90000 g/mol unimodal network. This network was the only sample tested that could be classified as "non-model" due to its large soluble fraction and high degree of swelling in toluene (w_{sol} = 5.48%, Q = 7.31 – Table 6.1). The 90000 g/mol chains in bimodal networks are incorporated into networks of significantly better quality (Table 6.1) due to the associated increase in

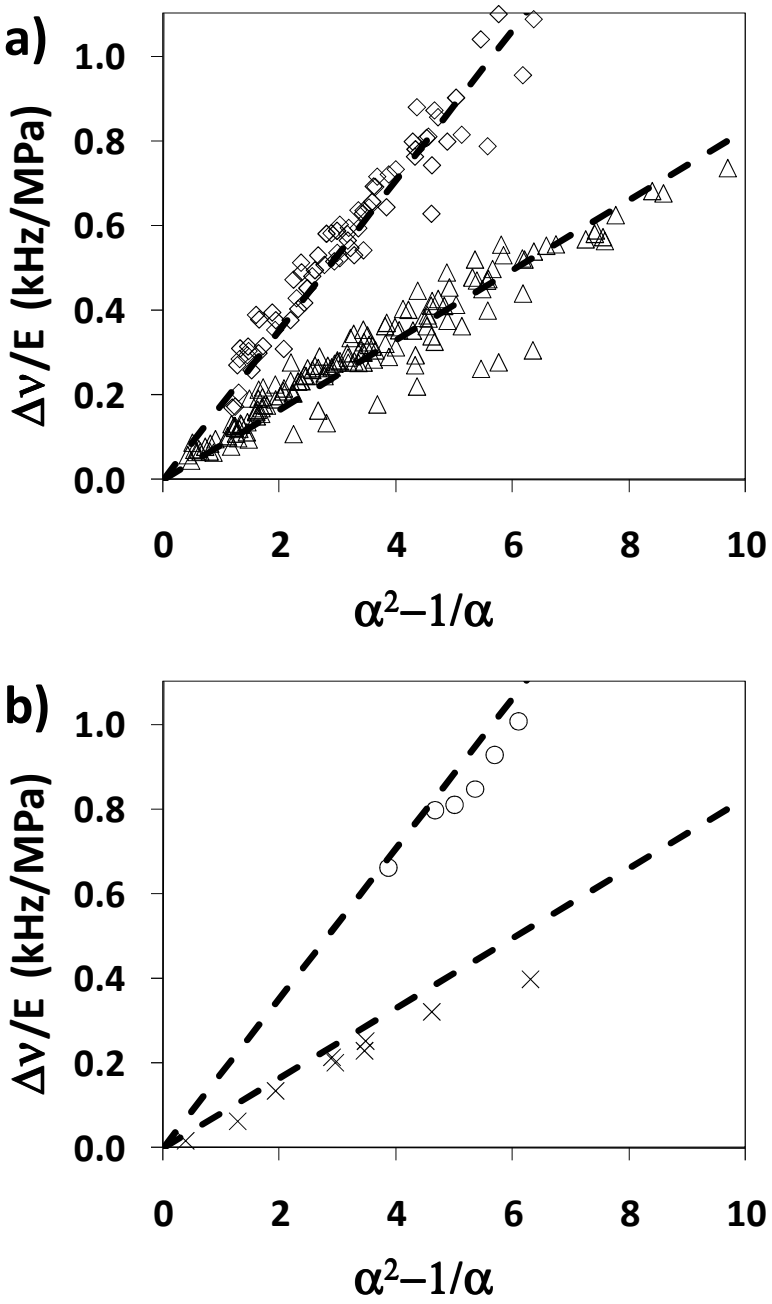

Figure 6.8. a) All data for the narrow ($\Delta\nu_n/E$) and wide ($\Delta\nu_w/E$) spectral splittings found in ^{2}H-NMR lineshapes of unimodal and bimodal networks and the best fit lines through these data. b) $\Delta\nu/E$ for the 90000 g/mol unimodal network (circles) and the 30000 g/mol ^{2}H-labeled free chains dissolved in a protonated 30000 g/mol network (x) plotted against the best fit lines generated in a).

cross-link density. The molar mass between effective junctions, which takes into account the presence of trapped entanglements along the elastic chains, can be calculated from:

$$M_c = 3\rho RT/E\,. \tag{3}$$

Taking $\rho = 0.97$ g/cm^3 for PDMS and elastic modulus values from Table 6.1, one can calculate $M_c = 27000$ and 12000 g/mol for the unimodal networks synthesized from 90000 and 36000 g/mol precursors, respectively. Therefore, elastic chains in both networks are expected to have about two effective junctions along their chain lengths, even though the 90,000 g/mol chains are almost three times longer than the 36000 g/mol chains. The lack of a visible "excluded volume" split $\Delta\nu_n$ can then be explained by the relative reduction of interchain interactions in the longer chain unimodal network. The presence of pendant chains and the removal of the relatively high fraction of soluble chains upon drying likely led to chain interspersion (non-trapped entanglements).[33,34] Upon uniaxial extension the chains primarily disintersperse,[35] diminishing the effect of excluded volume interactions. Consequently, the segment alignment is dominated by the movement of the cross-links. This effect appears to have eclipsed the contribution of chain segment interactions between pendant chains and the elastic network, since an increased fraction of pendant chains is expected in such non-model networks.[17] The relative lack of $\Delta\nu_n$ in the 90000 g/mol unimodal network causes it to show a higher degree of average segmental orientation with respect to elastic modulus than the other unimodal networks (Table 6.1). This effect is also demonstrated by the 36000 g/mol precursors reacted in the presence of 30% non-reactive chains. After the solvent chains are extracted, this network (36000d) shows a higher degree of segment orientation than the standard 36000 g/mol unimodal network. A higher contribution from disinterspersion of chains in the 36000d network

is expected due to its collapsed structure upon extraction. Table 6.1 also indicates a higher value of q for this network before removal of solvent chains (80.6 Hz/MPa) than after (73.3 Hz/MPa). This difference results from the decreased degree of intersegmental interactions between network chains when solvent chains are present.[33,34]

6.4 Conclusions

Segmental ordering in bimodal networks is investigated using ^{2}H-NMR. The average absolute value $\langle|v|\rangle$ of the spectra is computed to capture the presence of highly oriented segments. This allows for calculation of average chain segment order $\langle v \rangle$ by implementing a recently reported method.[15] Even in the rest state, the lineshapes of the short and long chain components are markedly different due to the different degree of motional restriction on each. The conformation of long chains is not affected when they are incorporated into a bimodal network structure. However, $\langle|v|\rangle_0$ values for short chains in undeformed networks evolve with bimodal composition as a result of the network topology.

Networks at about 90 mol % are of particular interest, since they have been demonstrated to produce optimal mechanical properties. Here, the high $\langle|v|\rangle_0$ value indicates increased motional restriction on the short chains that is likely the result of chains at a relatively high end-to-end distance during network formation. Further connections between microstructure and macroscopic properties are made by measuring ^{2}H-NMR spectra for samples that have been uniaxially stretched. These experiments clearly demonstrate the reapportionment of segmental orientation from long to short chains with increasing short chain concentration. When their concentration is at 60 mol %, the shorter chains are found to be protected from segmental alignment since they are clustered into small domains within a medium of

longer chains. Here, the segmental orientation is dominated by excluded volume interactions between neighboring chains.

Optimum mechanical properties found with 90 mol % short chains are primarily due to increased mechanical loading on the short chain matrix. Wide spectral wings for these ^{2}H-labeled short chains indicate that some of these chains are highly stretched. The segmental alignment of the short chains is at a maximum when their concentration is further increased, but the networks become increasingly brittle. Thus, the ductility afforded by the long chain component is essential to producing bimodal networks with enhanced mechanical properties. There are likely regions dominated by long chains within these optimal networks that allow the samples to stretch without fracture even as the short chains are increasingly loaded. Although the relative orientation of short and long chain segments clearly evolves with concentration, the ^{2}H-NMR experiments indicate that the overall segmental alignment normalized by the elastic modulus is equal across all bimodal network compositions.

REFERENCES

1. Chapellier, B.; Deloche, B.; Oeser, R. *Prog. Coll. Pol. Sci. S.* **1992**, *90*, 111-114.

2. Chapellier, B.; Deloche, B.; Oeser, R. *J. Phys. II* **1993**, *3*, 1619–1631.

3. Sotta, P. *Macromolecules* **1998**, *31*, 3872-3879.

4. Llorente, M. A.; Andrady, A. L.; Mark, J. E. *J. Polym. Sci., Polym. Phys.* **1981**, *19*, 621–630.

5. Mark, J. E.; Tang, M.-Y. *J. Polym. Sci., Polym. Phys.* **1984**, *22*, 1849–1855.

6. Galiatsatos, V.; Mark, J. E. *Macromolecules* **1987**, *20*, 2631-2632.

7. Subramanian, P. R.; Galiatsatos, V. *Makromol. Chem.-M. Symp.* **1993**, *76*, 233-240.

8. Viers, B. D.; Mark, J. E. *J. Inorg. Organomet. P.* **2007**, *17*, 283-288.

9. Hanyu, A.; Stein, R. S. *Makromol. Chem., Macromol. Symp.* **1991**, *45*, 189-203.

10. Besbes, S.; Bokobza, L.; Monnerie, L.; Bahar, I.; Erman, B. *Macromolecules* **1995**, *28*, 231–235.

11. Sotta, P. *Macromolecules* **1998**, *31*, 8417-8422.

12. Saalwächter, K. *J. Am. Chem. Soc.* **2003**, *125*, 14684-14685.

13. Saalwächter, K.; Ziegler, P.; Spyckerelle, O.; Haidar, B.; Vidal, A.; Sommer, J.-U. *J. Chem. Phys.* **2003**, *119*, 3468–3482.

14. Saalwächter, K.; Sommer, J.-U. *Macromol. Rapid Commun.* **2007**, *28*, 1455-1465.

15. Aguilera-Mercado, B. M.; Cohen, C.; Escobedo, F. A. submitted to *Macromolecules*.

16. Genesky, G. D.; Aguilera-Mercado, B. M.; Bhawe, D. M.; Escobedo, F. A.; Cohen, C. *Macromolecules* **2008**, *41*, 8231-8241.

17. Patel, S. K.; Malone, S.; Cohen, C.; Gillmor, J.; Colby, R. *Macromolecules* **1992**, *25*, 5241–5251.

18. Takahashi, H.; Shibyama, M.; Fujisawa, H.; Noruma, S. *Macromolecules* **1995**, *28*, 8824–8828.

19. Flory, P. J. *Principles of Polymer Chemistry*; Cornell University Press: Ithaca, NY, 1953.

20. Sotta, P.; Deloche, B. *Macromolecules* **1990**, *23*, 1999-2007.

21. Brereton, M. G. *Macromolecules* **1993**, *26*, 1152-1157.

22. McLoughlin, K.; Waldbieser, J. K.; Cohen, C.; Duncan, T. M. *Macromolecules* **1997**, *30*, 1044-1052.

23. Warner, M.; Callaghan, P. T.; Samulski, E. T.; *Macromolecules* **1997**, *30*, 4733-4736.

24. Deloche, B.; Beltzung, M.; Herz, J. *J. Phys. (Paris), Lett.* **1982**, *43*, 763-769.

25. Gronski, W.; Stadler, R.; Jacobi M. M. *Macromolecules* **1984**, *17*, 741-748.

26. Wu, W. L.; Jong, L.; Hanyu, A.; Coyne, L. D.; Stein, R. S. *Macromolecules* **1990**, *23*, 351–353.

27. Hecht, A.-M.; Horkay, F.; Geissler, E. *J. Phys. Chem. B* **2001**, *105*, 5637–5642.

28. Oikawa, H. *Polymer* **1992**, *33*, 1116–1119.

29. Ries, M. E.; Brereton, M. G.; Klein, P. G.; Ward, I. M.; Ekanayake, P.; Menge, H.; Schneider, H. *Macromolecules* **1999**, *32*, 4961-4968.

30. Yong, C. W.; Higgs, P. G. *Macromolecules* **1999**, *32*, 5062-5071.

31. Andrady, A. L.; Llorente, M. A.; Mark, J. E. *J. Chem. Phys.* **1980**, *72*, 2282–2290.

32. Kuhn, W.; Grün, F. *Kolloid Z.* **1942**, *101*, 248-271.

33. Urayama, K.; Kohjiya, S. *J. Chem. Phys.* **1996**, *104*, 3352-3359.

34. Sivasailam, K.; Cohen, C. *J. Rheol.* **2000**, *44*, 897-915.

35. Urayama, K.; Kohjiya, S. *Polymer* **1997**, *38*, 955-962.

FUTURE WORK

A number of interesting studies could be performed in light of the results of this thesis. Fatigue testing of these bimodal networks is one possibility. In this type of test, a uniaxial extension experiment would be performed repeatedly on the same strip of material up to the same elongation ratio to investigate the hysteresis and eventual failure of the material. While the model elastomers tested in Chapters 2 and 3 do not show stress-strain hysteresis, extension to near the failure point α_c would be interesting. Since the short chains are highly aligned with strain in optimal bimodal networks, these experiments might show more hysteresis as more short chains gradually ruptured under repeated loading.

Since most studies of bimodal networks have concentrated on PDMS, mechanical testing of bimodal networks synthesized from semi-flexible chains is another possibility. Polydiethylsiloxane (PDES) networks form a mesomorphic neck at high elongation ratios or low temperatures. One could synthesize PDES bimodal networks of varying compositions to assess the effect of bimodality on the mesophase formation.

Given the lineshape of the 90000 g/mol unimodal network reported in section 6.3.3, it would be interesting to perform ^{2}H-NMR studies of networks prepared with varying amounts of solvent chains (results for a single concentration are detailed at the end of section 6.3.3). Such networks would have differing degrees of contribution from inter-chain entanglements. Therefore, examination of the lineshapes of these networks when stretched would illustrate the relative contributions from the effect of cross-links and excluded volume interactions. Networks prepared in solvent would also be interesting to examine with fracture energy tests. These experiments might provide further insight into the effect of entanglements on the fracture process of

model end-linked networks.

Small angle neutron scattering (SANS) testing on the ^{2}H-labled samples from Chapters 5 and 6 would give a further experimental measure of the microstructures detailed in this thesis. SANS has been used to study bimodal networks, but not for networks with such widely ranging compositions. Such experiments, for instance, could corroborate the evidence for short chain clustering in 60 mol % short chain networks.